

DISSERTATION

CARBON-BASED ELECTRODES FOR ENVIRONMENTAL HEALTH APPLICATIONS

Submitted by

Kathleen E. Berg

Department of Chemistry

In partial fulfillment of the requirements

For the Degree of Doctor of Philosophy

Colorado State University

Fort Collins, Colorado

Summer 2019

Doctoral Committee:

Advisor: Charles Henry

Christopher Ackerson

Amber Krummel

Kevin Lear

Copyright by Kathleen E. Berg 2019

All Rights Reserved

## ABSTRACT

### CARBON-BASED ELECTRODES FOR ENVIRONMENTAL HEALTH APPLICATIONS

Environmental risk factors of air pollution and unsafe water are leading contributors to human morbidity and mortality, causing millions of deaths and diseases annually worldwide. Fine particulate matter (PM<sub>2.5</sub>) air pollution is linked to millions of deaths worldwide annually along with millions of cardiovascular and respiratory diseases. Unsafe water can contain heavy metals, including manganese (Mn), which high doses are linked to a variety of neurological and developmental diseases in humans. Analytical methods for testing for environmental risk factors such as fine PM and Mn still need improving. The primary focus of the dissertation here was to use carbon-based electrodes for improvements on environmental risk factor applications.

An electrochemical assay was developed and used to measure Mn(II) in aqueous samples with stencil printed carbon paste electrodes. Stencil printed carbon paste electrodes are a mixture of graphite and organic liquid; they are easy to fabricate, portable, and disposable. These electrodes also do not require modification before detecting Mn in aqueous samples, but 1,4-benzoquinone was added to the background electrolyte for improved precision. Mn was then detected in complex matrices of tea and yerba mate samples.

The focus is shifted from Mn detection to air pollution applications. A commercially available stencil printed carbon electrode was used for the dithiothreitol (DTT) assay, which is an assay commonly used to estimate the health effects of air pollution samples. The presented, improved DTT assay reduces reagents and increases sample throughput, both of which will help enable larger scale air pollution studies to be executed in the future. The DTT assay was then

further improved with a semi-automated system that further increases the sample throughput and reduces reagent volumes while reducing the required manual labor associated with liquid handling. The semi-automated system uses a custom carbon composite thermoplastic electrode (TPE). Changes were observed in the TPE response over time and are studied further.

The dissertation shifts focus to a more fundamental electrode characterization of high performing TPEs that were previously used because TPEs have a vast array of potential analytical applications, including environmental risk factor applications. Atomic force microscopy (AFM) and scanning electrochemical microscopy (SECM) were used for a thorough investigation of the local surface topography and electrochemistry of TPEs, which is needed to assess the cause of the excellent electrochemical properties. The evidence suggests that the TPEs behave as microelectrodes, which gives rise to their high electrochemical activity.

The amount of potential applications from TPEs is then increased by modifying the surface. TPEs, while being high performing and easy to pattern, have previously been limited by their solvent compatibility to aqueous solvents. Presented here is an alternative fabrication, which makes TPEs polar organic solvent compatible, that greatly increases the number of applications. The TPEs were then modified and functionalized in acetonitrile as a proof of concept that TPEs can be used in non-aqueous solvents and can have modified surfaces, which can lead to more applications.

The research here uses different carbon electrodes to advance method development of environmental risk factor quantification. Advances to Mn(II) detection and fine PM health impacts were made. Fundamental understandings were developed of carbon composite TPEs and then modified to show a large potential number of future applications for continual improvement of electrochemical sensing.

## ACKNOWLEDGEMENTS

I would like to thank my advisor, Chuck Henry, for all of the guidance, wisdom, and laughs he has given to me for my scientific and personal development. I can't image what graduate school would have been like with another advisor, and many of my future opportunities would not exist without him. I would also like to thank my committee members for their valuable time and feedback. Philippe Hapiot and Yann Leroux also deserve my appreciation for advising me during my time in France. My time in France would not have been possible without Philippe or Chuck.

I also would like to acknowledge Jaclyn Adkins and Scott Noblitt, who have also played important roles with my scientific development, and I appreciate their continued support and friendship. I also want to thank other Henry group members, past and present, who helped me in many different ways. There are too many to name, but I trust they know they helped me and hopefully know that I appreciate it. I would also like to thank the guys at Legacy, especially Ryan Holcomb and Robby Payne, for their training and expertise even when they didn't have to help. Outside of my research group, I would like to thank the other friends I have made while at CSU because their support has been invaluable.

I would also like to acknowledge those who helped my scientific development and research career before graduate school. Andrzej Rajca, Suchada Rajca, and Joe Paletta were helpful with their advice and teachings while I was at the University of Nebraska-Lincoln. I guess I wasn't meant to be a synthetic organic chemist though. I would also like to acknowledge L. Keith Woo for advising me while being a summer intern at the Ames Laboratory at Iowa State and Bob Angelici for his great encouragement.

I would lastly like to acknowledge those people whom I know from outside the context of school, whether they read this or not. I really appreciate the laughter, love, and support I have received from my family and friends during times of doubt, grief, and celebration (even and especially if they don't really understand what I'm doing). Again, there are too many to name here, but they likely know who they are. I will recognize Will Lassman for his constant encouragement, especially while I was in France and finishing up this dissertation. Throughout my life, I have received so much love and support from my father and sister, and I cannot express the impact they've had on me. Of course, none of this would have been possible without all of the love from my mother. It is a shame that she couldn't see me finish my Ph.D, but she taught me about life, love, and perseverance.

## TABLE OF CONTENTS

ABSTRACT.....	ii
ACKNOWLEDGEMENTS.....	iv
CHAPTER 1. INTRODUCTION TO CARBON-BASED ELECTRODES FOR ENVIRONMENTAL HEALTH APPLICATIONS .....	1
Introduction to Environmental Health .....	1
Introduction to Carbon Electrodes.....	4
Manganese Detection.....	5
DTT Assays .....	6
TPE Surface Investigation and Modification.....	8
REFERENCES .....	10
CHAPTER 2. MANGANESE DETECTION USING STENCIL-PRINTED CARBON INK ELECTRODES ON TRANSPARENCY FILM.....	14
Chapter Overview .....	14
Introduction.....	14
Experimental .....	17
Results and Discussion .....	19
Conclusion .....	25
REFERENCES .....	26
CHAPTER 3. ELECTROCHEMICAL DITHIOTHREITOL ASSAY FOR LARGE-SCALE PARTICULATE MATTER STUDIES .....	29
Chapter Overview .....	29

Introduction.....	30
Experimental .....	32
Results and Discussion .....	34
Conclusion .....	40
REFERENCES .....	41
CHAPTER 4. HIGH-THROUGHPUT, SEMI-AUTOMATED DITHIOTHREITOL ASSAY WITH UV/VIS OR ELECTROCHEMICAL DETECTION .....	
	43
Chapter Overview .....	43
Introduction.....	43
Experimental .....	47
Results and Discussion .....	52
Conclusion .....	58
REFERENCES .....	59
CHAPTER 5. SCANNING ELECTROCHEMICAL MICROSCOPY INVESTIGATION OF CARBON COMPOSITE THERMOPLASTIC SURFACES.....	
	62
Chapter Overview .....	62
Introduction.....	62
Experimental .....	65
Results and Discussion .....	66
Conclusion .....	73
REFERENCES .....	74
CHAPTER 6. INCREASING APPLICATIONS OF GRAPHITE THERMOPLASTIC ELECTRODES WITH ARYL DIAZONIUM GRAFTING .....	
	76

Chapter Overview .....	76
Introduction.....	76
Experimental.....	78
Results and Discussion .....	80
Conclusion .....	87
REFERENCES .....	89
CHAPTER 7. CONCLUSION.....	92
Future Directions .....	94
REFERENCES .....	96
APPENDIX 1. MONITORING REACTION KINETICS WITH INFRARED SPECTROSCOPY IN MICROFLUIDIC DEVICES.....	97
Appendix Overview .....	97
Introduction.....	97
Experimental .....	100
Results and Discussion .....	102
Conclusion .....	107
REFERENCES .....	110
APPENDIX 2. ELECTROCHEMICAL DETECTION OF 2-HYDROXYTEREPHTHALATE FOR IMPROVED PARTICULATE MATTER TOXICITY: A PROPOSAL.....	112
Appendix Overview .....	112
Introduction.....	114
Research Design and Methods.....	117
REFERENCES .....	124

## CHAPTER 1. INTRODUCTION TO CARBON-BASED ELECTRODES FOR ENVIRONMENTAL HEALTH APPLICATIONS

### **Introduction to Environmental Health**

Environmental risk factors, such as air pollution and unsafe water, are the leading contributors to the global burden of disease, causing millions of deaths and illnesses annually.<sup>1-6</sup> Human exposure to air pollution is associated with cardiovascular and respiratory diseases.<sup>7-9</sup> While unsafe water is directly linked to diarrheal and lower respiratory tract diseases,<sup>6</sup> excess heavy metal exposure via drinking and irrigation water can also lead to other diseases, including cancer, developmental diseases, and nervous system damage.<sup>10,11</sup> This introduction will discuss air pollution and heavy metal exposure further before introducing aqueous manganese detection, air pollution oxidative potential analysis, and the subsequent investigation and modification of the carbon-based electrodes used for the air pollution analysis.

#### *Particulate Matter Air Pollution*

Particulate matter (PM) consists of particles and liquid droplets suspended in the atmosphere that include acids, organics, metals, salts, soil, and dust from natural and anthropogenic sources.<sup>4,9,12</sup> PM is classified by the following aerodynamic equivalent diameters: PM<sub>10</sub> (coarse, less than 10  $\mu\text{m}$ ), PM<sub>2.5</sub> (fine, less than 2.5  $\mu\text{m}$ ), and PM<sub>0.1</sub> (ultrafine, less than 0.1  $\mu\text{m}$ ). PM<sub>10</sub> includes PM<sub>2.5</sub> unless indicated as the coarse fraction (PM<sub>2.5-10</sub>). Ultrafine PM has a large surface area with varying degrees of lung permeation. While coarse PM is toxic when deposited into the respiratory system, fine PM does pass through the larynx and ciliated airways and is argued to be more toxic.<sup>7,13</sup> The current air quality regulations limit PM mass concentration (annual mean of 10  $\mu\text{g m}^{-3}$  for fine PM and 20  $\mu\text{g m}^{-3}$  for coarse PM). PM composition, and thus

the corresponding toxicity, varies among locations, so recent studies suggest that PM mass concentration alone is a flawed health metric.<sup>14-17</sup>

PM toxicity is dependent on several factors, including size, concentration, and chemical composition.<sup>17,18</sup> The leading hypothesis for the mechanism of fine PM toxicity in humans is that the fine PM enters through the respiratory system and catalyzes reactive oxygen species (ROS) generation.<sup>18-22</sup> ROS are highly reactive oxygen-containing molecules (e.g. hydrogen peroxide, superoxide radical, hydroxyl radical, etc.). High levels of ROS equates to cellular stress, which is shown by inflammation, lipid peroxidation, DNA damage, and apoptosis.<sup>23-26</sup> PM oxidative potential, PM's ability to generate ROS with the corresponding antioxidant oxidation, is now measured and correlated to PM toxicity.<sup>27-36</sup>

There have been several developed assays for measuring PM oxidative potential that include cellular and acellular (chemical) assays. During the cellular assays, the cells are exposed to PM and the resulting ROS generation or oxidative stress markers are measured.<sup>15,23,37</sup> Cellular assays are thought to be an accurate representation of the human biological response but show inconsistent results between different cell culture methods and cell lines.<sup>26</sup> Of the chemical assays, there are direct and indirect ROS measurements. ROS can be directly detected with electron spin resonance (ESR) or high-performance liquid chromatography (HPLC) or fluorescence detection.<sup>31,38,39</sup> The direct ROS measurements often require complicated techniques and/or are not suited for higher throughput. Common indirect ROS measurement are thought to mimic the biological system for a faster screening tool than cellular assays and involve monitoring the loss (or gain in oxidized product) of ascorbic acid (AA), glutathione (GSH), and/or dithiothreitol (DTT) after PM exposure.<sup>40</sup> There is debate over the accuracy of AA and GSH assays depending on the PM composition because they are both sensitive to Cu and GSH is also sensitive to Fe.<sup>41,42</sup> The

DTT assay reacts with the widest range of compounds, including aromatic hydrocarbons and some metals, of tested assays.<sup>43-45</sup> Epidemiological evidence supports the DTT assay results being a relevant health metric for PM toxicity.<sup>22,31,40</sup>

### *Heavy Metal Exposure*

Heavy metals, often defined as elements with greater than 5 g cm<sup>-3</sup> density (but can include metalloids such as arsenic) are toxic at high concentrations but are usually found in trace quantities, ppb to less than 10 ppm.<sup>11</sup> As pollutants, they do not easily degrade and are incorporated into biologics and persist through the food chain.<sup>10</sup> Heavy metals are used in applications in industrial, agricultural, domestic, and technological applications, and human exposure has increased due to their environmental pollution.<sup>46</sup> Intake of the metals can occur from ingestion of contaminated food (vegetables that have been treated with waste water containing heavy metals) or drinking water.<sup>47-49</sup>

Heavy metal bioavailability and/or toxicity depends on many factors that include the concentration, complexation, oxidation state, and solubility.<sup>50</sup> It is known that cobalt, copper, chromium, iron, magnesium, manganese, molybdenum, nickel, selenium, and zinc are essential micronutrients for healthy biological function and deficiencies in these metals can lead to adverse health effects.<sup>51</sup> Other metals such as aluminum, antimony, arsenic, barium, beryllium, bismuth, cadmium, gallium, germanium, gold, indium, lead, lithium, mercury, nickel, platinum, silver, strontium, tellurium, thallium, tin, titanium, vanadium, and uranium are considered non-essential metals and have no established biological necessity.<sup>52</sup> Heavy metals have been reported to affect many cellular organelles and components, and ROS have been shown to play a role in the metal toxicity.<sup>53-56</sup>

While it is known that heavy metal exposure and PM air pollution can have severe negative health effects, accurate and precise quantitation is needed for a true risk assessment, which can lead to a better understanding and prevention of exposure.<sup>57</sup> Factors, such as cost and time, of the quantitation method can inhibit the risk assessment.<sup>58</sup> For example, the traditional DTT assay uses many consumable products, has a low throughput, and is used after the samples have been collected and transported to a laboratory for analysis.<sup>40</sup> The high cost and long turnaround time for sample analysis helps prevent large-scale studies of fine PM air pollution. Both heavy metal and PM health effects (via the DTT assay) measurements have shown promising improvements by using electrochemistry with carbon-based electrodes.<sup>59-63</sup>

### **Introduction to Carbon Electrodes**

Carbon is widely used as an electrode material for analytical and industrial electrochemistry.<sup>64</sup> Carbon electrodes are often attributed with the following advantages relative to other electrode materials: low cost, wide potential window, inert electrochemistry, and/or electrocatalytic activity to a variety of redox mechanisms.<sup>64,65</sup> Carbon electrodes are usually classified by their basic structure and hybridization, and most electrochemical activity is attributed to the edge plane as opposed to the basal plane, where the edge plane is the edge of the graphene plane and the basal plane is the “face” of the graphene plane.<sup>66,67</sup> There are many forms of high-performing carbon for electrochemistry, including graphene,<sup>68,69</sup> highly oriented pyrolytic graphite (HOPG),<sup>70</sup> carbon nanotubes (CNTs),<sup>71</sup> boron-doped diamond (BDD),<sup>72</sup> carbon fibers,<sup>73</sup> and carbon composite (or carbon paste) electrodes.<sup>74</sup> The properties that affect electrochemical behavior include surface structure, electronic structure, adsorption, electrocatalysis, and surface preparation.<sup>64</sup>

Carbon composite electrodes are a mixture of electroactive and inactive components and are often referred to as carbon paste electrodes.<sup>75-77</sup> Commonly, the electroactive component is graphite and the inactive component is an organic liquid, which makes these electrodes easier to pattern.<sup>78</sup> However, carbon paste electrodes suffer from low conductivity and electrochemical performance. Other carbon composite electrodes, made from carbon and an inactive solid material (e.g. a polymer), have been reported and have industrial and analytical applications.<sup>79,80</sup> Carbon composite and paste electrodes, relative to other carbon electrodes, often have low background current, but the inactive material can cause interferences.<sup>64</sup>

### **Manganese Detection**

Stencil printed carbon electrodes, a type of carbon paste electrode, give the advantages of low cost, disposability, and portability while retaining low detection limits.<sup>81</sup> Aqueous manganese (Mn) detection on stencil-printed carbon electrodes was investigated (Chapter 2, published in *Electroanalysis*).<sup>82</sup> Mn is an essential micronutrient, but high doses can lead to negative health effects, including manganism, which involves psychiatric and motor disturbances similar to Parkinson's disease.<sup>83,84</sup> Mn(II) is stable in aqueous environments and is often linked to water pollution that is still present in crops upon human consumption.<sup>85,86</sup> However, Mn(II) can be easily detected at relevant trace levels with electrochemistry. Cathodic stripping voltammetry (CSV) is an electrochemical technique where an oxidation potential is applied to oxidize Mn(II) to Mn(IV), followed by a negative, reducing sweep to Mn(II), resulting in a measurable current.<sup>87</sup> CSV is a popular choice for Mn(II) detection because it is sensitive, yields low detection limits, and can be performed on various modifications of carbon electrodes.<sup>87-89</sup> Mn(II) was detected on homemade stencil printed carbon electrodes with a 30 ppb limit of detection, and it was found that 1,4-benzoquinone and 3.5% NaCl addition to the background improved sensitivity and

reproducibility. An interference study from other metals was tested with the developed technique and was found to be susceptible to aluminum(III), iron(II), copper(II), and lead(II). Even with other metal interferences, Mn(II) was still successfully measured in yerba mate and green tea samples, which are known to have 2-2,000 ppm Mn depending on origin, brand, and preparation.<sup>90,91</sup> The stencil printed carbon electrodes are promising for measuring Mn in the field, which would yield spatial and temporal data.

### **DTT Assays**

Stencil printed carbon electrodes are used for another environmental risk factor, air pollution, using the DTT assay for PM oxidative potential analysis. The traditional DTT assay involved the following steps: (1) the PM sample is incubated with DTT in buffer, (2) an aliquot was removed and mixed with trichloroacetic acid, quenching reagent, at various times, (3) 5,5'-dithiobis(2-nitrobenzoic acid) (DTNB, Ellman's reagent) was added to the aliquot, and (4) the aliquot absorbance at 412 nm (5-mercapto-2-nitrobenzoic acid product of DTNB and DTT) was measured for indirect DTT detection.<sup>45</sup> The UV/vis assay is simple to perform and only requires common equipment, but only one sample per hour is analyzed, which makes large sample sizes difficult. A modified DTT assay without the additional reagents using electrochemical detection was later published with comparable accuracy and sensitivity.<sup>60</sup> The electrochemical assay, while saving on additional reagents, was not used by other research groups due to the homemade electrochemical device fabrication, making the electrochemical DTT assay seem not as simple. The current project began by performing the electrochemical DTT assay on a large (>100) amount of fine PM samples using commercially available electrochemical equipment, a wall jet flow cell with a replaceable stencil printed carbon electrode (Chapter 3, published in *Aerosol Science and Technology*).<sup>92</sup> An end-point assay (two time points) was shown to give the same DTT reactivity

as the kinetic assay (over three time points). After showing that the electrochemical detection yielded the same DTT rates, the electrochemical detection was applied to 211 samples from Honduras that were collected as part of a cookstove replacement project. The results were later used to show a link between household air pollution and prediabetes in women.<sup>93</sup> While the electrochemical DTT assay reduced reagents and increased sample throughput to five samples per hour, more work would be needed to semi-automate the DTT assay with a high sample throughput if large sample sizes could be easily analyzed.

There have only been a few attempts at automating the DTT assay with the most promising semi-automation still only processing one sample per hour.<sup>94</sup> The next project presented was the development of a semi-automated DTT assay using an HPLC autosampler with either electrochemical or UV/vis detection that resulted in an optimized sampling rate of six samples per hour while using less reagents (Chapter 4, submitted to *Environmental Science and Technology*). The UV/vis detection system's accuracy and precision were first established with Cu(II) as a model DTT oxidant.<sup>43</sup> Real samples from rural China were run with UV/vis detection. The same commercial electrochemical flow cell used previously for the DTT assay was used with an HPLC. While the commercial flow cell would work, the sampling rate was reduced to three samples per hour because of the required flow rate. To allow for a higher flow rate and thus higher sampling rate, a custom, homemade carbon electrode flow cell was used. The carbon electrode was a thermoplastic electrode (TPE) that can easily be molded while retaining good electrochemical properties.<sup>95</sup> While using the TPE for DTT detection, it was found the TPE was about four times more sensitive than the commercial flow cell, and the accuracy and precision of the TPE were then tested. After, real samples from Honduras, the same project as above, were analyzed using electrochemical detection with the TPE. However, after about six months of intermittent use, the

TPE began yielding variable results that suggested the electrode surface was changing over time and more active sites were possibly becoming exposed because of the increased current. The change in response over time from other TPEs has not been observed and warranted further investigation.

### **TPE Surface Investigation and Modification**

After demonstrating the utility of TPEs for DTT assays, I had the chance to perform fundamental studies to understand the characteristics of TPEs through a Chateaubriand Fellowship in Philippe Hapiot's laboratory at the Université de Rennes 1. TPEs are a mixture of carbon (graphite is usually used) and a thermoplastic that are easily shaped while giving good electrochemical performance. While carbon electrodes are typically difficult to pattern and/or have lower conductivity, TPEs are easily patternable into  $\mu\text{m}$ -sized features and have high conductivity and electron transfer kinetics.<sup>95,96</sup> It is hypothesized that TPEs have "active islands" of graphite that behave like microelectrodes, which was supported by the scanning electron microscopy (SEM) images. Though TPEs have been fabricated using poly(methyl methacrylate) (PMMA), cyclic olefin copolymer (COC), and polycaprolactone (PCL) with various carbon types, there has not been a thorough comparison of the different TPEs. I was presented with the opportunity to use scanning electrochemical microscopy (SECM) in France to conduct this investigation (Chapter 5, submitted to *Analytical Chemistry*). SECM is an electrochemical technique for investigating localized electrochemical surfaces and topography. An ultramicroelectrode (UME,  $\leq 20 \mu\text{m}$  diameter) is used to approach the substrate surface (TPE here), and the UME current either increases (positive feedback) or decreases (negative feedback) as the UME gets closer to the substrate (TPE here) surface. Surface imaging can be acquired to give a more global view of the heterogeneous surface and was used here. There were not large differences observed between COC

and PMMA TPEs, but there were large differences seen with changing carbon type and the thermoplastic:carbon ratio. As expected, the higher amount of carbon in the TPE lead to higher electrochemical activity with lower variation. PCL TPEs, which were the TPE type used in the DTT assay described above, were studied over time and found to have lower electrochemical activity after two weeks from fabrication. The results from this study will aid future TPE work by selecting the best TPE for the analyte of interest.

After investigating the electrochemical properties of TPEs, a new, organic-solvent compatible TPE was developed (Chapter 6, submitted to *Electrochimica Acta*). Previously fabricated TPEs were in PMMA templates, which limits solvent compatibility to aqueous solvents; however, this greatly reduces the applications to which TPEs can be applied because many electrochemical applications utilize non-aqueous solvents. Glass was used as a template with a COC TPE, so polar organic solvents are now compatible.<sup>97</sup> The TPE was then modified with various aryl diazonium salts in acetonitrile, and this is the first report of a surface modified TPE. Electrode modification is of great interest to many applications to achieve the desires sensing properties for the analyte of interest.<sup>98</sup> Aryl diazonium modification is popular because it's an easy and fast covalent bond formation to a variety of functional groups.<sup>99</sup> After modifying the surface with various aryl diazonium salts, post-modification click chemistry was successfully applied as a proof of concept. Click chemistry is also an easy and reliable modification technique that is a reaction between terminal alkynes and azides.<sup>100,101</sup> The click chemistry was performed with a ferrocene moiety that enabled a surface concentration value that was close to the theoretical limit and higher than previously observed on a glassy carbon electrode. The increased solvent compatibility and surface modification of TPEs here opens up the breadth of applications possible for the high performing TPEs.

In summary, excess heavy metal exposure and PM air pollution is detrimental to human health, and the goal of this dissertation was to develop better methods to quantitate exposure levels to each. Mn in aqueous samples was measured using carbon paste electrodes. Fine PM air pollution health effects are then estimated with an improved DTT assay that uses carbon electrodes. The same carbon electrodes used for the semi-automated DTT assay are then studied in more detail and modified to increase the number of future applications, including other environmental health risk applications.

## REFERENCES

1. J. O. Anderson, J. G. Thundiyil and A. Stolbach, *Journal of Medical Toxicology*, 2012, **8**, 166-175.
2. J. S. Apte, M. Brauer, A. J. Cohen, M. Ezzati and C. A. Pope, *Environmental Science & Technology Letters*, 2018.
3. A. J. Cohen, M. Brauer, R. Burnett, H. R. Anderson, J. Frostad, K. Estep, K. Balakrishnan, B. Brunekreef, L. Dandona, R. Dandona, V. Feigin, G. Freedman, B. Hubbell, A. Jobling, H. Kan, L. Knibbs, Y. Liu, R. Martin, L. Morawska, C. A. Pope, III, H. Shin, K. Straif, G. Shaddick, M. Thomas, R. van Dingenen, A. van Donkelaar, T. Vos, C. J. L. Murray and M. H. Forouzanfar, *The Lancet*, 2017, **389**, 1907-1918.
4. H. J. Forman and C. E. Finch, *Free Radical Biol. Med.*, 2018, **117**, 202-217.
5. W. H. Organization, *The world health report 2002: reducing risks, promoting healthy life*, World Health Organization, 2002.
6. E. Gakidou, A. Afshin, A. A. Abajobir, K. H. Abate, C. Abbafati, K. M. Abbas, F. Abd-Allah, A. M. Abdulle, S. F. Abera and V. Aboyans, *The Lancet*, 2017, **390**, 1345-1422.
7. J. S. Brown, T. Gordon, O. Price and B. Asgharian, *Particle and fibre toxicology*, 2013, **10**, 12.
8. G. Hoek, R. M. Krishnan, R. Beelen, A. Peters, B. Ostro, B. Brunekreef and J. D. Kaufman, *Environmental health*, 2013, **12**, 43.
9. O. M. Morakinyo, M. I. Mokgobu, M. S. Mukhola and R. P. Hunter, *International journal of environmental research and public health*, 2016, **13**, 592.
10. O. Akpor and M. Muchie, *International Journal of Physical Sciences*, 2010, **5**, 1807-1817.
11. L. Järup, *British medical bulletin*, 2003, **68**, 167-182.
12. C. Muhlfeld, B. Rothen-Rutishauser, F. Blank, D. Vanhecke, M. Ochs and P. Gehr, *American Journal of Physiology-Lung Cellular and Molecular Physiology*, 2008, **294**, L817-L829.
13. R. D. Brook, S. Rajagopalan, C. A. Pope, J. R. Brook, A. Bhatnagar, A. V. Diez-Roux, F. Holguin, Y. Hong, R. V. Luepker, M. A. Mittleman, A. Peters, D. Siscovick, S. C. Smith, L. Whitsel and J. D. Kaufman, *An Update to the Scientific Statement From the American Heart Association*, 2010, **121**, 2331-2378.
14. P. J. A. Borm, F. Kelly, N. Künzli, R. P. F. Schins and K. Donaldson, *Occupational and Environmental Medicine*, 2007, **64**, 73-74.
15. B. Crobeddu, L. Aragao-Santiago, L.-C. Bui, S. Boland and A. Baeza Squiban, *Environ. Pollut.*, 2017, **230**, 125-133.
16. L. Ntziachristos, J. R. Froines, A. K. Cho and C. Sioutas, *Particle and Fibre Toxicology*, 2007, **4**, 5.
17. M. Steenhof, I. Gosens, M. Strak, K. J. Godri, G. Hoek, F. R. Cassee, I. S. Mudway, F. J. Kelly, R. M. Harrison and E. Lebret, *Particle and fibre toxicology*, 2011, **8**, 26.
18. A. De Vizcaya-Ruiz, M. Gutiérrez-Castillo, M. Uribe-Ramirez, M. Cebrián, V. Mugica-Alvarez, J. Sepúlveda, I. Rosas, E. Salinas, C. Garcia-Cuéllar and F. Martínez, *Atmos. Environ.*, 2006, **40**, 583-592.
19. A. A. Alfadda and R. M. Sallam, *BioMed Research International*, 2012, **2012**.

20. W. Y. Tuet, S. Fok, V. Verma, M. S. Tagle Rodriguez, A. Grosberg, J. A. Champion and N. L. Ng, *Atmos. Environ.*, 2016, **144**, 335-344.
21. K. Donaldson, V. Stone, A. Seaton and W. MacNee, *Environ. Health Perspect.*, 2001, **109**, 523-527.
22. J. T. Bates, R. J. Weber, J. Abrams, V. Verma, T. Fang, M. Klein, M. J. Strickland, S. E. Sarnat, H. H. Chang, J. A. Mulholland, P. E. Tolbert and A. G. Russell, *Environmental Science & Technology*, 2015, **49**, 13605-13612.
23. N. Li, C. Sioutas, A. Cho, D. Schmitz, C. Misra, J. Sempf, M. Wang, T. Oberley, J. Froines and A. Nel, *Environ. Health Perspect.*, 2003, **111**, 455.
24. I. S. Mudway, N. Stenfors, S. T. Duggan, H. Roxborough, H. Zielinski, S. L. Marklund, A. Blomberg, A. J. Frew, T. Sandström and F. J. Kelly, *Arch. Biochem. Biophys.*, 2004, **423**, 200-212.
25. I. Rahman and I. Adcock, *European respiratory journal*, 2006, **28**, 219-242.
26. Y. Wang, M. J. Plewa, U. K. Mukherjee and V. Verma, *Atmos. Environ.*, 2018, **179**, 132-141.
27. J. Charrier, N. Richards-Henderson, K. Bein, A. McFall, A. Wexler and C. Anastasio, *Atmospheric Chemistry and Physics*, 2015, **15**, 2327-2340.
28. J. G. Charrier and C. Anastasio, *Environmental Science & Technology*, 2015, **49**, 9317-9325.
29. T. Fang, V. Verma, J. Bates, J. Abrams, M. Klein, M. Strickland, S. Sarnat, H. Chang, J. Mulholland and P. Tolbert, *Atmospheric Chemistry & Physics Discussions*, 2015, **15**.
30. D. Gao, T. Fang, V. Verma, L. Zeng and R. J. Weber, *Atmospheric Measurement Techniques*, 2017, **10**, 2821.
31. N. A. H. Janssen, A. Yang, M. Strak, M. Steenhof, B. Hellack, M. E. Gerlofs-Nijland, T. Kuhlbusch, F. Kelly, R. Harrison, B. Brunekreef, G. Hoek and F. Cassee, *Sci. Total Environ.*, 2014, **472**, 572-581.
32. N. Li, T. Xia and A. E. Nel, *Free Radical Biol. Med.*, 2008, **44**, 1689-1699.
33. T. Moreno, F. J. Kelly, C. Dunster, A. Oliete, V. Martins, C. Reche, M. C. Minguillón, F. Amato, M. Capdevila, E. de Miguel and X. Querol, *Atmos. Environ.*, 2017, **148**, 230-238.
34. E. Vidrio, C. H. Phuah, A. M. Dillner and C. Anastasio, *Environmental Science & Technology*, 2009, **43**, 922-927.
35. A. Yang, A. Jedynska, B. Hellack, I. Kooter, G. Hoek, B. Brunekreef, T. A. J. Kuhlbusch, F. R. Cassee and N. A. H. Janssen, *Atmos. Environ.*, 2014, **83**, 35-42.
36. E. Vidrio, H. Jung and C. Anastasio, *Atmos. Environ.*, 2008, **42**, 4369-4379.
37. A. P. Landreman, M. M. Shafer, J. C. Hemming, M. P. Hannigan and J. J. Schauer, *Aerosol Sci. Technol.*, 2008, **42**, 946-957.
38. S. Fuller, F. Wragg, J. Nutter and M. Kalberer, *Atmos. Environ.*, 2014, **92**, 97-103.
39. H. Shen and C. Anastasio, *Atmos. Environ.*, 2012, **46**, 665-668.
40. J. T. Bates, T. Fang, V. Verma, L. Zeng, R. J. Weber, P. E. Tolbert, J. Y. Abrams, S. E. Sarnat, M. Klein, J. A. Mulholland and A. G. Russell, *Environmental Science & Technology*, 2019, **53**, 4003-4019.
41. K. J. Godri, R. M. Harrison, T. Evans, T. Baker, C. Dunster, I. S. Mudway and F. J. Kelly, *PloS one*, 2011, **6**, e21961.
42. Q. Xiong, H. Yu, R. Wang, J. Wei and V. Verma, *Environmental science & technology*, 2017, **51**, 6507-6514.

43. J. G. Charrier and C. Anastasio, *Atmospheric chemistry and physics (Print)*, 2012, **12**, 11317-11350.
44. V. Verma, T. Fang, H. Guo, L. King, J. Bates, R. Peltier, E. Edgerton, A. Russell and R. Weber, *Atmospheric Chemistry and Physics*, 2014, **14**, 12915-12930.
45. A. K. Cho, C. Sioutas, A. H. Miguel, Y. Kumagai, D. A. Schmitz, M. Singh, A. Eiguren-Fernandez and J. R. Froines, *Environ. Res.*, 2005, **99**, 40-47.
46. P. B. Tchounwou, C. G. Yedjou, A. K. Patlolla and D. J. Sutton, *Experientia supplementum (2012)*, 2012, **101**, 133-164.
47. C. W. Quinn, D. M. Cate, D. D. Miller-Lionberg, T. Reilly III, J. Volckens and C. S. Henry, *Environmental science & technology*, 2018, **52**, 3567-3573.
48. S. Khan, Q. Cao, Y. Zheng, Y. Huang and Y. Zhu, *Environ. Pollut.*, 2008, **152**, 686-692.
49. M. R. Noll, *Journal of Environmental Quality*, 2003, **32**, 374.
50. J. Hamelink, P. F. Landrum, H. Bergman and W. H. Benson, *Bioavailability: physical, chemical, and biological interactions*, CRC press, 1994.
51. W. H. Organization, 1996.
52. L. W. Chang, L. Magos and T. Suzuki, *Toxicology of metals*, Taylor & Francis US, 1996.
53. S. Wang and X. Shi, *Mol. Cell. Biochem.*, 2001, **222**, 3-9.
54. D. Beyersmann and A. Hartwig, *Arch. Toxicol.*, 2008, **82**, 493.
55. P. B. Tchounwou, J. A. Centeno and A. K. Patlolla, *Mol. Cell. Biochem.*, 2004, **255**, 47-55.
56. A. K. Patlolla, C. Barnes, C. Yedjou, V. Velma and P. B. Tchounwou, *Environmental Toxicology: An International Journal*, 2009, **24**, 66-73.
57. C. Monn, *Atmos. Environ.*, 2001, **35**, 1-32.
58. G. Davies and D. Whyatt, *Transactions in GIS*, 2009, **13**, 229-246.
59. K. A. Koehler, J. Shapiro, Y. Sameenoi, C. Henry and J. Volckens, *Aerosol Sci. Technol.*, 2014, **48**, 489-497.
60. Y. Sameenoi, K. Koehler, J. Shapiro, K. Boonsong, Y. Sun, J. Collett, J. Volckens and C. S. Henry, *J. Am. Chem. Soc.*, 2012, **134**, 10562-10568.
61. J. Barton, M. B. G. García, D. H. Santos, P. Fanjul-Bolado, A. Ribotti, M. McCaul, D. Diamond and P. Magni, *Microchimica Acta*, 2016, **183**, 503-517.
62. D. Jagner, *Analyst*, 1982, **107**, 593-599.
63. J. Wang, *Electroanalysis: An International Journal Devoted to Fundamental and Practical Aspects of Electroanalysis*, 2005, **17**, 1341-1346.
64. R. L. McCreery, *Chem. Rev.*, 2008, **108**, 2646-2687.
65. W. Zhang, S. Zhu, R. Luque, S. Han, L. Hu and G. Xu, *Chem. Soc. Rev.*, 2016, **45**, 715-752.
66. X. Ji, C. E. Banks, W. Xi, S. J. Wilkins and R. G. Compton, *The Journal of Physical Chemistry B*, 2006, **110**, 22306-22309.
67. R. L. McCreery and M. T. McDermott, *Anal. Chem.*, 2012, **84**, 2602-2605.
68. A. K. Geim, *science*, 2009, **324**, 1530-1534.
69. A. K. Geim and K. S. Novoselov, in *Nanoscience and Technology: A Collection of Reviews from Nature Journals*, World Scientific, 2010, pp. 11-19.
70. A. N. Patel, M. G. Collignon, M. A. O'Connell, W. O. Hung, K. McKelvey, J. V. Macpherson and P. R. Unwin, *J. Am. Chem. Soc.*, 2012, **134**, 20117-20130.
71. E. T. Thostenson, Z. Ren and T.-W. Chou, *Compos. Sci. Technol.*, 2001, **61**, 1899-1912.

72. J. Xu, M. C. Granger, Q. Chen, J. W. Strojek, T. E. Lister and G. M. Swain, *Anal. Chem.*, 1997, **69**, 591A-597A.
73. S. Chand, *Journal of materials science*, 2000, **35**, 1303-1313.
74. D. E. Tallman and S. L. Petersen, *Electroanalysis*, 1990, **2**, 499-510.
75. I. Švancara, K. Vytrás, K. Kalcher, A. Walcarius and J. Wang, *Electroanalysis*, 2009, **21**, 7-28.
76. I. Švancara, A. Walcarius, K. Kalcher and K. Vytrás, *Open Chemistry*, 2009, **7**, 598-656.
77. R. N. Adams, *Anal. Chem.*, 1958, **30**, 1576-1576.
78. S. Sharma and M. Madou, *Bioinspired Biomim. Nanobiomater*, 2012, **1**, 252-265.
79. P. H. M. Buzzetti, G. C. de Oliveira, A. L. M. Azevedo, R. C. Michel, E. A. Ponzio and F. S. Semaan, *Advances in materials science research*, 2015, **21**, 1-23.
80. A. Regel and S. Lunte, *Electrophoresis*, 2013, **34**, 2101.
81. J. Adkins, K. Boehle and C. Henry, *Electrophoresis*, 2015.
82. K. E. Berg, J. A. Adkins, S. E. Boyle and C. S. Henry, *Electroanalysis*, 2016, **28**, 679-684.
83. S. Bleich, D. Degner, R. Sprung, A. Riegel, W. Poser and E. Rütther, 2014.
84. M. G. Baker, S. R. Criswell, B. A. Racette, C. D. Simpson, L. Sheppard, H. Checkoway and N. S. Seixas, *Scandinavian Journal of Work Environment & Health*, 2015, **41**, 94-101.
85. E. A. Malecki, *Brain Research Bulletin*, 2001, **55**, 225-228.
86. F. A. Jan, M. Ishaq, S. Khan, I. Ihsanullah, I. Ahmad and M. Shakirullah, *J. Hazard. Mater.*, 2010, **179**, 612-621.
87. O. M. S. Filipe and C. M. A. Brett, *Talanta*, 2003, **61**, 643-650.
88. C. E. Banks, J. Kruusma, R. R. Moore, P. Tomcik, J. Peters, J. Davis, S. Komorsky-Lovric and R. G. Compton, *Talanta*, 2005, **65**, 423-429.
89. J. Y. Jin, F. Xu and T. Miwa, *Electroanalysis*, 2000, **12**, 610-615.
90. V. L. Cordoba Braganca, P. Melnikov and L. Z. Zanoni, *Biol. Trace Elem. Res.*, 2011, **144**, 1197-1204.
91. K. Wrobel, K. Wrobel and E. M. C. Urbina, *Biol. Trace Elem. Res.*, 2000, **78**, 271-280.
92. K. E. Berg, L. R. Turner, M. L. Benka-Coker, S. Rajkumar, B. N. Young, J. L. Peel, M. L. Clark, J. Volckens and C. S. Henry, *Aerosol Sci. Technol.*, 2019, 1-8.
93. S. Rajkumar, M. L. Clark, B. N. Young, M. L. Benka - Coker, A. M. Bachand, R. D. Brook, T. L. Nelson, J. Volckens, S. J. Reynolds and C. L'Orange, *Indoor air*, 2018.
94. T. Fang, V. Verma, H. Guo, L. King, E. Edgerton and R. Weber, *Atmospheric Measurement Techniques*, 2015, **8**, 471.
95. K. J. Klunder, Z. Nilsson, J. B. Sambur and C. S. Henry, *J. Am. Chem. Soc.*, 2017, **139**, 12623-12631.
96. E. Noviana, K. J. Klunder, R. B. Channon and C. S. Henry, *Anal. Chem.*, 2019, **91**, 2431-2438.
97. P. S. Nunes, P. D. Ohlsson, O. Ordeig and J. P. Kutter, *Microfluidics and nanofluidics*, 2010, **9**, 145-161.
98. A. J. Bard, *Journal*, 1983.
99. M. Delamar, R. Hitmi, J. Pinson and J. M. Saveant, *J. Am. Chem. Soc.*, 1992, **114**, 5883-5884.
100. J. E. Moses and A. D. Moorhouse, *Chem. Soc. Rev.*, 2007, **36**, 1249-1262.
101. W. H. Binder and R. Sachsenhofer, *Macromol. Rapid Commun.*, 2007, **28**, 15-54.

## CHAPTER 2. MANGANESE DETECTION USING STENCIL-PRINTED CARBON INK ELECTRODES ON TRANSPARENCY FILM

### Chapter Overview

Manganese (Mn) was determined using square-wave cathodic stripping voltammetry (CSV) with inexpensive, stencil-printed carbon electrodes generated on transparency films. Using an optimized pH 5.0 ammonium acetate buffer and 1,4-benzoquinone, a detection limit as low as 500 nM (30 ppb) was achieved. 1,4-Benzoquinone improved peak potential reproducibility and height, while addition of 3.5% NaCl to the background solution approximately doubled the sensitivity ( $\mu\text{A/ppm}$ ). Tolerance tests were conducted and the method was found to be resilient to chromium(VI), iron(III), magnesium(II), nickel(II), and zinc(II), but susceptible to aluminum(III), copper(II), iron(II), and lead(II) at concentration ratios at or below one. This technique was successfully used to measure Mn levels in yerba mate and green tea samples as an example application. This work was published in *Electroanalysis*.<sup>1</sup> Jaclyn Adkins advised and supervised the experiments. Sarah Boyle worked on this project, but the data is not presented here nor in the manuscript.

### Introduction

Manganese (Mn) is an essential micronutrient that can be toxic if ingested at high concentrations. Chronic exposure to elevated Mn concentrations has been linked to a number of pathologies, including Parkinson's disease.<sup>2-5</sup> The toxicity varies with oxidation states of Mn. Mn(II) is associated with toxicity to mitochondria and is commonly linked to water pollution due to its stability in aqueous systems, while Mn(VII) is rare in aqueous environments.<sup>6-8</sup> Elevated levels of Mn occur from environmental and anthropogenic sources. Tea and yerba mate beverages contain a significant amount of Mn, with reports ranging from 2 to 2,000 ppm, depending on

location of origin, brand, and method of preparation.<sup>9-11</sup> Mn content can be determined with various methods, with atomic absorption spectroscopy (AAS) and inductively coupled plasma mass spectrometry (ICP-MS) being the most common.<sup>12-14</sup> Most of these methods, however, suffer from a lack of portability, high costs, and delayed response time, making them impractical for field measurements.<sup>15,16</sup>

Electrochemistry is an alternative detection technique that can meet both portability and low detection limit requirements necessary for effective in-field use. Recently, inexpensive microfluidic paper-based analytical devices ( $\mu$ PADs) and electrochemical paper-based analytical devices (ePADs) have shown promising diagnostic potential for public health and environmental monitoring due to their reduced analytical costs while maintaining similar performance to commercial electrode systems.<sup>17-21</sup> For example, Ruecha *et al.* were able to determine sub-ppb levels of Zn(II), Cd(II), and Pb(II) with chemically modified carbon screen-printed electrodes using square-wave anodic stripping voltammetry.<sup>22</sup> Besides using paper, printing electrodes onto commercial transparency film is becoming a practical option due to the chemical compatibility and disposability of the polypropylene material.<sup>22,23</sup> Electrode performance is also improved on transparency film relative to paper because the carbon ink remains on the substrate surface compared to penetrating into the porous cellulose paper, leading to a higher electrode conductivity.<sup>22,24</sup>

Stripping voltammetry is an electrochemical detection technique that can provide quantifiable, trace detection of numerous metals.<sup>15,16,25-51</sup> Anodic stripping voltammetry (ASV) is a popular electrochemical method for trace metal determination, but is not optimal for Mn measurements due to the strongly negative potential (-1.70 V vs. SCE) required for the reduction of Mn(II) to Mn(0). Initially, because of its broader potential range, Hg electrodes were used with

ASV to accommodate the reduction potential, but this was not optimal due to the low solubility of Mn in Hg.<sup>31,37,40,45</sup> ASV detection of Mn is also challenged by interference from H<sup>+</sup> reduction, which increases detection limits of Mn.<sup>25,26,36,45,48</sup>

Cathodic stripping voltammetry (CSV) is an alternative detection mode that has promise for measuring Mn. It is more sensitive and gives lower detection limits for Mn than ASV by avoiding Hg solubility issues and H<sup>+</sup> reduction interferences.<sup>25,26,45,48</sup> In CSV, a positive oxidation potential is applied to oxidize Mn(II) to Mn(IV), where Mn(IV) is electrodeposited onto the electrode surface as MnO<sub>2</sub>.<sup>30</sup> A negative potential sweep is then applied to reduce the Mn(IV) back to Mn(II), resulting in the measurable removal of Mn from the electrode surface. As in ASV, the Mn concentration can be deduced from current peak height and/or area. Previously used electrode materials for CSV of Mn include boron-doped diamond,<sup>25,50</sup> palladium/copper,<sup>16</sup> and various modifications of carbon.<sup>15,26-28,30,34,36,41-43,48,49,51</sup> These electrodes can be expensive and/or require larger sample volume compared to the carbon electrodes in this work.

This work presents a simple and inexpensive fabrication method for disposable, transparency film-based electrodes to measure Mn in aqueous solutions using square-wave CSV. The addition of 1,4-benzoquinone was found to improve the electrochemical performance. To our knowledge, this has not been reported for stripping voltammetry. The addition of 1,4-benzoquinone and 3.5% NaCl was found to significantly improved sensitivity and reproducibility relative to the buffer solutions alone. The developed method is relatively resistant to interferences from Cr(VI), Fe(III), Mg(II), Ni(II), and Zn(II). It is susceptible to interferences from Al(III), Cu(II), Fe(II), and Pb(II). Using the optimized system, Mn was measured in various tea and yerba mate samples for an illustrative application; results were compared to traditional AAS measurements.

## Experimental

### *Materials*

Carbon ink (E3178, Ercon Incorporated, Wareham, MA, USA), graphite (< 20  $\mu\text{m}$ , Sigma-Aldrich, St. Louis, MO, USA), and transparency film (3M, Saint Paul, MN, USA) were used for electrode production. Glacial acetic acid (EMD, Darmstadt, Germany) and ammonium hydroxide (Mallinckrodt, Phillipsburg, PA, USA) were diluted in 18.2  $\text{M}\Omega \cdot \text{cm}$  water from a MilliPore (Billerica, MA, USA) Milli-Q system. The 1000 mg/L Mn atomic absorption standard, 1,4-benzoquinone (BQ), catechol, Tris(2,2'-bipyridyl)dichlororuthenium(II) hexahydrate (RuBiPy), and ferrocenecarboxylic acid were purchased from Sigma-Aldrich. p-aminophenol (PAP) was obtained from MilliPore, and p-nitrophenol (PNP) was purchased from TCI America (Portland, OR). Interfering metal solutions were prepared as received without drying from aluminum(III) sulfate hydrate, iron(II) sulfate heptahydrate, lead atomic absorption standard, and zinc(II) nitrate hexahydrate (Sigma-Aldrich). Copper(II) sulfate hexahydrate, magnesium(II) chloride hexahydrate, and potassium dichromate were purchased from Fisher Scientific (Pittsburg, PA, USA). Iron(III) chloride hexahydrate was purchased from Mallinckrodt (Phillipsburg, PA, USA) and nickel(II) sulfate hexahydrate was from Acros (Geel, Belgium). Loose leaf Traditional Blend yerba mate was purchased from Nativa Yerba Mate Incorporated (Saint Paul, MN, USA), and tea bags containing Traditional Yerba Mate were purchased from Guayaki (Sebastopol, CA, USA). Green Tea Superfruit, Mixed Berry was purchased from Lipton (London, United Kingdom). All tea samples were sent to the Colorado State University Veterinary Diagnostic Laboratory for Mn validation using flame atomic absorption spectroscopy (FAAS).

Electrochemical experiments were performed using either a CHI 660B (CH Instruments, Austin, TX) or an eDAQ EA161 Potentiostat and EC201 e-Corder (Denistone East, Australia).

The square-wave stripping voltammetry parameters were as follows: deposition time of 180 s, deposition potential of +0.85 V, final potential of -1 V, incremental potential of 0.004 V, amplitude of 0.105 V, frequency of 15 Hz, and variable sensitivity. All measurements were performed in a three-electrode configuration using carbon counter, working, and pseudo-reference electrodes.

### *Procedure*

Stencils for the three-electrode devices were designed using CorelDRAW software and cut from transparency films using a 30 W CO<sub>2</sub> laser cutter (Epilog Laser, Golden, CO, USA). The electrode dimensions are shown in Figure 2.1. A 5:13 (w/w) graphite-carbon ink mixture was

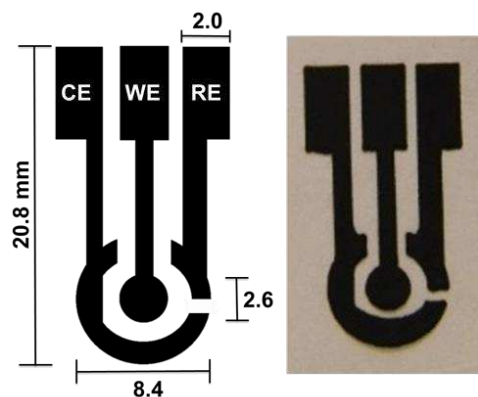


**Figure 2.1:** Schematic and picture of the three-electrode system. All dimensions reported in mm. CE = counter electrode, WE = working electrode, and RE = reference electrode.

stencil printed onto transparency film to create the carbon working, pseudo-reference, and auxiliary electrodes. The electrodes were then dried in a 65 °C oven for 30 min. In this study, each batch of electrodes required a new Mn calibration curve, most likely due to the volatility of the carbon ink solvent, leading to varying batch-to-batch ink compositions. The buffer used for all experiments was 0.05 M acetic acid titrated with 0.125 M ammonium hydroxide to an optimized pH of 5.0.<sup>28,36</sup> Standard Mn solutions were diluted from the atomic absorption standard with the buffer. 1,4-benzoquinone standards (4-12 mM) were prepared daily in buffer. The sample well can

hold between 40 and 80  $\mu\text{L}$ . A 60  $\mu\text{L}$  total volume containing 57  $\mu\text{L}$  of Mn solution and 3  $\mu\text{L}$  of benzoquinone (or other respective redox additive) solution was used for all voltammetry experiments.

A 3.5% w/w NaCl addition to the buffer was used to dilute the Mn AAS solution where indicated. PAP (9.9 mM), PNP (18 mM), catechol (21 mM), ferrocenecarboxylic acid (3.9 mM), and RuBiPy (8.9 mM) solutions were made and tested with 9.0  $\mu\text{M}$  (490 ppb) Mn in NaCl added buffer solution. Interfering metal solutions were made with ratios of 1, 10, 100, 1,000, and 10,000 ppm metal to 18  $\mu\text{M}$  (1 ppm) Mn diluted in NaCl-containing buffer with benzoquinone. Loose leaf yerba mate tea was produced by adding leaves (170 mg) to 70  $^{\circ}\text{C}$  water (17 g) for 45 min, cooling to room temperature ( $23 \pm 2$   $^{\circ}\text{C}$ ), and then filtering (Whatman No. 1) the leaves from solution. The bags of yerba mate and green tea were both prepared by adding the respective tea bag to 200 mL of 75  $^{\circ}\text{C}$  water for 45 min, and cooling to room temperature. All brewed teas were then diluted with water to achieve concentrations within linear calibration curves. Equal volumes of diluted sample solution and a doubly concentrated background solution with benzoquinone were tested.

## **Results and Discussion**

Inexpensive, disposable stencil-printed carbon ink electrodes produced on commercially available polypropylene overhead transparency film (Figure 2.1) were used for Mn determination using CSV with a 180 s deposition time. Stencil printing of these electrodes was a simple, one-step, alternative method for producing low-cost carbon electrodes. In this study, each electrode was used only once, and results were not compared between batches of electrodes due to the variability of signal between batches. The 180 s deposition time was chosen as a result of an optimization study performed of 180, 230, and 360 s deposition times that all gave similar limits of detection. It was found that 0.85 V deposition potential yielded the highest current, while higher

(> 0.90 V) potentials resulted in other interfering peaks. Other CSV parameters were chosen from previously reported literature values.<sup>41</sup> The limit of detection was determined by real measurements of Mn, which was higher than the calculated limit of detection from blank samples. A Mn reduction peak was observed at 0.4 V, and peak height ( $I_p$ ) was used for analysis. However, the Mn peak had variable  $I_p$  ( $7 \pm 1 \mu\text{A}$  standard deviation) and potential ( $430 \pm 60 \text{ mV}$ ).

To improve the stability of the peak potential and height, 1,4-benzoquinone was added to the Mn solutions, initially with the intent to be used as an internal standard due to the non-interfering reduction peak. Figure 2.2 shows multiple voltammograms with and without

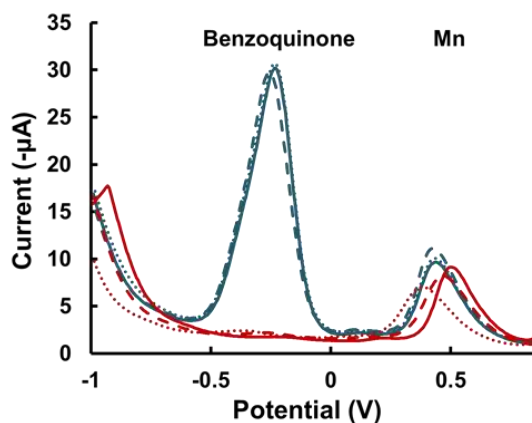


**Figure 2.2:** Multiple scans with (blue) and without (red) 1,4-benzoquinone at  $8.0 \mu\text{M}$  (440 ppb) Mn. Benzoquinone reduction peak occurs at  $-0.3 \text{ V}$ , Mn is at  $0.4 \text{ V}$ .

benzoquinone at a constant Mn concentration of  $8.0 \mu\text{M}$  (440 ppb). The relative standard deviation, RSD, of the peak potential decreased to 1.3% ( $385 \pm 5 \text{ mV}$ ) from 14%, and the  $I_p$ 's RSD decreased to 2.5% ( $12 \pm 0.3 \mu\text{A}$ ) from 14%. The improvement in performance was unexpected and led to further studies in an attempt to understand the underlying mechanism. Benzoquinones have shown to display electrocatalytic oxidation properties in other studies.<sup>52-54</sup> Hydroquinones have also been oxidized to the benzoquinone in the presence of  $\text{MnO}_2$ ,<sup>55</sup> which is the form of Mn deposited in CSV. The presence of 1,4-hydroquinone in the solution could affect the Mn detection. It is also possible that the benzoquinone acts as a reference couple, improving the performance of the

pseudo- reference electrode. To investigate this further, the reversible redox couples PAP, PNP, catechol, RuBiPy, and ferrocenecarboxylic acid were tested with the Mn CSV technique (Figure 2.3). PAP's reduction peak has a shoulder that interferes with the Mn peak and was not analyzed

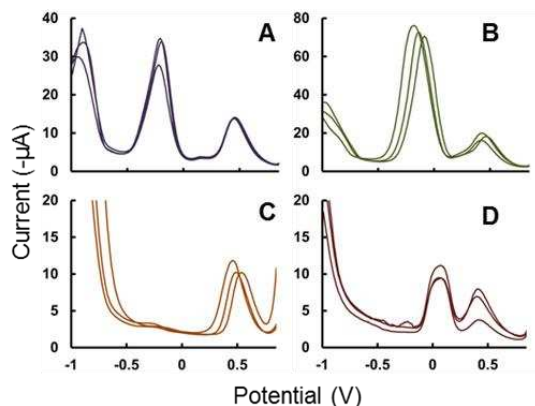


**Figure 2.3:** CSV scans with 9.0  $\mu\text{M}$  (490 ppb) Mn with A) 1,4-benzoquinone, B) catechol, C) PNP, and D) ferrocenecarboxylic acid.

further. Catechol and ferrocenecarboxylic acid, however, do have reduction peaks within this experimental potential window. The Mn  $I_p$  ( $\mu\text{A} \pm$  standard deviation of  $n = 3$ ) with 9.0  $\mu\text{M}$  (490 ppb) Mn were the following: Mn only,  $12.33 \pm 0.57$ ; benzoquinone,  $11.43 \pm 0.28$ ; ferrocenecarboxylic acid,  $4.38 \pm 1.90$ ; catechol,  $12.85 \pm 1.62$ ; PNP,  $8.58 \pm 1.08$ ; RuBiPy,  $16.06 \pm 1.48$ . The peak potentials ( $\text{V} \pm$  standard deviation of  $n = 3$ ) with 9.0  $\mu\text{M}$  (490 ppb) Mn were the following: Mn only,  $0.44 \pm 0.06$ ; benzoquinone,  $0.45 \pm 0.01$ ; ferrocenecarboxylic acid,  $0.41 \pm 0.01$ ; catechol,  $0.44 \pm 0.03$ ; PNP,  $0.49 \pm 0.04$ ; RuBiPy,  $-0.60 \pm 0.03$ . Only ferrocenecarboxylic acid stabilizes the Mn reduction peak potential but does not stabilize  $I_p$ . Using an external Ag/AgCl reference electrode dipped into the solution was also attempted with similar parameters but did not yield a Mn reduction peak. While these results do not definitively deny the electrode potential stabilization hypothesis, they cast doubt on its validity given none of the compounds had the same stabilization effect as 1,4-benzoquinone. At this point, the exact mechanism for the signal improvement obtained with 1,4-benzoquinone remains elusive and is being investigated further.

Calibration curves were required for each new batch of electrodes, possibly due to the volatility of the ink solvent, leading to variability in batch-to-batch ink compositions. Calibration curves of relative peak currents of Mn/benzoquinone (vs.  $[\text{Mn}]/[\text{benzoquinone}]$ ) were compared to calibration curves of Mn  $I_p$  vs.  $[\text{Mn}]$ . The absolute  $I_p$  calibration curves had equal or higher coefficients of determination ( $R^2$ , 0.9924 to 0.9999) than relative  $I_p$  calibration curves (0.9657 to 0.9999), but both analysis techniques are used for comparison. While using 1,4-benzoquinone, the limit of detection was 500 nM (30 ppb), and the response curve was linear from 0.5-25  $\mu\text{M}$  (0.030-1.4 ppm) with a 180 s deposition time. With the addition of 3.5% w/w NaCl to mimic seawater, the sensitivity of Mn  $I_p$  increased from 17 to 28  $\mu\text{A}/\text{ppm}$  Mn, and the relative  $I_p$  sensitivity approximately doubled from 11.5 to 21.5. The addition of NaCl did not change limit of detection or quantification. Single concentration measurements in a solution containing 3.5% w/w KCl exhibited the same  $I_p$  as 3.5% w/w NaCl. It is not known why the salt water solution yields larger sensitivity, but it is potentially related to the higher ionic strength and therefore conductivity. When dealing with higher ionic strength solutions, such as seawater, a commonly measured environmental source of Mn,<sup>13,25,39,41,43,56-58</sup> this suggests that precautions need to be taken to ensure the accuracy of detected Mn concentrations. Sample detection in different matrices could be calibrated by preparing standard solutions with conductivities that match the sample conductivity, or by diluting all analyte solutions in a common electrolyte.

Tolerance ratio tests with potential interfering species were performed, and the results are listed in Table 2.1. Interfering metal solutions were made with ratios of 1, 10, 100, 1,000, and 10,000 ppm metal to 18  $\mu\text{M}$  (1 ppm) Mn diluted in NaCl-containing buffer with benzoquinone. Listed are the tolerance ratios, the concentration ratio of the metal to Mn that were significantly changed; both Mn analysis methods, Mn  $I_p$  and relative  $I_p$ , are reported. The method of comparing

relative  $I_p$  is generally more robust. This is most likely because the interfering metals affect the Mn and benzoquinone similarly. The two metals that have less interference with Mn  $I_p$  than relative  $I_p$  are Cu(II) and Mg(II). Presence of Mg(II) increased the relative  $I_p$  but decreased the Mn  $I_p$ . Cr(VI), Fe(III), and Mg(II) increased the relative  $I_p$  below a 100:1 ratio and gave reduction peaks that interfered with the benzoquinone peak caused interference at ratios greater than 100. Zn(II) and Ni(II) were only seen to have interferences at ratios greater than 1,000 when analyzing the relative  $I_p$  but significantly interfered with the Mn  $I_p$  at ratios greater than 10. Zn is known to form a stable complex with copper and could be added to remove the copper interference [81]. The mechanism of interference is unclear at this time, and future work will need to address eliminating the interference from these metals.

**Table 2.1:** Tolerance ratios of various metals for measuring Mn with Mn  $I_p$  alone and relative to benzoquinone peak. <sup>[a]</sup> The interfering metal peak was overlapping with the benzoquinone peak at higher concentrations. <sup>[b]</sup> The  $I_p$ /relative  $I_p$  value increased.

Metal	Relative Peak Tolerance Ratio	Mn Peak Tolerance Ratio
Al (III)	<1	<1
Cu (II)	<1	>1
Fe (II)	<1	<1
Pb (II)	<1	<1
Cr (VI)	>100 <sup>[a][b]</sup>	>10 <sup>[b]</sup>
Fe (III)	>100 <sup>[a][b]</sup>	>100 <sup>[b]</sup>
Mg (II)	>100 <sup>[a][b]</sup>	>1,000
Ni (II)	>1,000	>10
Zn (II)	>1,000	>10

Mn is commonly found in tea and yerba mate.<sup>8,59-63</sup> The detected Mn levels for yerba mate and green tea samples for analysis of Mn  $I_p$  and relative  $I_p$  are reported (Table 2.2, Figure 2.4)

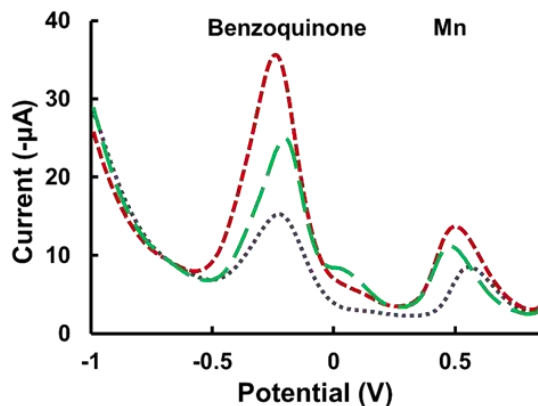


**Figure 3.2:** Representative tea voltammograms. Bagged mate (red, short dash) and green tea (purple, dotted) have 6.5 mM benzoquinone. Loose leaf mate (green, long dash) has 8.8 mM benzoquinone standard.

using the standard calibration method. With Mn  $I_p$  analysis, one sample was accurately predicted. Using relative  $I_p$ , two of the three tea samples tested included the FAAS value within the 95% confidence interval. This method detected higher concentrations of Mn than FAAS reported. Based on the tolerance study, Cr(VI), Fe(III), and Mg(II) are all likely to increase the relative  $I_p$ , but it could be from the presence of Mg(II) due to the lowered detected concentrations with the Mn  $I_p$  analysis. Mg(II) is also known to occur in yerba mate samples based on previous studies and nutrition labels.<sup>9-11</sup>

**Table 2.2:** Mn in tea samples measured from relative  $I_p$  and Mn  $I_p$ . ( $\alpha = 0.05$ ;  $n = 3$ ).

Sample	Mn by Relative $I_p$ (ppm)	Mn by Mn Peak (ppm)	Mn (FAAS) (ppm)
Loose Leaf Yerba Mate	13 ± 4.5	11.2 ± 1.9	11.80
Bag Yerba Mate	9.9 ± 4.0	8.0 ± 0.42	5.65
Green Tea	3.1 ± 1.2	0.97 ± 0.57	2.45

## Conclusion

A carbon electrode system, made from commercially available carbon ink/graphite stenciled onto transparency film, was fabricated to determine Mn(II) content with CSV. It has the advantages of being simple, economical, and suitable for field measurements with a detection limit as low as 500 nM (30 ppb) Mn. Measured manganese concentrations using this technique agreed with a traditional atomic absorbance spectroscopy method for two tea and yerba mate samples. Because this method is susceptible to interferences from Al(III), Cu(II), Fe(II), and Pb(II), future work will need to address and eliminate the interferences from these commonly found metals, in order to apply this to a broader range of aqueous samples.

## REFERENCES

1. K. E. Berg, J. A. Adkins, S. E. Boyle and C. S. Henry, *Electroanalysis*, 2016, **28**, 679-684.
2. M. G. Baker, S. R. Criswell, B. A. Racette, C. D. Simpson, L. Sheppard, H. Checkoway and N. S. Seixas, *Scandinavian Journal of Work Environment & Health*, 2015, **41**, 94-101.
3. S. Bleich, D. Degner, R. Sprung, A. Riegel, W. Poser and E. Rütter, 2014.
4. M. A. Khan, N. Castro-Guerrero and D. G. Mendoza-Cozatl, *Frontiers in Plant Science*, 2014, **5**.
5. R. Witholt, R. H. Gwiazda and D. R. Smith, *Neurotoxicology and Teratology*, 2000, **22**, 851-861.
6. E. Kendüzler, A. R. Türker and Ö. Yalçinkaya, *Talanta*, 2006, **69**, 835-840.
7. E. A. Malecki, *Brain Research Bulletin*, 2001, **55**, 225-228.
8. S. Wen and X. Zhu, *Food Analytical Methods*, 2014, **7**, 291-297.
9. V. L. Cordoba Braganca, P. Melnikov and L. Z. Zanoni, *Biol. Trace Elem. Res.*, 2011, **144**, 1197-1204.
10. R. V. Garcia, I. Basualdo, I. Peralta, M. deHerebia and S. Caballero, *Archivos Latinoamericanos De Nutricion*, 1997, **47**, 77-80.
11. K. Wrobel, K. Wrobel and E. M. C. Urbina, *Biol. Trace Elem. Res.*, 2000, **78**, 271-280.
12. S. H. Babu, K. S. Kumar, K. Suvadhan, K. Kiran, D. Rekha, L. Krishnaiah, K. Janardhanam and P. Chiranjeevi, *Environ. Monit. Assess.*, 2007, **128**, 241-249.
13. M. N. Gandhi and S. M. Khopkar, *Anal. Sci.*, 1992, **8**, 233-236.
14. I. L. Garcia, F. O. Sobejano and M. H. Cordoba, *Analyst*, 1991, **116**, 517-520.
15. J. Y. Jin, F. Xu and T. Miwa, *Electroanalysis*, 2000, **12**, 610-615.
16. W. Kang, X. Pei, A. Bange, E. N. Haynes, W. R. Heineman and I. Papautsky, *Anal. Chem.*, 2014, **86**, 12070-12077.
17. J. Adkins, K. Boehle and C. Henry, *Electrophoresis*, 2015.
18. D. M. Cate, J. A. Adkins, J. Mettakoonpitak and C. S. Henry, *Anal. Chem.*, 2015, **87**, 19-41.
19. D. M. Cate, W. Dungchai, J. C. Cunningham, J. Volckens and C. S. Henry, *Lab Chip*, 2013, **13**, 2397-2404.
20. W.-J. Lan, E. J. Maxwell, C. Parolo, D. K. Bwambok, A. B. Subramaniam and G. M. Whitesides, *Lab Chip*, 2013, **13**, 4103-4108.
21. Z. Nie, C. A. Nijhuis, J. Gong, X. Chen, A. Kumachev, A. W. Martinez, M. Narovlyansky and G. M. Whitesides, *Lab Chip*, 2010, **10**, 477-483.
22. N. Ruecha, N. Rodthongkum, D. M. Cate, J. Volckens, O. Chailapakul and C. S. Henry, *Anal. Chim. Acta*.
23. B. E. Wilson, W. H. Smyrl and A. Stein, *J. Electrochem. Soc.*, 2014, **161**, A700-A703.
24. P. Rattanarat, W. Dungchai, D. Cate, J. Volckens, O. Chailapakul and C. S. Henry, *Anal. Chem.*, 2014, **86**, 3555-3562.
25. C. E. Banks, J. Kruusma, R. R. Moore, P. Tomcik, J. Peters, J. Davis, S. Komorsky-Lovric and R. G. Compton, *Talanta*, 2005, **65**, 423-429.
26. C. M. A. Brett and M. Neto, *J. Electroanal. Chem.*, 1989, **258**, 345-355.
27. H. S. El-Desoky, I. M. Ismail and M. M. Ghoneim, *J. Solid State Electrochem.*, 2013, **17**, 3153-3167.

28. N. A. El-Maali and D. A. El-Hady, *Anal. Chim. Acta*, 1998, **370**, 239-249.
29. O. A. Farghaly, *Talanta*, 2004, **63**, 497-501.
30. O. M. S. Filipe and C. M. A. Brett, *Talanta*, 2003, **61**, 643-650.
31. M. M. Ghoneim, A. M. Hassanein, E. Hammam and A. M. Beltagi, *Fresenius J. Anal. Chem.*, 2000, **367**, 378-383.
32. E. A. Hutton, S. B. Hocevar, B. Ogorevc and M. R. Smyth, *Electrochem. Commun.*, 2003, **5**, 765-769.
33. E. A. Hutton, B. Ogorevc, S. B. Hocevar and M. R. Smyth, *Anal. Chim. Acta*, 2006, **557**, 57-63.
34. T. Ishiyama and T. Tanaka, *Tetsu to Hagane-Journal of the Iron and Steel Institute of Japan*, 1996, **82**, 923-928.
35. S. Legeai, S. Bois and O. Vittori, *J. Electroanal. Chem.*, 2006, **591**, 93-98.
36. F. F. Lima, T. F. Tormin, E. M. Richter and R. A. A. Munoz, *Microchem. J.*, 2014, **116**, 178-182.
37. C. Locatelli and G. Torsi, *J. Electroanal. Chem.*, 2001, **509**, 80-89.
38. M. Nimmo and G. Fones, *Anal. Chim. Acta*, 1994, **291**, 321-328.
39. R. J. O'Halloran, *Anal. Chim. Acta*, 1982, **140**, 51-58.
40. J. Opydo, in *Proceedings of Ecopole 2009, Vol 3 No 2*, eds. M. Waclawek, M. Kraitr, J. Skrzypski and W. Waclawek, 2009, vol. 3, pp. 355-358.
41. J. S. Roitz and K. W. Bruland, *Anal. Chim. Acta*, 1997, **344**, 175-180.
42. N. Y. Stozhko, N. A. Malakhova, M. V. Fyodorov and K. Z. Brainina, *J. Solid State Electrochem.*, 2008, **12**, 1219-1230.
43. T. Tanaka, T. Muramatsu, N. Takada and A. Mizuike, *Bunseki Kagaku*, 1993, **42**, 587-591.
44. G. Tölg, *Angew. Chem.*, 1986, **98**, 764-764.
45. G. Vandijck and F. Verbeek, *Anal. Chim. Acta*, 1971, **54**, 475-&.
46. J. Wang, *Electroanalysis*, 2005, **17**, 1341-1346.
47. J. Wang and J. M. Lu, *Electrochem. Commun.*, 2000, **2**, 390-393.
48. W. Yue, A. Bange, B. L. Riehl, B. D. Riehl, J. M. Johnson, I. Papautsky and W. R. Heineman, *Electroanalysis*, 2012, **24**, 1909-1914.
49. J. W. Di and F. Zhang, *Talanta*, 2003, **60**, 31-36.
50. A. J. Saterlay, J. S. Foord and R. G. Compton, *Analyst*, 1999, **124**, 1791-1796.
51. G. B. Slepchenko, T. M. Gindullina, V. I. Deryabina, Y. N. Smirnova and E. A. Nesterov, *Xv International Scientific Conference Chemistry and Chemical Engineering in Xxi Century Dedicated to Professor L.P. Kulyov*, 2014, **10**, 383-390.
52. T. Ikeda, I. Katasho, M. Kamei and M. Senda, *Agricultural and biological chemistry*, 1984, **48**, 1969-1976.
53. R. T. Kachoosangi, G. G. Wildgoose and R. G. Compton, *Anal. Chim. Acta*, 2008, **618**, 54-60.
54. H. R. Zare, N. Nasirizadeh and M. Mazloun Ardakani, *J. Electroanal. Chem.*, 2005, **577**, 25-33.
55. M. B. McBride, *Soil Science Society of America Journal*, 1987, **51**, 1466-1472.
56. V. V. Kuznetsov, S. Y. Kladiti, E. A. Filatova and A. V. Kolesnikov, *Mendeleev Commun.*, 2014, **24**, 365-367.
57. A. V. Wegorzewski and T. Kuhn, *Marine Geology*, 2014, **357**, 123-138.
58. J. Wu, S. Roshan and G. Chen, *Mar. Chem.*, 2014, **166**, 9-24.
59. A. Ashenef, *Food Additives & Contaminants Part B-Surveillance*, 2014, **7**, 30-36.

60. A. A. Gouda, *Spectrochimica Acta Part a-Molecular and Biomolecular Spectroscopy*, 2014, **131**, 138-144.
61. P. Pohl, E. Stelmach and A. Szymczycha-Madeja, *Food Chem.*, 2014, **163**, 31-36.
62. G. Ucar, D. Bakircioglu and Y. B. Kurtulus, *J. Anal. Chem.*, 2014, **69**, 420-425.
63. Q. Xu, Y. Wang, G. Jin, D. Jin, K. Li, A. Mao and X. Hu, *Sensors and Actuators B-Chemical*, 2014, **201**, 274-280.

## CHAPTER 3. ELECTROCHEMICAL DITHIOTHREITOL ASSAY FOR LARGE-SCALE PARTICULATE MATTER STUDIES

### Chapter Overview

Particulate matter (PM) air pollution is associated with human morbidity and mortality. Measuring PM oxidative potential has been shown to provide a predictive measurement between PM exposure and adverse health impacts. The dithiothreitol (DTT) assay is commonly used to measure the oxidative potential of PM<sub>2.5</sub> (PM less than 2.5  $\mu\text{m}$  aerodynamic diameter). In the common, kinetic form of this assay, the decay of DTT is quantified over time (indirectly) using 5,5'-dithiobis(2-nitrobenzoic acid) (DTNB, Ellman's reagent) via UV/vis absorbance spectroscopy. The loss of DTT can also be quantified directly using electrochemical detection. The objectives of this work were (1) to evaluate the electrochemical assay, using commercially available equipment, relative to the UV/vis absorbance assay, and (2) to apply the electrochemical method to a large (>100) number of PM<sub>2.5</sub> aerosol filter samples. Also presented here is the comparison an end-point assay to the kinetic assay, in an attempt to reduce the time, labor, and materials necessary to quantify PM oxidative potential. The end-point, electrochemical assay gave comparable results to the UV/vis absorbance assay for PM filter sample analysis. Finally, high filter mass loadings (higher than about 0.5  $\mu\text{g}$  PM per  $\text{mm}^2$  filter) lead to sub-optimal DTT assay performance, which suggests future studies should limit particle mass loadings on filters. This work was published in *Aerosol Science and Technology*.<sup>1</sup> Laurelle R. Turner's contribution to the work was planning and performing the PM<sub>2.5</sub> oxidative potential measurements with electrochemical DTT detection; Megan Benka-Coker, Sarah Rajkumar, and Bonnie Young contributed to the published work by collecting and weighing the filters. Kevin Klunder measured the PM<sub>2.5</sub> oxidative potential with UV/vis absorbance detection.

## Introduction

Human exposure to particulate matter (PM) air pollution has been linked to adverse health effects and millions of premature deaths worldwide each year.<sup>2-4</sup> The toxicological mechanism(s) of PM are still being elucidated, but one common hypothesis is that PM generates reactive oxygen species (ROS) leading to increased oxidative stress and inflammation in the body.<sup>5-7</sup> PM oxidative potential, the PM's ability to oxidize target molecules, is arguably a more biologically relevant measurement of PM toxicity as opposed to PM mass alone.<sup>8-11</sup> PM oxidative potential is hypothesized to be more relevant to human health because PM composition is not uniform, and each PM component has different reactivities with biological systems.<sup>10,12</sup>

The oxidative potential of a PM sample can be measured through antioxidant loss monitoring.<sup>8,10</sup> Crobeddu *et al.*<sup>13</sup> argue that ascorbic acid and glutathione depletion assays show the best correlation to intracellular ROS. Other studies, however, have shown a lack of association between ascorbate and health outcomes, likely due to ascorbate's high reactivity in the presence of Cu(II).<sup>14,15</sup> Glutathione depletion is also sensitive to Cu and Fe.<sup>16</sup> Another drawback of antioxidant depletion assays is the time required for sample incubation, which decreases the sample throughput. The glutathione depletion assay takes approximately four hours,<sup>17</sup> and the ascorbic acid assay takes one to two hours<sup>10,14,18</sup> but is often run simultaneously with glutathione for four hours.<sup>17,19</sup> A more thorough comparison of PM oxidative potential measurements can be found elsewhere.<sup>20</sup>

Dithiothreitol (DTT), a reducing agent known to react with a large number of chemicals relative to other antioxidants, is frequently used for *in vitro* quantification of PM oxidative potential.<sup>8,12,21-23</sup> In the DTT assay, PM oxidizes DTT to the disulfide, and the remaining DTT is quantified over time. DTT reactivity with PM has been correlated with relevant biomarkers of

inflammation and oxidative stress in human studies<sup>24</sup> and *in vivo* assays.<sup>13,25</sup> DTT concentration is commonly quantified with 5,5'-dithiobis(2-nitrobenzoic acid) (DTNB, Ellman's reagent), which reacts with DTT to form 2-nitro-5-thiobenzoic acid (TNB), a chromophore that can be quantified with 412 nm light. DTT concentration can also be directly measured via electrochemistry.<sup>26</sup> The electrochemical detection method yields comparable results as UV/vis detection but eliminates additional reagents and reduces PM sample mass requirements.<sup>27,28</sup> While there are advantages to the electrochemical detection of DTT, the assay described by Sameenoi *et al.* is limited to those who have electrode and microfluidic device fabrication equipment, which involves a large, upfront investment of equipment and labor.

Here, a modified version of the electrochemical DTT assay developed by Sameenoi *et al.* is presented using commercially available equipment. This new DTT assay uses a commercially available wall-jet flow cell with replaceable electrodes. While an end-point assay format can be used with UV/vis or electrochemical detection, it has not been applied to either DTT detection method to our knowledge. Kinetic and end-point assay formats were compared and gave comparable results. The single (post-initial) time point further simplifies the assay by reducing labor and consumable goods. The DTT reactivity of water-soluble extracts from PM<sub>2.5</sub> filter samples collected during field studies in Honduras, separated into personal and area/indoor exposure, was also tested against the UV/vis assay developed by Charrier and coworkers,<sup>21</sup> modified from the original published UV/vis assay developed by Cho and coworkers.<sup>8</sup> The Charrier *et al.* assay modifications are the addition of 50:50 trifluoroethanol (TFE):water, before DTT addition, to the PM solution and the Chelex treatment of phosphate buffer to remove transition metals (where Cho *et al.* used EDTA). Unlike EDTA, the Chelex is filtered out prior to the DTT assay and will not interfere with the assay results. Here, unlike many previous assays,

including those developed by Cho *et al.* and Charrier *et al.*, we do not use a chemical quenching agent, further reducing consumables. This study evaluates the combined effectiveness (accuracy, ease of use, reduced cost, and reduced assay time) of the electrochemical and end-point DTT assay on a large-scale study of aerosol filter samples, applicable to users without access to custom electrochemical methods.

## **Experimental**

### *Materials*

Electrochemical experiments were performed using a CHI 812 potentiostat (CHI Instruments, Austin, TX). Purified (18.2 M $\Omega$ ·cm) water was used for all experiments (MilliPore Milli-Q system, Billerica, MA, USA). Dithiothreitol (DTT), 2,2,2-trifluoroethanol (TFE), and Chelex® 100 mesh were purchased from Sigma-Aldrich (St. Louis, MO, USA). Sodium phosphate monobasic and sodium phosphate dibasic were purchased from Fisher Scientific (Pittsburg, PA, USA). 5,5'-dithiobis(2-nitrobenzoic acid) (DTNB, Ellman's reagent) was purchased from Pierce Chemical (Dallas, TX, USA).

### *DTT Assay*

Filter samples were handled with plastic forceps and ceramic scissors to minimize possible metal contamination.<sup>12</sup> Prior results from Charrier *et al.* have suggested that targeting 10  $\mu\text{g}/\text{mL}$  PM in the DTT assay gives the most consistent results.<sup>21</sup> Unless otherwise stated, the massed filter samples were cut to achieve the target concentration of 10  $\mu\text{g}/\text{mL}$  PM using between 0.5 and 1 mL total volume of fresh 75  $\mu\text{M}$  DTT in 0.1 M Chelex-treated sodium phosphate buffer (pH 7.4). The filters were initially wetted with 15  $\mu\text{L}$  of 50:50 TFE:water (v:v) in a 1.5 mL centrifuge tube (Eppendorf, Hamburg, Germany). Samples were incubated in the DTT solution at 37 °C in a water bath for 30 min. The reaction was then effectively halted in a  $5 \pm 3$  °C water bath for five min.<sup>27</sup>

Sample aliquots were intermittently injected into the wall-jet flow cell (FLWCL, DropSens, Spain) at 85  $\mu\text{L}/\text{min}$ . The working electrode (DropSens 410 SPE, DropSens, Spain) was held at +0.3 V vs. Ag/AgCl. A calibration curve was generated for each electrode used prior to running the assay. The relative value of initial peak currents were measured and adjusted to the lab blank filter reactivity rate, divided by the summation of the incubation and cooling time (35 min). For the UV/vis assay, 400  $\mu\text{L}$  of 75  $\mu\text{M}$  DTNB was added to discrete 100  $\mu\text{L}$  DTT aliquots over a 45-min period (approximately 0, 15, 30, and 45 min) and analyzed immediately at 412 nm (Agilent 8453, Santa Clara, CA, USA) with a molar absorptivity of  $14\,150\ \text{M}^{-1}\ \text{cm}^{-2}$  used for concentration calculations.

### *Filter Sampling*

Air sampling filters (n=105 personal and n=106 area samples) were collected from March 3 through April 30, 2015 as part of a Honduras cookstove study as previously reported.<sup>29</sup> One blank filter was collected every two weeks.  $\text{PM}_{2.5}$  was sampled onto 37-mm PTFE-coated glass fiber filters (Fiberfilm<sup>TM</sup> T60A20, Pall Corporation, KY, USA) using Triplex Cyclones (BGI, Mesa Labs, Butler NJ, USA) and AirChek XR5000 pumps (SKC Inc., Eighty Four, PA, USA) operating at 1.5 L/min for 24 hrs. The filters were equilibrated for at least 24 hrs and then pre-weighed to the nearest microgram at Colorado State University (CSU) using a microbalance (Mettler-Toledo microbalance model MX5, Columbus, OH, USA). After collection of the  $\text{PM}_{2.5}$  sample, filters were stored at -22 °C and then transported to CSU, equilibrated, and post-weighed. The filters were then stored in a -80 °C freezer until tested. The whole filter particle mass is the difference in masses before and after collection, accounting for the mean change in field blanks. Personal filters were collected near the participant's breathing zone; area filters were collected 76-127 cm from the stovetop in the participants' kitchens. Each household had one personal and one

area exposure filter; therefore the two data sets from personal and area exposure are not independent from each other.

## Results and Discussion

### Assay Validation

The electrochemical DTT assay has been reported as an accurate, precise, and simple assay that also uses less consumable materials than the UV/vis absorbance assay by eliminating DTNB addition and lowering the DTT solution volumes.<sup>27,28</sup> The first assay steps (extracting the filter, adding DTT, and removing aliquots) are comparable between the absorbance and electrochemical assays (Figure 3.1). The hydrophobic filter is initially wetted with a TFE/water solution and then

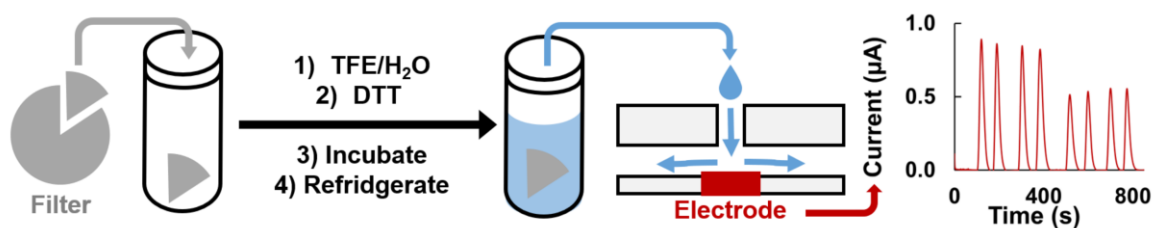


**Figure 3.1:** Schematic of the filter extraction and electrochemical assay. A filter piece is cut and massed, extracted into TFE/water, then DTT in phosphate buffer is added for a known PM concentration. The solution is incubated at 37 °C and then thermally quenched in 5 °C fridge. Aliquots are removed and analyzed with flow injection chronoamperometry. Example data shown where the peak current is decreasing over time, with replicates.

extracted into a phosphate buffer solution of DTT.<sup>30</sup> The timing of the removal of aliquots is discussed below. However, with the electrochemical system, flow injection analysis is used and the aliquot is directly injected into the detector system in a similar manner as described by Sameenoi *et al.* (2012). The direct DTT injection replaces indirect detection with the DTNB chromophore, eliminating the need for extra reagents, decreasing assay costs, and removing the added labor and uncertainty associated with indirect detection. For the electrochemical system presented here, only commercially available equipment, a DropSens poly(methyl methacrylate)

(PMMA) wall-jet flow cell with DropSens screen-printed carbon electrodes with a built-in reference electrode, was used to validate the electrochemical assay. While we opted to use DropSens components, there are numerous commercially available potentiostats, electrodes, and flow cells that could achieve the same results. Our system has a limit of detection (LOD), calculated as three times the standard deviation of the blank, of 8.45  $\mu\text{M}$  DTT. The current signal was  $0.0137 \pm 0.0006 \mu\text{A}/\mu\text{M}$  DTT (n=24). Additionally, one person can analyze five samples per hour using the electrochemical flow cell system, which is a higher rate than the approximate one sample per hour with either the two-person manual or semi-automated absorbance assays reported previously.<sup>23</sup>

Besides the electrochemical assay presented here eliminating the time, labor, and consumables associated with preparing, adding, and mixing a quenching and developing reagent, we have combined it here with an end-point assay to further reduce the time and labor. End-point assays are commonly used to simplify kinetic analyses.<sup>31-34</sup> The original assay continually removes aliquots from the DTT chemical reaction, which leads to additional labor, time, and materials<sup>8</sup>. In the example of the semi-automated system developed by Fang *et al.*,<sup>23</sup> there would still be a benefit from eliminating the reagents and measuring fewer time points because the reagent solutions would not have to be purchased or prepared, and assay time would be reduced from about 60 to 30 minutes per sample, potentially leading to higher sample throughput at a lower cost. To help reduce time and labor requirements that limit large-scale aerosol studies, we evaluated the ability to reduce the number of time points needed for the DTT reaction rate calculation. We compared removing multiple aliquots over time to using one, post-initial, time point, also referred to as an end-point assay. The end-point assay principle can be applied to both the electrochemical and UV/vis assays due to the linear reactivity of DTT used in the DTT assay. With the linear reactivity

of DTT and having a proper calibration curve for accurate and precise measurements,<sup>35</sup> the DTT rate can be accurately calculated from two time points. Replicates at each time point are still needed to decrease the uncertainty. The DTT reactivity of the same filter was used at two different PM concentrations, 5 and 10  $\mu\text{g}/\text{mL}$ , with the multiple aliquot (kinetic) and the end-point assays. As seen in Figure 3.2, measured DTT consumption rates between the end-point and kinetic assays

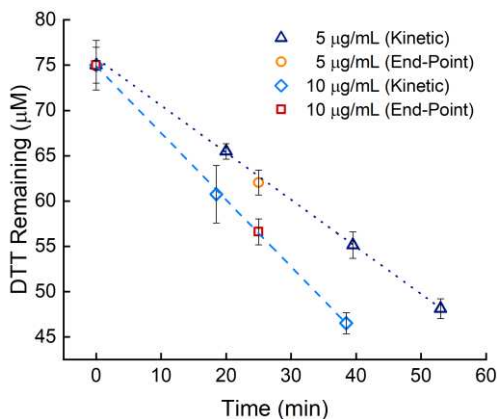


**Figure 3.2:** Comparison of DTT loss with the end-point and kinetic assays for 2 different PM concentrations: 5  $\mu\text{g}/\text{mL}$  (orange circles and navy triangles, respectively,  $509 \pm 9 \text{ nM min}^{-1}$  loss rate) and 10  $\mu\text{g}/\text{mL}$  (red squares and blue diamonds, respectively,  $740 \pm 20 \text{ nM min}^{-1}$  loss rate). Error bars represent the standard deviation of three replicates.

fall along the same line (for a given PM concentration). The DTT reactivity of both PM filter pieces at 5  $\mu\text{g}/\text{mL}$  was  $509 \pm 9$  ( $n=12$  for each assay type)  $\text{nM DTT min}^{-1}$ , and both 10  $\mu\text{g}/\text{mL}$  PM DTT reactivities were  $740 \pm 20$  ( $n=9$  for each assay type)  $\text{nM DTT min}^{-1}$ . The end-point assay was therefore used during the rest of this study.

#### *Evaluation of Mass-Normalized Bias*

Potential DTT reactivity bias in a mass-normalized PM system has recently been reported.<sup>21</sup> Charrier *et al.* show that DTT reactivity is not always linear with extracted PM concentration, most likely due to high Cu concentration in the samples, as Cu(II) has a non-linear reactivity with DTT, yielding higher DTT reactivity at lower PM concentrations when it is PM-mass normalized. Charrier *et al.* state the need for 10  $\mu\text{g}/\text{mL}$  extracted PM concentration to be

compared between studies to reduce the mass-reactivity bias. The linearity of several samples was tested for bias with the mass-normalized response (Figure 3.3). Three of the four filter samples

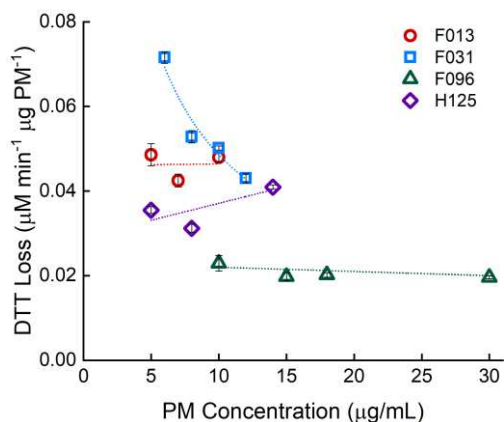


**Figure 3.3:** Determining bias in mass-normalized response with four random filter samples (F013, F031, F096, H125) at various PM concentrations. Filters F013, F096, and H125 have no significant slope at a 95% confidence level. Filter F031 has a power fit of  $y = 0.2403x^{-0.694}$  with  $R^2$  of 0.95. Error bars represent standard deviation of three replicates.

show no mass-normalized (i.e., the 95% confidence interval about the slope contains zero). One filter, F031, had a significant negative slope with a linear fit ( $-0.004 \pm 0.001$ ,  $R^2=0.88$ ) but has an improved coefficient of determination with a non-linear fit. A power function fit yields a coefficient of determination of 0.95. This is likely due to a higher Cu concentration in the filter sample, yielding a non-linear mass-normalized response, as seen previously.<sup>21</sup> To help alleviate the potential bias in the large-scale study, a PM concentration of 10 µg/mL was used for evaluation of real filter samples, as suggested by Charrier *et al.*

#### *Evaluation of Honduras Cookstove Study PM<sub>2.5</sub> Filter Samples*

The electrochemical and absorbance assays have previously been shown to give similar results.<sup>27</sup> Here, the modified electrochemical DTT assay was also compared against the UV/vis assay with real aerosol filter samples using Deming regression analysis,<sup>36</sup> which incorporates the error of both methods into the fit. The same filters were used for comparison, and the extraction technique was the same for both assays. The Deming regression best fit results in a line with a

slope of 1.05 and an intercept of 0.119 (Figure 3.4), and the correlation coefficient of 0.79. The

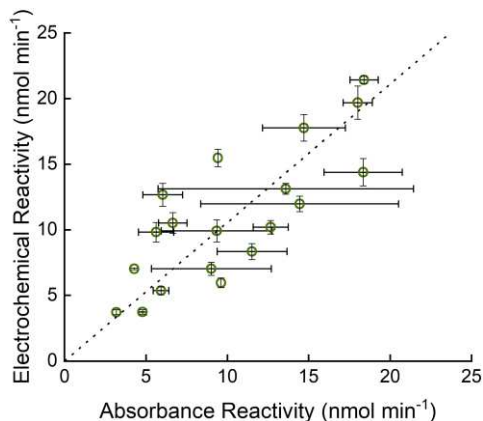


**Figure 3.4:** Comparison of filter DTT reactivity of the absorbance assay with electrochemical assay using Deming regression (dashed line is the best fit from the regression analysis,  $y=1.05x+0.119$ ) of 19 filter samples.  $R^2=0.63$ . Error bars represent standard deviation of three replicates of three different filter pieces.

standard deviation values of the two assays should not be directly compared as the electrochemical assay utilized lab blanks (filters that were not exposed to the field), and the absorbance assay utilized field blanks, as either can be used with the DTT assay.

After comparing the modified electrochemical DTT assay to the UV/Vis assay, the practicality of using the electrochemical assay with a large sample size was addressed. In this study, we tested 211 filters collected in Honduras as part of an epidemiology cookstove project.<sup>29</sup> The filter samples were separated into area and personal exposures. The average area exposure DTT reactivity rate ( $\text{nmol DTT min}^{-1} \text{ m}^{-3}$ ) was 9.38 with a reactivity range between 0.460 and 31.8. Personal exposures showed an average DTT reactivity rate ( $\text{nmol DTT min}^{-1} \text{ m}^{-3}$ ) of 5.90 with a reactivity range between 1.03 and 18.4.

Even though the same PM concentration was used, there was a limitation found within this filter sample set. It has been assumed that the DTT reactivity is unaffected by the collected filter's whole filter particle mass (WFPM, the filter's change in mass during collection), and to our knowledge, this assumption has not been tested. With the assumption that the total collected PM

mass does not affect the DTT assay results, as long as the extracted PM concentration is consistent, a linear relationship would be expected between the WFPM-normalized reactivity (DTT reactivity multiplied by WFPM) relative to the WFPM of the filters, with the resulting slope being equivalent to the average DTT reactivity of the samples. However, a strong linear relationship is not seen with the filters tested here (Figure 3.5) as the coefficients of variation,  $R^2$ , are 0.33 and 0.27 for the area and personal sample sets, respectively. With the area exposure filter samples (Figure 3.5), a deviation from linearity is clearly seen above about 0.5 mg WFPM. The non-linearity above 0.5 mg could be explained by the large mass loadings on the filter hindering mass transport of the PM into the bulk solution and/or inaccessibility of the DTT to PM buried on the filter, causing lower reactivity per PM mass than expected. This limit to mass loadings could also simply be a limitation of the extraction method used here. The same deviation from linearity is not clearly seen with the personal exposure filters (Figure 3.5) as the PM mass loadings do not exceed 0.8 mg and less than

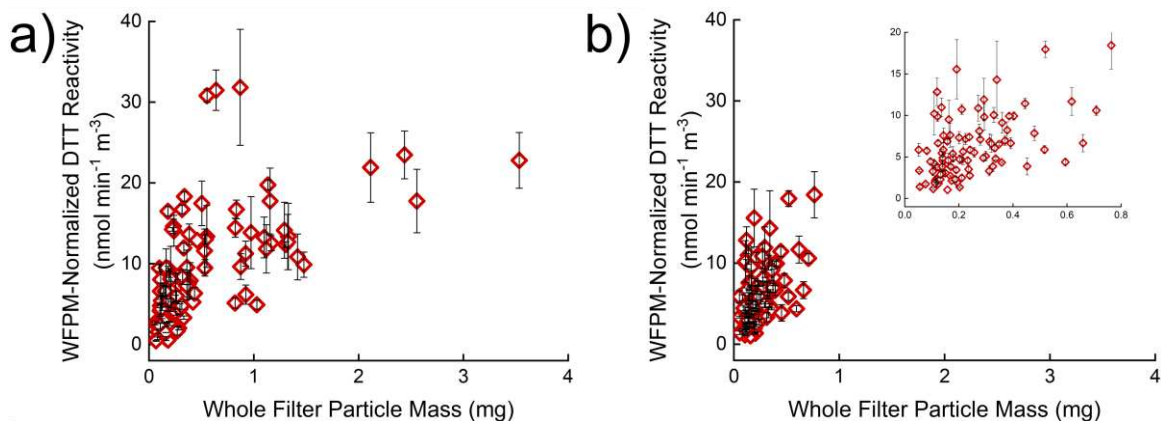


**Figure 3.5:** Comparison of normalized reactivity vs. whole filter particle mass in a) 106 area and b) 105 personal filter samples. Normalized reactivity is the DTT reactivity rate ( $\text{nmol DTT min}^{-1} \text{mg}^{-1} \text{PM m}^{-3} \text{air}$ ) multiplied by the whole filter particle mass ( $\text{mg PM}$ ). The units have been simplified in regards to grams of PM. Error bars represent three replicates of three filter sections.

10% of the filter mass loadings are greater than 0.5 mg. The filter type and the PM source, as the samples tested here were driven by wood burning, might also have an influence on the value where the deviation from linearity is seen. Future work is required to confirm if the deviation from

linearity at high WFPM is from the mass transport or the extraction method used here. If it is a mass transport problem, future PM studies should be cognizant of the mass loadings onto the filter and the bias it introduces into the DTT assay. If the extraction method presented here is used, then mass loadings should remain smaller than about 0.5 mg per 37 mm filter, equivalent to 0.5  $\mu\text{g}$  PM per  $\text{mm}^2$  of filter, but future work will solidify this cautionary statement. If another extraction method is used, then the linearity of WFPM-normalized reactivity should still be tested in the range of filter mass loadings to confirm no bias with high WFPM.

## **Conclusion**

In this work, an electrochemical system was developed to directly measure DTT using commercially available electrodes in a wall-jet flow cell. The system was validated through comparison to the UV/vis assay, and this work is the first time that the electrochemical DTT assay has been applied to a large sample size (211 samples). The time and labor was reduced by using an end-point assay instead of the kinetic assay. The presented end-point assay can also be used in the future during a UV/vis detection DTT assay. The assay showed deviation from expected linearity between filter  $\text{PM}_{2.5}$  mass and the WFPM-normalized DTT reactivity with high mass loadings likely due to a slow mass transport or the inability of DTT to react with PM components. Future studies will need to address the observed lower reactivity at high mass loadings by limiting mass loadings onto filters. Future work will need to test if the linear deviation is from the PM source, filter type, extraction method, or another factor. The end-point electrochemical assay presented here increases the sample throughput to five samples per hour, but future work should seek to improve sample throughput further. The sample throughput also involves constant manual labor, so an automated system would also be beneficial to address for future large-scale studies to reduce the prohibitive cost of labor.

## REFERENCES

1. K. E. Berg, L. R. Turner, M. L. Benka-Coker, S. Rajkumar, B. N. Young, J. L. Peel, M. L. Clark, J. Volckens and C. S. Henry, *Aerosol Sci. Technol.*, 2019, 1-8.
2. A. J. Cohen, M. Brauer, R. Burnett, H. R. Anderson, J. Frostad, K. Estep, K. Balakrishnan, B. Brunekreef, L. Dandona, R. Dandona, V. Feigin, G. Freedman, B. Hubbell, A. Jobling, H. Kan, L. Knibbs, Y. Liu, R. Martin, L. Morawska, C. A. Pope, III, H. Shin, K. Straif, G. Shaddick, M. Thomas, R. van Dingenen, A. van Donkelaar, T. Vos, C. J. L. Murray and M. H. Forouzanfar, *The Lancet*, 2017, **389**, 1907-1918.
3. O. M. Morakinyo, M. I. Mokgobu, M. S. Mukhola and R. P. Hunter, *International journal of environmental research and public health*, 2016, **13**, 592.
4. M.-A. Kioumourtzoglou, J. D. Schwartz, M. G. Weiskopf, S. J. Melly, Y. Wang, F. Dominici and A. Zanobetti, *Environ. Health Perspect.*, 2016, **124**, 23.
5. A. De Vizcaya-Ruiz, M. Gutiérrez-Castillo, M. Uribe-Ramirez, M. Cebrián, V. Mugica-Alvarez, J. Sepúlveda, I. Rosas, E. Salinas, C. Garcia-Cuéllar and F. Martínez, *Atmos. Environ.*, 2006, **40**, 583-592.
6. A. A. Alfadda and R. M. Sallam, *BioMed Research International*, 2012, **2012**.
7. J. O. Anderson, J. G. Thundiyil and A. Stolbach, *Journal of Medical Toxicology*, 2012, **8**, 166-175.
8. A. K. Cho, C. Sioutas, A. H. Miguel, Y. Kumagai, D. A. Schmitz, M. Singh, A. Eiguren-Fernandez and J. R. Froines, *Environ. Res.*, 2005, **99**, 40-47.
9. R. D. Brook, S. Rajagopalan, C. A. Pope, J. R. Brook, A. Bhatnagar, A. V. Diez-Roux, F. Holguin, Y. Hong, R. V. Luepker, M. A. Mittleman, A. Peters, D. Siscovick, S. C. Smith, L. Whitsel and J. D. Kaufman, *An Update to the Scientific Statement From the American Heart Association*, 2010, **121**, 2331-2378.
10. N. A. H. Janssen, A. Yang, M. Strak, M. Steenhof, B. Hellack, M. E. Gerlofs-Nijland, T. Kuhlbusch, F. Kelly, R. Harrison, B. Brunekreef, G. Hoek and F. Cassee, *Sci. Total Environ.*, 2014, **472**, 572-581.
11. P. J. A. Borm, F. Kelly, N. Künzli, R. P. F. Schins and K. Donaldson, *Occupational and Environmental Medicine*, 2007, **64**, 73-74.
12. J. G. Charrier and C. Anastasio, *Atmospheric chemistry and physics (Print)*, 2012, **12**, 11317-11350.
13. B. Crobeddu, L. Aragao-Santiago, L.-C. Bui, S. Boland and A. Baeza Squiban, *Environ. Pollut.*, 2017, **230**, 125-133.
14. T. Fang, V. Verma, J. Bates, J. Abrams, M. Klein, M. Strickland, S. Sarnat, H. Chang, J. Mulholland and P. Tolbert, *Atmospheric Chemistry & Physics Discussions*, 2015, **15**.
15. E. Vidrio, H. Jung and C. Anastasio, *Atmospheric Environment*, 2008, **42**, 4369-4379.
16. K. J. Godri, R. M. Harrison, T. Evans, T. Baker, C. Dunster, I. S. Mudway and F. J. Kelly, *PloS one*, 2011, **6**, e21961.
17. I. S. Mudway, N. Stenfors, S. T. Duggan, H. Roxborough, H. Zielinski, S. L. Marklund, A. Blomberg, A. J. Frew, T. Sandström and F. J. Kelly, *Arch. Biochem. Biophys.*, 2004, **423**, 200-212.
18. A. Yang, A. Jedynska, B. Hellack, I. Kooter, G. Hoek, B. Brunekreef, T. A. J. Kuhlbusch, F. R. Cassee and N. A. H. Janssen, *Atmos. Environ.*, 2014, **83**, 35-42.

19. J. G. Ayres, P. Borm, F. R. Cassee, V. Castranova, K. Donaldson, A. Ghio, R. M. Harrison, R. Hider, F. Kelly, I. M. Kooter, F. Marano, R. L. Maynard, I. Mudway, A. Nel, C. Sioutas, S. Smith, A. Baeza-Squiban, A. Cho, S. Duggan and J. Froines, *Inhalation Toxicology*, 2008, **20**, 75-99.
20. Y. Wang, M. J. Plewa, U. K. Mukherjee and V. Verma, *Atmos. Environ.*, 2018, **179**, 132-141.
21. J. G. Charrier, A. S. McFall, K. K. T. Vu, J. Baroi, C. Olea, A. Hasson and C. Anastasio, *Atmos. Environ.*, 2016, **144**, 325-334.
22. Q. Xiong, H. Yu, R. Wang, J. Wei and V. Verma, *Environmental science & technology*, 2017, **51**, 6507-6514.
23. T. Fang, V. Verma, H. Guo, L. King, E. Edgerton and R. Weber, *Atmospheric Measurement Techniques*, 2015, **8**, 471.
24. R. J. Delfino, N. Staimer, T. Tjoa, D. L. Gillen, J. J. Schauer and M. M. Shafer, *Journal of Exposure Science and Environmental Epidemiology*, 2013, **23**, 466.
25. N. Li, C. Sioutas, A. Cho, D. Schmitz, C. Misra, J. Sempf, M. Wang, T. Oberley, J. Froines and A. Nel, *Environ. Health Perspect.*, 2003, **111**, 455.
26. Y. Sameenoi, M. M. Mensack, K. Boonsong, R. Ewing, W. Dungchai, O. Chailapakul, D. M. Cropek and C. S. Henry, *Analyt.*, 2011, **136**, 3177-3184.
27. Y. Sameenoi, K. Koehler, J. Shapiro, K. Boonsong, Y. Sun, J. Collett, J. Volckens and C. S. Henry, *J. Am. Chem. Soc.*, 2012, **134**, 10562-10568.
28. K. A. Koehler, J. Shapiro, Y. Sameenoi, C. Henry and J. Volckens, *Aerosol Sci. Technol.*, 2014, **48**, 489-497.
29. S. Rajkumar, M. L. Clark, B. N. Young, M. L. Benka - Coker, A. M. Bachand, R. D. Brook, T. L. Nelson, J. Volckens, S. J. Reynolds and C. L'Orange, *Indoor air*, 2018.
30. E. Vidrio, C. H. Phuah, A. M. Dillner and C. Anastasio, *Environmental Science & Technology*, 2009, **43**, 922-927.
31. A. Karadag, B. Ozcelik and S. Saner, *Food analytical methods*, 2009, **2**, 41-60.
32. C. Boozer, G. Kim, S. Cong, H. Guan and T. Londergan, *Curr. Opin. Biotechnol.*, 2006, **17**, 400-405.
33. W. L. Daniel, M. S. Han, J.-S. Lee and C. A. Mirkin, *J. Am. Chem. Soc.*, 2009, **131**, 6362-6363.
34. K. A. Giuliano, J. R. Haskins and D. L. Taylor, *Assay and drug development technologies*, 2003, **1**, 565-577.
35. S. D. Noblitt, K. E. Berg, D. M. Cate and C. S. Henry, *Anal. Chim. Acta*, 2016, **915**, 64-73.
36. P. J. Cornbleet and N. Gochman, *Clin. Chem.*, 1979, **25**, 432-438.

## CHAPTER 4. HIGH-THROUGHPUT, SEMI-AUTOMATED DITHIOTHREITOL ASSAY WITH UV/VIS OR ELECTROCHEMICAL DETECTION

### Chapter Overview

Fine particulate matter (PM<sub>2.5</sub>) is a leading environmental risk factor for adverse health outcomes, including cardiovascular and respiratory morbidity, and premature mortality. PM<sub>2.5</sub> oxidative potential is a relatively new paradigm for exploring health risks associated with the various chemical compositions of ambient PM<sub>2.5</sub>. PM<sub>2.5</sub> oxidative potential is commonly measured with the dithiothreitol (DTT) assay. DTT is mixed with an aqueous PM<sub>2.5</sub> sample extract, and the DTT loss rate is measured. However, the DTT assay is time consuming and laborious, with only a few reported automation attempts. A semi-automated DTT assay is introduced and evaluated using a traditional HPLC combined with either UV/vis absorbance or electrochemical detection that has comparable accuracy and sensitivity. Commercial and custom-made electrochemical detectors are also compared before measuring ambient PM<sub>2.5</sub> filter samples. The optimized, semi-automated assay can process six samples per hour (an 83% time savings compared to one sample per hour with manual analysis). Cost becomes significant for large-scale studies and was also considered; electrochemical detection produced a 40% consumables cost savings compared to UV/vis detection. This work has been submitted to *Environmental Science and Technology*. Xiaoying Li ran the UV/vis absorbance detection on filters from China. Kaylee Clark worked on the project but the data is not presented here.

### Introduction

Human exposure to fine particulate matter (PM<sub>2.5</sub>, particles with aerodynamic diameter less than 2.5 μm) is a leading contributor to the global burden of disease with a well-established link to several million premature deaths annually, as well as millions of cardiovascular- and

respiratory-related hospitalizations.<sup>1-4</sup> In 2015, PM<sub>2.5</sub> exposure was estimated to contribute to 4.2 million premature deaths (7.6% of total global mortality). A recent study estimated that achieving the World Health Organization's air quality guideline of 10 µg/m<sup>3</sup> (as an annual average outdoor PM<sub>2.5</sub> concentration) would result in life expectancy increases of 0.6 years, the same magnitude as eliminating *both* breast and lung cancer worldwide.<sup>5</sup> Current air quality regulations focus on limiting the mass concentration of PM<sub>2.5</sub> in outdoor air; however, recent research suggests that PM mass concentration is likely an imperfect predictor of risk for health effects because the composition (and potential toxicology) of PM can vary substantially even though mass concentration may remain constant.<sup>6-10</sup> A leading hypothesis for PM<sub>2.5</sub> toxicity is that PM<sub>2.5</sub> generates reactive oxygen species (ROS), which leads to oxidative stress and systemic inflammation.<sup>11-15</sup> Thus, the oxidative potential of PM has been proposed as a complementary measure to PM<sub>2.5</sub> mass concentration.<sup>6,16,17</sup>

A widely used chemical assay to estimate PM oxidative potential is the dithiothreitol (DTT) assay.<sup>18-23</sup> The DTT assay has been shown to correlate with relevant biological markers that correspond to oxidative stress and inflammation.<sup>8,24</sup> To perform the assay, DTT is mixed with the extracted PM<sub>2.5</sub> sample, and the remaining DTT is quantified over time. The magnitude of DTT loss is related to the PM oxidative potential. Despite the widespread use of the DTT assay, there is not a singular protocol practiced across all laboratories. In the original published assay,<sup>7</sup> a known (but variable between 5 and 40 µg/mL) PM sample concentration was incubated with 100 µM DTT in pH 7.4 potassium phosphate buffer at 37 °C. Trichloroacetic acid was added to quench the reaction at various times between 15 and 90 min, and an aliquot was removed and mixed with ethylenediaminetetraacetic acid (EDTA) and 5,5-dithio-bis-(2-nitrobenzoic acid) (Ellman's reagent, DTNB). DTNB reacts with DTT to form 5-mercapto-2-nitrobenzoic acid (TNB), which

is quantified spectroscopically at 412 nm. Since the initial publication, subsequent studies have varied the following parameters: the incubated concentration of PM,<sup>25</sup> the addition of a filter wetting agent,<sup>26</sup> the time points at which DTT concentration is measured,<sup>27,28</sup> the quenching reagent,<sup>29</sup> the use of Chelex instead of EDTA,<sup>30</sup> and an alternative DTT detection method.<sup>29</sup> The modifications, described in greater detail below, were typically made to improve the assay, but the inconsistencies among the DTT assays can cause confusion and lead to inaccurate comparisons between laboratories.

While DTT oxidation potential is reported as PM mass-normalized to account for higher DTT decay rates at higher PM concentrations, Charrier *et al.* found that the mass-normalized DTT response is non-linear with some PM samples due to some individual components' non-linear DTT response, as shown with samples high in copper and manganese.<sup>25</sup> The authors suggested that future studies use a fixed extraction concentration of 10 µg PM/mL for interstudy comparisons. Another contribution Anastasio's group made to the DTT assay was made using 2,2,2-trifluoroethanol (TFE) as a Teflon filter wetting agent to improve PM extraction into the aqueous solution.<sup>26</sup> TFE use now varies between laboratories. Another variable is the time at which the DTT concentration is monitored to calculate the DTT loss rate, and many studies do not report it. Often, the DTT concentration is measured multiple times over 60 minutes.<sup>25,28</sup> A recent study reported on the accuracy of using an end-point assay using two time points (0 and 25 min) and found comparable results between multiple measurements and the end-point assay,<sup>27</sup> and there are also other research groups who measure DTT concentration at 0 and 60 minutes.<sup>8,31,32</sup> While differences in when the DTT concentration is measured has a relatively minor impact on the reported PM oxidative potential, the use of EDTA can significantly impact assay performance and reliability. After reporting that EDTA lowered the DTT response from metals and quinone

components of PM,<sup>30</sup> Charrier *et al.* recommended using Chelex-treated buffers to reduce background effects without reducing the DTT response. However, many studies still use EDTA in the DTT assay.<sup>28,33-36</sup> Trichloroacetic acid is another reagent used in the DTT assay to quench the reaction between DTT and PM<sub>2.5</sub> before DTNB quantitative analysis. An effective alternative to eliminating trichloroacetic acid (thereby also eliminating the cost and labor associated with the reagent addition) for quenching the reaction has been to chill the samples at 4 °C for thermal quenching.<sup>29</sup> The same study also demonstrated the feasibility of direct electrochemical quantification of DTT for PM oxidation potential, which yielded DTT rates comparable to those determined when UV/vis was the detection method. The electrochemical detection method decreases the amount of reagents and PM sample mass needed for the assay.<sup>27</sup>

The DTT assay, as originally published, has the major limitation of being labor and time intensive, having long turnaround time from sample collection to results, and requiring many reagents. To address these problems, there have been several reports of semi-automated assays that reduce time and reagents.<sup>27-29,37-39</sup> Samake *et al.* used a plate reader to automate a portion of the UV/vis detection. While this approach was an improvement, no automation of liquid handling was noted.<sup>37</sup> Another study shortened the results turnaround time to 30 min by utilizing a microfluidic paper-based analytical device ( $\mu$ PAD), but this assay would be difficult to automate.<sup>39</sup> An alternative electrochemical detection method presented by Sameenoi *et al.* eliminates trichloroacetic acid and DTNB (and associated costs and labor), while also enabling online monitoring when coupled to a particle-into-liquid sampler (PILS).<sup>29,38</sup> Another online DTT assay that uses a mist chamber and automated syringe pump was recently developed by Puthussery *et al.*<sup>40</sup> It was recently reported that a higher analysis rate to five samples per hour with one person (as compared to one sample per hour with two persons<sup>28</sup>) using electrochemical detection,<sup>27</sup> but

our approach did not yet automate liquid handling. The only report found thus far using liquid handling automation is by Fang *et al.*, where programmable syringe pumps were used to develop the most automated DTT assay.<sup>28</sup> The system can analyze approximately one sample per hour, be left unattended for 24 h, and be monitored remotely. To our knowledge, while there are many advantages to this assay relative to the fully manual system, the sample processing rate is still relatively slow.

The objective of the work herein was to develop an alternative approach to a semi-automated DTT assay with the following characteristics: a higher sample throughput than previous semi-automated systems, implemented modifications from the original assay, and easily accessible to other laboratories with similar equipment. The system uses a high-performance liquid chromatography (HPLC) pump and autosampler programmed to mix reagents and inject aliquots. The use of the system is demonstrated with aerosol filter samples using two detection options: UV/vis absorbance (already integrated into the HPLC) and electrochemical (custom-made or commercially available flow cell integrated into the HPLC). The developed method here has comparable accuracy and precision as the previously published DTT assays. Both detection options have sampling rates of six samples per hour, equivalent to an 83% time savings compared to the existing semi-automated systems. The non-reusable products (i.e. consumables) associated with the electrochemical detection presents a 40% cost savings relative to the UV/vis detection.

## **Experimental**

### *Materials*

All chemicals used were reagent grade and used as received with solution preparation in 18.2 M $\Omega$ ·cm water (MilliPore Milli-Q system, Billerica, MA, USA). DTT was purchased from Acros Organics (NJ, USA). CuSO<sub>4</sub>, DTNB, Chelex® 100 resin, potassium phosphate monobasic,

and potassium phosphate dibasic were purchased from Sigma-Aldrich (MO, USA). An Ultimate 3000 HPLC (Thermo Fisher Scientific, MA, USA) was used with a pH 7.4 phosphate buffer eluent at 1 mL/min for the UV/vis detection and electrochemical detection with the custom TPE flow cell. The commercial electrochemical flow cell (FLWCL, DropSens, Spain) was run with a commercial 3-electrode set up (DropSens 410 SPE, DropSens, Spain) with a pH 7.4 phosphate buffer eluent at 0.085mL/min. Details related to the custom TPE electrochemical flow cell construction are provided in the Supporting Information. All electrochemical experiments were operated using a PalmSens4 potentiostat and peak height (as customary with electrochemical wall jet flow cells<sup>41,42</sup>) was analyzed using PStTrace software (Palmsens, Houten, Netherlands).

#### *Semi-automated DTT Assay*

0.1 M potassium phosphate, pH 7.4 buffer was Chelex®-treated for at least one week and the chelex was decanted prior to use. Air sampling filters were handled with ceramic scissors and plastic forceps to avoid metal contamination. The filters were cut and weighed to achieve a target concentration of 10 µg PM per mL buffer while using between 100 and 1500 µL total buffer volume. Before buffer addition, the filters were wetted with 15 µL of 50:50 TFE:water (v:v) in a 1.5 mL centrifuge tube. Buffer was added, and the samples were sonicated at 37 °C for 30 min. 90 µL was removed from the centrifuge tubes into HPLC vials (300 µL polypropylene plastic, Waters, MA, USA). 10 µL of 1 mM DTT (100 µM final concentration) was added to each vial, including a blank buffer for each sample set, and mixed with either a multi-channel pipette (Integra Voyager, Integra Biosciences Corp, NH, USA) or by the HPLC. For UV/vis absorbance detection, two vials of each extracted PM were prepared (initial and 35 min). After a known reaction time, 10 µL of 3 mM DTNB in buffer was injected and mixed into the DTT vial. Three separate 10 µL aliquots were injected into the HPLC UV/vis detector at 412 nm for a total of six measurements per sample.

Peak area was used for DTT calibration and subsequent quantification. For electrochemical detection, a 10  $\mu\text{L}$  aliquot was injected into the electrochemical flow cell; this injection was repeated five times ( $n=6$  total) unless otherwise stated. The potentiostat was held at +0.3 V vs Ag/AgCl, and current was measured. Current peak height ( $I_p$ ,  $\mu\text{A}/\text{cm}^2$ ) was used for DTT calibration and subsequent quantification. The calculated DTT rate is blank subtracted and is calculated as previously reported.<sup>43</sup>

### *Honduras Filter Sampling*

Air sampling filters ( $n=105$  personal and  $n=106$  area samples) were collected from March 3 through April 30, 2015 as part of a Honduras cookstove study as previously reported.<sup>44</sup> One blank filter was collected every two weeks.  $\text{PM}_{2.5}$  was sampled onto 37-mm PTFE-coated glass fiber filters (Fiberfilm<sup>TM</sup> T60A20, Pall Corporation, KY, USA) using Triplex Cyclones (BGI, Mesa Labs, Butler NJ, USA) and AirChek XR5000 pumps (SKC Inc., Eighty Four, PA, USA) operating at 1.5 L/min for 24 hrs. The filters were equilibrated for at least 24 hrs and then pre-weighed to the nearest microgram at Colorado State University (CSU) using a microbalance (Mettler-Toledo microbalance model MX5, Columbus, OH, USA). After collection of the  $\text{PM}_{2.5}$  sample, filters were stored at  $-22\text{ }^\circ\text{C}$  and then transported to CSU, equilibrated, and post-weighed. The filters were then stored in a  $-80\text{ }^\circ\text{C}$  freezer until tested. The whole filter particle mass is the difference in masses before and after collection, accounting for the mean change in field blanks. Personal filters were collected near the participant's breathing zone; area filters were collected 76-127 cm from the stovetop in the participants' kitchens. Each household had one personal and one area exposure filter; therefore the two data sets from personal and area exposure are not independent from each other. The filters collected here have been previously used and analysed in other studies.<sup>27,44</sup>

### *China Filter Sampling*

The outdoor air pollution filter samples were collected in two neighboring villages in Yu County (112.55°-113.49° E, 37.57°-38.31° N) of Yangquan City, Shanxi Province in China. Yu County is in the east of Shanxi Province and southwest of Beijing, approximately 400 kilometers away. The two villages where sampling took place are located approximately 9-10 km from the primary urban center of Yu County. Although coal mining in the region has been a long-standing driver of economic activity, active coal mining in the area surrounding these two villages has ceased recently, following government shutdowns of small and low-grade companies. Several small refractory manufacturing industries are within 10 km of the two villages. The residents in one of the two villages primarily use coal for cooking and heating, while natural gas is the major energy for cooking and heating in the other village. Cooking emission and coal burning are the likely major sources of air pollution in these two villages, as local traffic is limited, consisting mostly of infrequent trips by private cars and motorcycles.

One four-channel sampler (Gas village: TH-16 A, Tianhong, China; Coal village: RT-AP4, Ruite, China) was set up to collect 24-h ambient PM<sub>2.5</sub> samples in the center of each village. The flow rate of the sampler was 16.7 L/min. Two 47 mm PTFE and quartz filters were collected at the same time. Four sets of field blanks were collected at both sites. In total, 36 sets of PTFE and quartz filters were collected from January 1-24, 2018. All filter samples were transported to the field laboratory and immediately stored in a -20 °C freezer. Following completion of the field sampling campaign, all samples were transported by plane to Colorado State University, where they were stored in a -20 °C freezer prior to mass measurement and oxidative potential analyses. The PTFE filters (Zefluor, Pall Life Sciences) were conditioned for 24-h (21-22 °C, 30-34% humidity) and weighed in triplicate on a microbalance (Mettler Toledo XS3DU) with 1- $\mu$ g

resolution before and after sample collection. The average of the three readings was taken as each filter weight, unless two weights differed by more than 5  $\mu\text{g}$ , in which case the filters were weighed more times until there were three weights within 5  $\mu\text{g}$ . Filter gross masses were blank-corrected using the mean value of blank filters ( $8 \pm 8 \mu\text{g}$ ), and  $\text{PM}_{2.5}$  concentrations were calculated by dividing by the sampled air volume.

#### *Custom TPE Flow Cell Fabrication*

The homemade TPE electrochemical flow cell template was fabricated with a poly(methyl methacrylate) (PMMA, Optix, Plaskolite) that was cut 30 W  $\text{CO}_2$  laser cutter (Epilog Laser, Golden, CO, USA) with a working electrode diameter of 2.5 mm and a counter circling the working electrode (Figure 4.1). The reference electrode was an external Ag/AgCl placed in the outlet. The

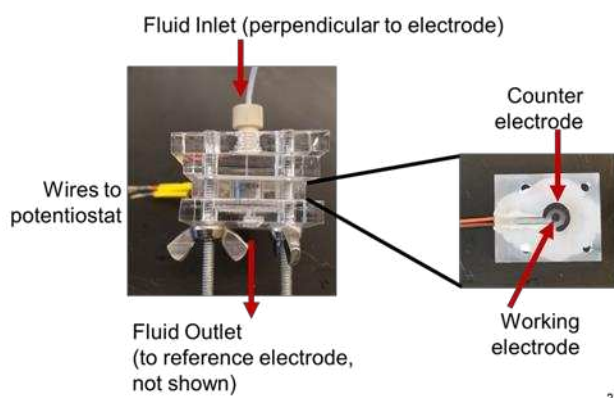


**Figure 4.1:** Picture of assembled custom TPE flow cell. The counter and working electrode are graphite-CoPC-PCL, which is perpendicular to the fluid inlet, and the reference electrode is placed in the fluid outlet, not shown.

device was bolted together with o-rings between each layer. The device consisted of 4 layers: tapped fluid inlet connection, fluid inlet with spacer of 100  $\mu\text{m}$ -thick Scotch tape, the electrode, and the outlet. The working and counter electrodes were made as described previously. Polycaprolactone (PCL, Thermomorph) was dissolved in dichloromethane. 7-11 micron graphite (Alfa Aesar, MA, USA) was added in a 1:3 PCL:Graphite ratio by weight with 20% cobalt(II) phthalocyanine (CoPC) weight relative to graphite was added for thiol detection. The graphite-

CoPC-PCL was thoroughly mixed, and the dichloromethane was evaporated. The resulting graphite plastic was then heat pressed into the template. The excess PCL was sanded off. Wires were connected with conductive silver paint (SPI, PA, USA) and then covered with PCL to be a flat surface. The electrode was sanded daily on 3000 grit sandpaper.

## Results and Discussion

### *Semi-automated Assay Development*

A higher throughput alternative approach was sought here to conduct the DTT assay by programming an HPLC to perform the liquid handling steps after PM<sub>2.5</sub> collected on filters are extracted in TFE and buffer. The automation was initially performed using an HPLC pump, autosampler, and UV/vis detector. Example peaks and the resulting DTT calibration curve are shown in Figure 4.2. DTT detection linearity, sensitivity, and precision are evident from the

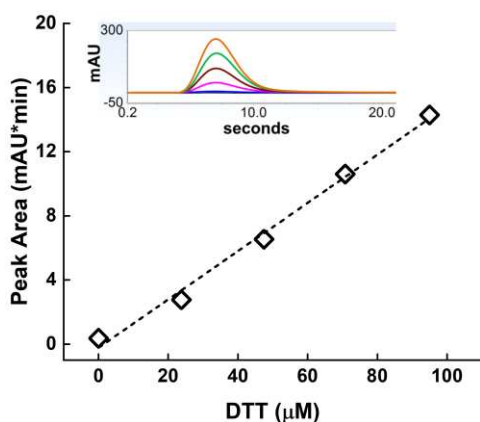


**Figure 4.2:** Example HPLC UV/vis detection peaks (inset) and corresponding calibration curve. The dashed line is the linear regression with  $\text{Peak Area} = (0.150 \pm 0.007)[\text{DTT}] - (0.2 \pm 0.4)$ ,  $R^2$  of 0.991. Standard deviation error bars (all  $\leq 5\%$  relative standard deviation) are not visible from  $n=5$  replicate measurements conducted at each DTT concentration.

calibration curve, and the coefficient of determination ( $R^2$ ) is 0.991. For the DTT assay to measure oxidative potential, the HPLC was programmed to inject and mix DTT into a vial containing sample, followed by DTNB, and then finally injecting a sample aliquot for detection. Two vials were used for each extracted filter sample for two separate time points (0 and 35 min) for an end-

point assay. The programmed mixing consists of withdrawing the final solution volume from the vial and reinjecting it into the same vial using the HPLC's integrated syringe. The DTNB was then injected and mixed into each vial. Automating DTT and DTNB injection and mixing into the samples provided a three sample per hour throughput rate. When a multi-channel pipette was used to inject and mix the DTT with the same volumes, the sample throughput rate doubled to six samples per hour with three DTT measurements at each of the two time points.

#### Assay Validation

The system's accuracy was tested with Cu(II) as a positive control for DTT oxidation (Figure 4.3). The published blank-subtracted DTT decay rate ( $\mu\text{M min}^{-1}$ ) is  $1.06[\text{Cu}]^{0.442}$ .<sup>30</sup> Our

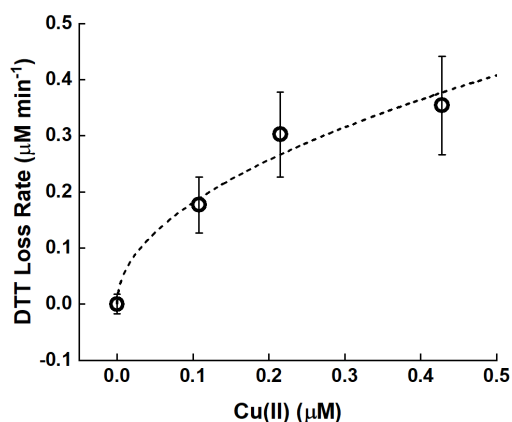


**Figure 4.3:** DTT decay rate at four Cu(II) concentrations. The dashed line is the best fit line, where  $\text{DTT rate} = 0.58[\text{Cu}]^{0.5}$ . Error bars represent the standard deviation from the linear DTT rates at each Cu concentration ( $n=6$ ).

measured blank-subtracted DTT decay rate ( $\mu\text{M min}^{-1}$ ) was  $0.58[\text{Cu}]^{(0.5 \pm 0.1)}$ , where the uncertainty is the 95% confidence interval of the fit from the four Cu(II) concentrations. The error bars represent the standard deviation from six measurements at each Cu(II) concentration. Our measured reaction rate constant of 0.58 is lower than the published value of 1.06, likely because the DTT loss rate was performed at room temperature whereas the literature value is measured at 37 °C and given the dependence of the reaction rate constant on solution conditions (e.g. temperature, pH, ionic strength). The literature partial order, 0.442, does fall within the 95%

confidence interval of our measured partial order of  $0.5 \pm 0.1$ , and demonstrates that the DTT in this study is likely reacting as it has in previous studies.

### *Electrochemical Detection*

The DTT assay with electrochemical detection requires fewer reagents while providing comparable sensitivity to UV/vis detection. Instead of injecting and mixing the DTNB before removing an aliquot of sample solution for analysis, an aliquot was taken at various times after the DTT reaction began. The aliquot was injected into an electrochemical flow cell instead of the HPLC's UV/vis detector. Electrochemical detection with a commercial flow cell was also tested. The commercial flow cell is advantageous to laboratories without electrochemical fabrication equipment. However, the maximum flow rate of the commercial flow cell is 0.085 mL/min. The injections are synchronized with the HPLC pump to ensure reproducibility, and the lower flow rate caused a delay in the injection rate to ensure the injection was synchronized with the pump. The injection time delay resulted in a sampling rate of three samples per hour when using the commercial flow cell (about half the rate of the custom-made electrochemical flow cell). Example DTT injection peaks and calibration curve are shown in the Figure 4.4. Filter samples were not

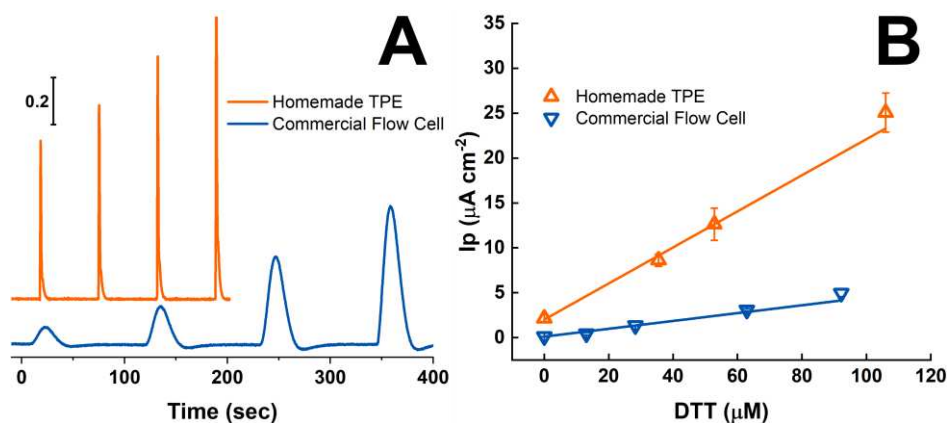


**Figure 4.4:** Examples of electrochemical DTT detection injection peaks (A, scale bar is 0.2  $\mu\text{A}$ ) and calibration curves (B) comparing the custom TPE and commercial DropSens flow cells. The linear regression for the custom TPE flow cell calibration curve is  $(0.218 \pm 0.009)[\text{DTT}] + (1.5 \pm 0.6)$ ,  $R^2$  of 0.973, and the commercial flow cell is  $(0.053 \pm 0.003)[\text{DTT}] - (0.1 \pm 0.1)$ ,  $R^2$  of 0.993. Error bars represent one standard deviation about the mean ( $n=4$ ).

tested with the commercial flow cell because of the lower flow rate. Numerous commercial electrochemical flow cells exist and can be tested at a higher flow rate to achieve a higher sampling rate.

To operate an electrochemical flow cell such that it is capable to withstand higher flow rates and thus higher sampling rates, a custom TPE electrochemical flow cell was designed and fabricated<sup>45</sup> using a composite carbon electrode. The flow cell costs less than \$1, is reusable, and has a maximum flow rate >1 mL/min. Example DTT injection peaks and calibration curves are shown in Figure 4.4. For the electrochemical DTT assay, a quenching reagent was not used to save time and consumables. Measuring only two time points here would not give uncertainty (or precision here) in the measurements because replicates cannot be done at the same reaction time, as with the UV/vis assay. The linear least squares regression uncertainty with the lab blank uncertainty propagated (as a real sample would be numerically treated) was calculated with an increasing number of time points (Figure 4.5) from five filter samples, collected as described

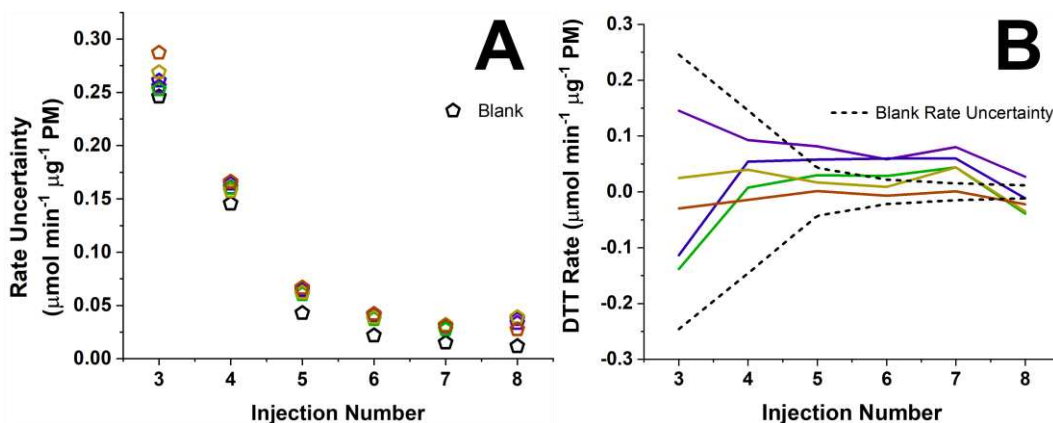


**Figure 4.5:** The DTT rate uncertainty, determined from repeated analysis of samples extracted from multiple different filter-based samples, as a function of the number of injections (A). The blank error was propagated. The corresponding filters' blank-subtracted rates (B). The two dashed black lines are the blank rate uncertainty.

elsewhere.<sup>44</sup> There are significant differences ( $p < 0.05$ , ANOVA one-way test performed with Microsoft Excel) in the filter sample rate uncertainties based on the number of injections, from

three to six. The F-critical value was 5.32 with F values of 47.31 (three vs four injections), 50.71 (four vs five), and 7.60 (five vs six). The blank was not included in the calculations. There were not significant differences in the uncertainties between six and seven injections ( $p > 0.05$ , F value of 3.31). Therefore, six time points (injections) were used in the electrochemical detection study ( $n=6$ ). The impact of decreasing uncertainty can also be seen in Figure 4.5. The blank-subtracted rates of the corresponding filters are also shown, where the black dotted line is the uncertainty of the lab blank. All of the rates are within the blank uncertainty until over five injection time points.

#### *Detection Method Comparison*

The semi-automated system with either UV/vis or electrochemical detection was developed to analyze real filter samples from two different locations (Figure 4.6) that vary with respect to

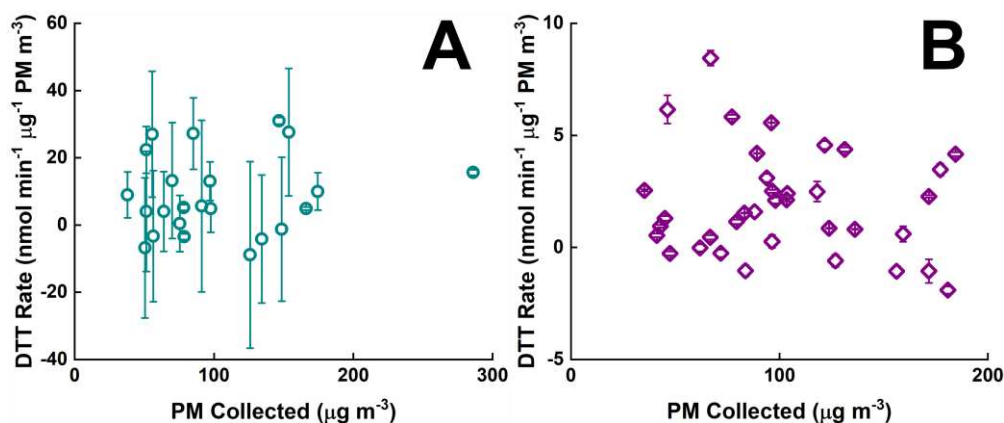


**Figure 4.6:** DTT rates of PM<sub>2.5</sub> filter samples from different sources tested with electrochemical detection (A, dark cyan circle, source: Honduras) and the automated UV/vis detection (B, purple diamond, source: China). Error bars represent linear regression uncertainty from  $n=6$ .

aerosol abundance and composition. The semi-automated system successfully measured the oxidative potential of 59 ambient PM<sub>2.5</sub> filter samples in under 10 hours (each unique sample was analyzed six times). The varied standard deviations between ambient PM<sub>2.5</sub> samples collected in Honduras have been seen before with these same samples using either detection motif and therefore are likely not a result of the detection method used, also as previously discussed.<sup>27</sup> The

differences between the standard deviations between the two collection sites can likely be attributed to the PM<sub>2.5</sub> components in each of the samples and each of their corresponding filter extraction efficiencies, DTT oxidation rates, and uncertainty.<sup>30,46</sup>

Both the UV/vis and electrochemical detection (with the custom TPE flow cell) allowed for an analysis rate of six samples per hour, and the manual labor was only associated with the sample preparation. The sensitivities (instrument response per unit concentration of DTT, calculated from the DTT calibration curves) of the UV/vis and electrochemical detection are 0.150 mAU\*min/ $\mu$ M DTT and 0.218 Ip/ $\mu$ M DTT, respectively. Although these reported sensitivities are different, they are comparable and more than sufficient for the DTT assay. The current consumables cost per sample (as calculated upon publication) of the UV/vis detection is \$2.50, but the electrochemical detection is cheaper at \$1.50 per sample (Table 1), equivalent to the electrochemical detection providing a 40% cost savings per 100 filters analyzed. The cost difference is a result of the extra reagents and vials required for the UV/vis detection. The electrochemical detection does require a flow cell and a potentiostat. Our custom TPE flow cell is reusable and costs less than \$1, while the commercial DropSens flow cell is currently about \$1000 with reusable (up to about 30 injections) electrodes.

**Table 4.1:** Comparison between UV/vis absorbance detection and electrochemical detection with our custom TPE flow cell or a commercial DropSens flow cell

	UV/Vis	Custom TPE	Commercial
Rate (samples per hour)	6	6	3
Consumables Cost (\$ per sample)	2.50	1.50	1.60
Sensitivity (per $\mu$ M DTT)	0.150 mAU min	0.218 $\mu$ A cm <sup>-2</sup>	0.053 $\mu$ A cm <sup>-2</sup>
Other Equipment Needed		Potentiostat	Potentiostat

After six months of intermittent use, the custom TPE flow cell results changed. The Ip response on calibration curves increased and were inconsistent between day-to-day runs. The DTT Ip should decrease over time because DTT concentration is decreasing over time as it reacts with

PM<sub>2.5</sub>. However, the  $I_p$  was seen to stay relatively constant or increase over time (Figure 4.7). The

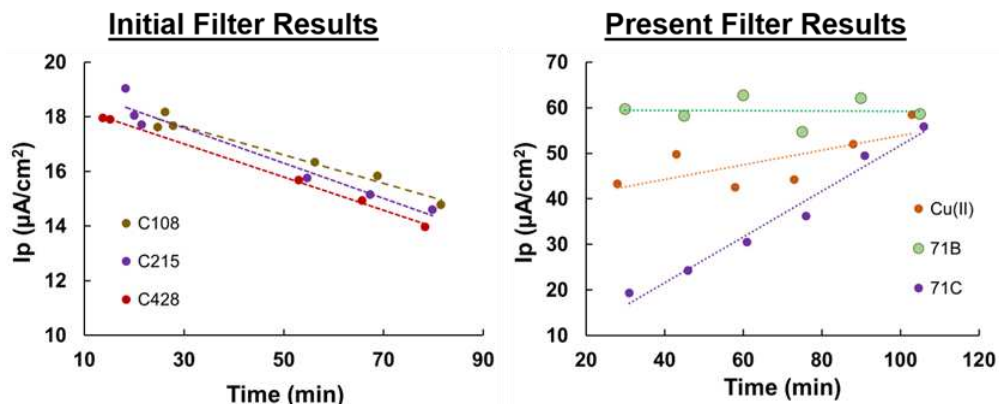


**Figure 4.7:**  $I_p$ , as measured with custom TPE flow cell, of various filters (C108, C215, C428, 71B, 71C) and Cu(II) positive control. Initial filter results were taken when the custom TPE flow cell was less than three months after fabrication, and the present filter results were taken after about six months after fabrication.

higher response after a prolonged period of time suggests that the electrode surface is changing and more active sites are becoming exposed. It is currently unclear how the surface is changing nor what active site(s) are being exposed. Further investigation into TPEs is needed.

## Conclusion

Even though an HPLC was used here for the liquid handling, other autosamplers and flow pumps are likely suitable for automation. Reducing cost and time associated with performing DTT assays with aerosol samples can lower barriers to incorporating oxidative potential analysis at a larger scale in exposure, environmental health, and epidemiologic studies. Doing so could provide new insight on spatial and temporal patterning in multiple PM measurements, including personal exposures. The DTT assay provides a measure of oxidative activity associated with the PM in the sample, and this may shed important light on human health impacts of particulate matter pollution, a leading environmental health risk factor worldwide. Further work needs to be done with TPEs to determine the change in response after an extended period of time.

## REFERENCES

1. A. J. Cohen, M. Brauer, R. Burnett, H. R. Anderson, J. Frostad, K. Estep, K. Balakrishnan, B. Brunekreef, L. Dandona, R. Dandona, V. Feigin, G. Freedman, B. Hubbell, A. Jobling, H. Kan, L. Knibbs, Y. Liu, R. Martin, L. Morawska, C. A. Pope, III, H. Shin, K. Straif, G. Shaddick, M. Thomas, R. van Dingenen, A. van Donkelaar, T. Vos, C. J. L. Murray and M. H. Forouzanfar, *The Lancet*, 2017, **389**, 1907-1918.
2. O. M. Morakinyo, M. I. Mokgobu, M. S. Mukhola and R. P. Hunter, *International journal of environmental research and public health*, 2016, **13**, 592.
3. G. Hoek, R. M. Krishnan, R. Beelen, A. Peters, B. Ostro, B. Brunekreef and J. D. Kaufman, *Environmental health*, 2013, **12**, 43.
4. E. Gakidou, A. Afshin, A. A. Abajobir, K. H. Abate, C. Abbafati, K. M. Abbas, F. Abd-Allah, A. M. Abdulle, S. F. Abera and V. Aboyans, *The Lancet*, 2017, **390**, 1345-1422.
5. J. S. Apte, M. Brauer, A. J. Cohen, M. Ezzati and C. A. Pope, *Environmental Science & Technology Letters*, 2018.
6. P. J. A. Borm, F. Kelly, N. Künzli, R. P. F. Schins and K. Donaldson, *Occupational and Environmental Medicine*, 2007, **64**, 73-74.
7. A. K. Cho, C. Sioutas, A. H. Miguel, Y. Kumagai, D. A. Schmitz, M. Singh, A. Eiguren-Fernandez and J. R. Froines, *Environ. Res.*, 2005, **99**, 40-47.
8. B. Crobeddu, L. Aragao-Santiago, L.-C. Bui, S. Boland and A. Baeza Squiban, *Environ. Pollut.*, 2017, **230**, 125-133.
9. H. J. Forman and C. E. Finch, *Free Radical Biol. Med.*, 2018, **117**, 202-217.
10. L. Ntziachristos, J. R. Froines, A. K. Cho and C. Sioutas, *Particle and Fibre Toxicology*, 2007, **4**, 5.
11. A. A. Alfadda and R. M. Sallam, *BioMed Research International*, 2012, **2012**.
12. J. O. Anderson, J. G. Thundiyil and A. Stolbach, *Journal of Medical Toxicology*, 2012, **8**, 166-175.
13. A. De Vizcaya-Ruiz, M. Gutiérrez-Castillo, M. Uribe-Ramirez, M. Cebrián, V. Mugica-Alvarez, J. Sepúlveda, I. Rosas, E. Salinas, C. Garcia-Cuéllar and F. Martínez, *Atmos. Environ.*, 2006, **40**, 583-592.
14. A. Campbell, M. Oldham, A. Becaria, S. Bondy, D. Meacher, C. Sioutas, C. Misra, L. Mendez and M. Kleinman, *Neurotoxicology*, 2005, **26**, 133-140.
15. J. T. Bates, R. J. Weber, J. Abrams, V. Verma, T. Fang, M. Klein, M. J. Strickland, S. E. Sarnat, H. H. Chang, J. A. Mulholland, P. E. Tolbert and A. G. Russell, *Environmental Science & Technology*, 2015, **49**, 13605-13612.
16. R. D. Brook, S. Rajagopalan, C. A. Pope, J. R. Brook, A. Bhatnagar, A. V. Diez-Roux, F. Holguin, Y. Hong, R. V. Luepker, M. A. Mittleman, A. Peters, D. Siscovick, S. C. Smith, L. Whitsel and J. D. Kaufman, *An Update to the Scientific Statement From the American Heart Association*, 2010, **121**, 2331-2378.
17. N. A. H. Janssen, A. Yang, M. Strak, M. Steenhof, B. Hellack, M. E. Gerlofs-Nijland, T. Kuhlbusch, F. Kelly, R. Harrison, B. Brunekreef, G. Hoek and F. Cassee, *Sci. Total Environ.*, 2014, **472**, 572-581.
18. V. Verma, T. Fang, H. Guo, L. King, J. Bates, R. Peltier, E. Edgerton, A. Russell and R. Weber, *Atmospheric Chemistry and Physics*, 2014, **14**, 12915-12930.

19. T. Fang, V. Verma, J. Bates, J. Abrams, M. Klein, M. Strickland, S. Sarnat, H. Chang, J. Mulholland and P. Tolbert, *Atmospheric Chemistry & Physics Discussions*, 2015, **15**.
20. M. Visentin, A. Pagnoni, E. Sarti and M. C. Pietrogrande, *Environ. Pollut.*, 2016, **219**, 72-79.
21. Q. Xiong, H. Yu, R. Wang, J. Wei and V. Verma, *Environmental science & technology*, 2017, **51**, 6507-6514.
22. J. T. Bates, R. J. Weber, V. Verma, T. Fang, C. Ivey, C. Liu, S. E. Sarnat, H. H. Chang, J. A. Mulholland and A. Russell, *Atmos. Environ.*, 2018, **193**, 158-167.
23. J. T. Bates, T. Fang, V. Verma, L. Zeng, R. J. Weber, P. E. Tolbert, J. Y. Abrams, S. E. Sarnat, M. Klein, J. A. Mulholland and A. G. Russell, *Environmental Science & Technology*, 2019, **53**, 4003-4019.
24. N. Li, C. Sioutas, A. Cho, D. Schmitz, C. Misra, J. Sempf, M. Wang, T. Oberley, J. Froines and A. Nel, *Environ. Health Perspect.*, 2003, **111**, 455.
25. J. G. Charrier, A. S. McFall, K. K. T. Vu, J. Baroi, C. Olea, A. Hasson and C. Anastasio, *Atmos. Environ.*, 2016, **144**, 325-334.
26. E. Vidrio, C. H. Phuah, A. M. Dillner and C. Anastasio, *Environmental Science & Technology*, 2009, **43**, 922-927.
27. K. E. Berg, L. R. Turner, M. L. Benka-Coker, S. Rajkumar, B. N. Young, J. L. Peel, M. L. Clark, J. Volckens and C. S. Henry, *Aerosol Sci. Technol.*, 2019, 1-8.
28. T. Fang, V. Verma, H. Guo, L. King, E. Edgerton and R. Weber, *Atmospheric Measurement Techniques*, 2015, **8**, 471.
29. Y. Sameenoi, K. Koehler, J. Shapiro, K. Boonsong, Y. Sun, J. Collett, J. Volckens and C. S. Henry, *J. Am. Chem. Soc.*, 2012, **134**, 10562-10568.
30. J. G. Charrier and C. Anastasio, *Atmospheric chemistry and physics (Print)*, 2012, **12**, 11317-11350.
31. H. Jiang, M. Jang, T. Sabo-Attwood and S. E. Robinson, *Atmos. Environ.*, 2016, **131**, 382-389.
32. H. Jiang, M. Jang and Z. Yu, *Atmospheric Chemistry and Physics*, 2017, **17**, 9965-9977.
33. Y. Wang, M. J. Plewa, U. K. Mukherjee and V. Verma, *Atmos. Environ.*, 2018, **179**, 132-141.
34. J. Wang, X. Lin, L. Lu, Y. Wu, H. Zhang, Q. Lv, W. Liu, Y. Zhang and S. Zhuang, *Sci. Total Environ.*, 2019, **649**, 969-978.
35. Q. Li, A. Wyatt and R. M. Kamens, *Atmos. Environ.*, 2009, **43**, 1037-1042.
36. A. Eiguren-Fernandez, E. Di Stefano, D. A. Schmitz, A. L. N. Guarieiro, E. M. Salinas, E. Nasser, J. R. Froines and A. K. Cho, *Journal of the Air & Waste Management Association*, 2015, **65**, 270-277.
37. A. Samake, G. Uzu, J. Martins, A. Calas, E. Vince, S. Parat and J. Jaffrezo, *Scientific reports*, 2017, **7**, 10978.
38. K. A. Koehler, J. Shapiro, Y. Sameenoi, C. Henry and J. Volckens, *Aerosol Sci. Technol.*, 2014, **48**, 489-497.
39. Y. Sameenoi, P. Panymeesamer, N. Supalakorn, K. Koehler, O. Chailapakul, C. S. Henry and J. Volckens, *Environmental Science & Technology*, 2013, **47**, 932-940.
40. J. V. Puthussery, C. Zhang and V. Verma, *Atmospheric Measurement Techniques*, 2018, **11**, 5767-5780.
41. W. J. Albery and C. M. Brett, *Journal of Electroanalytical Chemistry and Interfacial Electrochemistry*, 1983, **148**, 211-220.

42. J. Yamada and H. Matsuda, *Journal of Electroanalytical Chemistry and Interfacial Electrochemistry*, 1973, **44**, 189-198.
43. J. Charrier, N. Richards-Henderson, K. Bein, A. McFall, A. Wexler and C. Anastasio, *Atmospheric Chemistry and Physics*, 2015, **15**, 2327-2340.
44. S. Rajkumar, M. L. Clark, B. N. Young, M. L. Benka - Coker, A. M. Bachand, R. D. Brook, T. L. Nelson, J. Volckens, S. J. Reynolds and C. L'Orange, *Indoor air*, 2018.
45. K. J. Klunder, Z. Nilsson, J. B. Sambur and C. S. Henry, *J. Am. Chem. Soc.*, 2017, **139**, 12623-12631.
46. K. Bein and A. Wexler, *Atmos. Environ.*, 2015, **107**, 24-34.

## CHAPTER 5. SCANNING ELECTROCHEMICAL MICROSCOPY INVESTIGATION OF CARBON COMPOSITE THERMOPLASTIC SURFACES

### Chapter Overview

Despite having wider solvent windows, less fouling, and lower cost, carbon electrodes typically suffer from lower conductivity and greater difficulty to pattern relative to noble metal electrodes. Recently introduced carbon composite thermoplastic electrodes (TPEs), however, have high electrochemical activity, are easy to pattern into  $\mu\text{m}$ -sized features, and remain inexpensive. TPE's electrochemical response changes with the carbon and thermoplastic type used, but there has not been an extensive study on why these electrodes perform so well. In this work, the first thorough characterization of the different carbon and thermoplastic types is presented using scanning electrochemical microscopy (SECM) imaging with ferrocene (Fc), ferrocyanide ( $\text{Fe}(\text{CN})_6^{3-/4-}$ ), and dopamine to investigate the electrochemical surface heterogeneity. Experiments show that TPEs behave as a network of interacting microelectrodes made by active islands isolated within less active areas. Higher carbon content in TPEs yielded higher electrochemical activity with lower variation, and judicious choice of graphite types yielded higher dopamine response than the other carbon types. The study here also presents data that will aid future work by helping determine which TPE is best for the analyte of interest. This work has been submitted to *Analytical Chemistry*.

### Introduction

Electrochemistry has a vast array of applications in technology, including batteries, pollutant sensors, and health-related monitors.<sup>1,2</sup> Commercial examples include the lithium-ion battery frequently used in portable electronics,<sup>3</sup> and blood glucose monitors with enzyme-based electrode systems.<sup>4</sup> Common electrode materials consist of noble metals and carbon. Metals have

high conductivity and are easily patterned but typically suffer from higher cost, fouling, and narrow potential windows.<sup>1</sup> Carbon is an attractive, low-cost substitute due to its abundance and biocompatibility, but carbon electrodes typically suffer from lower conductivity and can be difficult to pattern. Screen printed electrodes are usually the easiest carbon electrode to pattern but usually also have the lowest performance of carbon-based electrodes.<sup>5,6</sup> Additional patterning methods do exist but often require complicated techniques and/or extreme temperatures,<sup>7-10</sup> adding to the cost and limiting the choice of substrate materials. The need of low-cost, high performing electrodes still exists.

Carbon composite electrodes fabricated from graphite and a polymeric binder are a promising alternative to improve electrode performance.<sup>11-17</sup> There has been a recent revitalization of using carbon composite thermoplastic electrodes (TPEs) using a simple, solvent-assisted fabrication method.<sup>18-20</sup> TPEs are an inexpensive thermoplastic and carbon mixture that retain similar physical properties to the thermoplastic, resulting in easy electrode fabrication and patterning into  $\mu\text{m}$ -sized features, while also retaining excellent electrochemical performance from the carbon additive. Of the four carbon types initially tested by Klunder *et al.*,<sup>18</sup> measured conductivities were up to 70 times higher than commonly available screen-printed carbon electrodes. TPEs were found to be kinetically comparable to Pt and significantly faster than other commercial carbon electrodes. TPEs have been fabricated with a variety of carbon types (graphite and carbon black) and thermoplastics, including poly(methyl methacrylate) (PMMA), cyclic olefin copolymer (COC) and polycaprolactone (PCL). TPE electrochemical performance depends on the carbon, thermoplastic, and their corresponding ratio. However, there has not yet been a thorough comparison of the different carbon and thermoplastic types. It is currently unclear as to what gives rise to the thermoplastic and carbon mixture electrodes' high conductivity and electron transfer

kinetics. It has been possibly attributed to “active islands” of graphite that leads to microelectrode-type behavior, as previously characterized with other carbon composite electrodes.<sup>21-23</sup>

The fundamental electrochemistry of TPEs was sought to be understood, focusing on the electrochemical heterogeneity. The electrodes’ electrochemical heterogeneity can be compared using scanning electrochemical microscopy (SECM). SECM is a well-known electrochemical technique for probing the local-scale electrochemical activity and topography, as opposed to more classical bulk solution analyses (e.g. cyclic voltammetry) that provide a global view of the surface.<sup>24-27</sup> In feedback mode,<sup>26,28</sup> an electroactive species is generated at the ultramicroelectrode (UME, <20  $\mu\text{m}$  diameter) that diffuses to the substrate surface, interacts with the substrate, and then diffuses back to the UME, creating a change in the electrochemical current. When the local surface area is reactive, the UME current increases as the tip distance from the surface decreases (and vice versa with a non-reactive surface) because the electroactive species has increased surface interaction. If the electrode-substrate distance is held constant (as common with 2-dimensional images), higher current values correspond to more reactive surface areas. TPEs can be tested similarly to a modified surface due to the heterogeneity of the carbon and thermoplastic.

Here, the surfaces and localized electrochemistry of TPEs are investigated as a function of thermoplastic, carbon type, and the ratio of thermoplastic to carbon. The first measurement of the surface roughness of the TPEs was using atomic force microscopy (AFM), and then proceeded with SECM for a thorough comparison of the local electrochemical activity of PMMA, COC, and PCL TPEs fabricated with four different carbon types (three graphites and a carbon black) at two different thermoplastic:carbon ratios. Ferrocene (Fc), ferrocyanide ( $\text{Fe}(\text{CN})_6^{3-/4-}$ ), and dopamine were used as redox probes to perform SECM imaging to yield more information about the electrochemical surface characteristics. It was found that carbon type and ratio has a larger effect

on the electrochemical activity than thermoplastic type, but it is also observed that the PCL TPE's electrochemical activity decreases over time. The data presented will aid future carbon and thermoplastic type selection for TPE fabrication across a range of analytes.

## Experimental

All solutions were prepared with 18.2 M $\Omega$ ·cm water (Milli-Q system, Billerica, MA, USA), and the chemicals were reagent grade from Sigma-Aldrich (MO, USA). TPE carbon types used were 7-11  $\mu$ m graphite ("11  $\mu$ m", 99%, Alfa Aesar, MA, USA), 3569 graphite ("3569", 99.9% carbon, 96.9% is  $\leq$ 75  $\mu$ m, Asbury Graphite Mills Inc, NJ, USA), MG-1599 ("MG", Great Lakes Graphite Inc., MA, USA), and acetylene carbon black ("Black", 50 nm, STREM chemicals Inc., MA, USA). TPEs were fabricated as previously described.<sup>18,19</sup> Briefly, PMMA (Optix, Plaskolite), COC (8007, TOPAS, MI, USA), and PCL (ThermoMorph) were dissolved in ethyl acetate, toluene, and dichloromethane, respectively. Carbon was added in specified ratios to the thermoplastic solution by mass (1:4 thermoplastic:carbon is equivalent to 80% carbon by mass) and thoroughly mixed. The solvent was evaporated (partially for PMMA and COC, fully for PCL), and the carbon composite material was heat pressed into 2.5 mm-diameter holes in PMMA templates. The excess carbon composite material was removed by sanding. TPEs were freshly polished with P4000 (5  $\mu$ m grit) sand paper before measurements. For the PCL TPEs studied over time, the PCL electrodes were stored in air between measurements after fabrication and then freshly polished with P4000 sand paper.

AFM measurements were performed with an NT-MDT Ntegra microscope in tapping mode using ACTA tips (AppNano Inc, CA, USA) on freshly polished TPEs. All images were 10 x 10  $\mu$ m<sup>2</sup> with 400 x 400 data points. Data analysis was performed with Gwyddion software.<sup>29</sup> SECM measurements were performed using a homemade setup to that described by Lhenry *et al.*,<sup>30</sup> with

an Autolab PGSTAT 12 (Metrohm, Utrecht, Netherlands) potentiostat. The SECM setup is equipped with an adjustable stage for the tilt angle correction and controlled by the SECMx software written by Wittstock, G., *et al.*<sup>31</sup> SECM measurements were performed using a typical 3-electrode configuration in feedback mode, with a 10  $\mu\text{m}$  diameter Pt electrode (CH Instruments Inc, TX, USA) as the tip working electrode, Ag/AgCl (saturated KCl) reference electrode, and a Pt wire as a counter electrode. The applied potential at the tip electrode was at the diffusion plateau of the mediator to allow for fast electron transfer at the tip electrode. TPEs were not electrically connected (unbiased conditions). Tilt angle was manually corrected before imaging following a classical three points procedure.  $100 \times 100 \mu\text{m}^2$  images were taken at L (d/a) of 1, and values are reported as normalized current ( $i/i_{\text{inf}}$ ). 1 mM Fc(MeOH)<sub>2</sub> in 0.1 M H<sub>2</sub>SO<sub>4</sub> and 1 mM K<sub>4</sub>Fe(CN)<sub>6</sub> in 0.5 M KCl images were taken as  $50 \times 2 \mu\text{m}$ , and 1 mM L-dopamine in 0.1 M H<sub>2</sub>SO<sub>4</sub> were taken as  $25 \times 4 \mu\text{m}$ . Images were acquired at room temperature. SECM image data analysis was performed with Gwyddion software.

## Results and Discussion

TPEs fabricated with four different carbon types (three graphites: “11  $\mu\text{m}$ ”, “3569”, “MG” and one carbon black, “Black”, that have been previously tested by the Henry group for relatively high conductivity and low capacitance).<sup>20</sup> Three different thermoplastics (PMMA, COC, and PCL) were tested for variances in surface roughness and electrochemical heterogeneity. Due to differences in solvents and melting temperatures, PMMA and COC are fabricated similarly (partial solvent evaporation), while PCL’s fabrication enables a more rapid throughput of electrodes due to complete solvent evaporation before molding the PCL electrode.<sup>20</sup> The ratios of thermoplastic to carbon are the lowest and highest carbon masses possible across all thermoplastic types while still enabling a working electrode. For example, the carbon black cannot be fabricated with higher

than a 1:1 thermoplastic:carbon black ratio because the electrode material breaks apart after solvent evaporation, but the conductivity is too low below a 3:1 thermoplastic:carbon black ratio to be a practical electrode. Therefore, the 3:1 and 1:1 thermoplastic:carbon black ratios were measured. 1:1 and 1:5 thermoplastic:carbon ratios were measured with both the 11  $\mu\text{m}$  and 3569 graphites, and 1:1 and 1:4 thermoplastic:MG ratios were measured here.

### Topographic Surface Characterization of TPEs

TPE surface roughness has not previously been measured below approximately 1  $\mu\text{m}$  height resolution. Before beginning SECM studies on the surfaces, AFM measurements were carried out to evaluate surface roughness for accurate SECM data. The surface roughness for each electrode composition is shown in Figure 5.1. The PMMA TPEs have surface roughness' (across

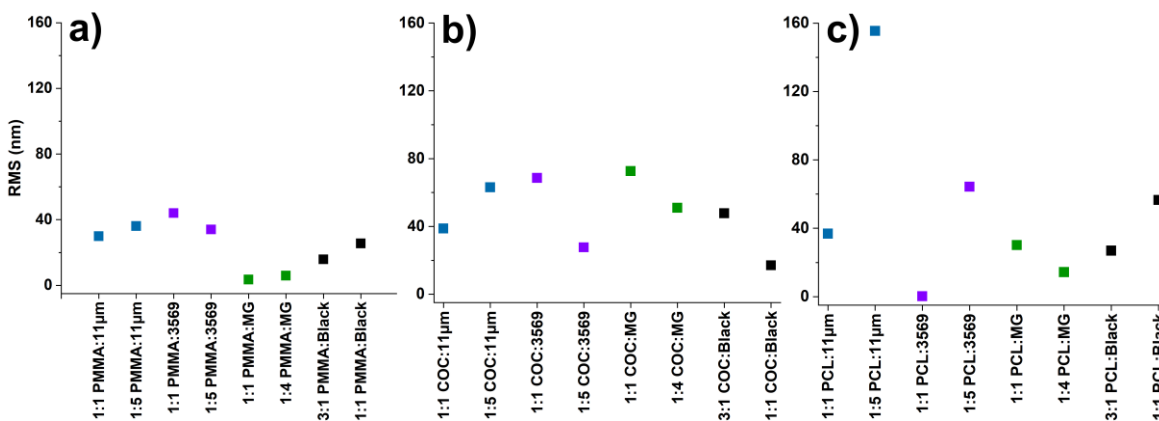


**Figure 5.1:** AFM surface roughness, reported as RMS in nm, of (a) PMMA, (b) COC, and (c) PCL TPEs after polishing.

all carbon types and ratios) ranging from 4 to 44 nm root mean square (RMS) with the average being 24 nm. The PMMA TPEs surface roughness average and range are lower than COC and PCL TPEs, both with an average of 48 nm and ranges of 17-73 and 0.2-155 nm, respectively. Even though the carbon particle sizes range from 500 nm to 75  $\mu\text{m}$ , there does not appear to be any overt trends between the carbon types. It is thus likely that the carbon type has little effect on the surface

roughness of TPEs and that the observed surface roughness is the direct result of the electrode polishing.

### Comparing SECM Approach Curves and Images

The TPEs' localized electrochemical activity was then investigated using SECM imaging and approach curves. An example image of 1:1 PMMA:MG with a ferrocene redox probe is shown in Figure 5.2. The surface has heterogeneous electrochemical activity with an average normalized

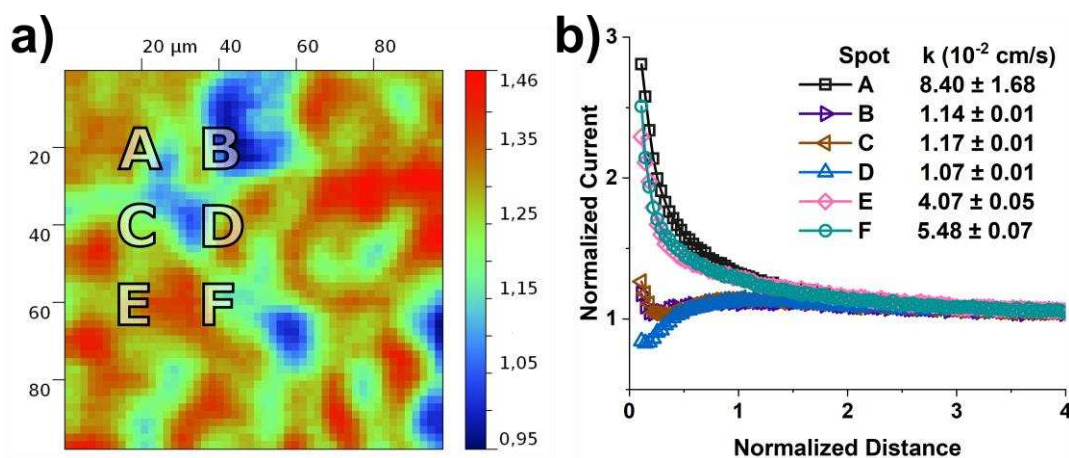


**Figure 5.2:** 1:1 PMMA:MG TPE (a) SECM image and (b) approach curves taken with  $\text{Fc}(\text{MeOH})_2$  at points A, B, C, D, E, and F with apparent rate constant ( $k$ ,  $10^{-2}$  cm  $\text{s}^{-1}$ ) values calculated from fitted approach curves. Both were taken with a  $10 \mu\text{m}$  diameter Pt UME. Image is  $100 \times 100 \mu\text{m}^2$ , and the scale bar values are the normalized current ( $i/i_{\text{inf}}$ ) (image mean value is 1.27).

current value ( $i/i_{\text{inf}}$ ) of 1.27 and an RMS of 0.091. The observed heterogeneous activity agrees well with the previously published SEM images of TPEs, where there are island-type configurations of carbon and thermoplastic across the surfaces.<sup>18,19</sup> Six approach curves were also taken at the points indicated on the image (A, B, C, D, E, and F) shown in Figure 5.2 with the same ferrocene redox probe. Approach curves show an increase of the normalized current with decreasing normalized tip-sample distance corresponding to positive feedback. Approach curve shape analysis indicates that the kinetics are controlled by the electron transfer between the oxidized redox probe and the surface. The resulting apparent rate constant,  $k$ , values are listed in Figure 5.2. As expected, at locations with the higher relative normalized current ( $i/i_{\text{inf}}$ ) (red on the SECM image), higher  $k$

values are derived and vice versa with lower relative normalized currents (blue on the SECM image). The lower electrochemical activity island between points C and D corresponds to the lower  $k$  values in these areas. In more active areas, rate constant values in the range of  $4-8 \cdot 10^{-2} \text{ cm s}^{-1}$  are obtained indicating a fast electron exchange between the surface and the molecule in solution. Thus, the image presented supports the hypothesis that TPEs have microelectrode-type behavior due to graphite with “highly active islands”. The image also yields a better global view of the electrode surface electrochemical activity relative to a few approach curves. Image analysis is continued with here.

### Electrochemical mapping of PMMA and COC TPEs

For the complete surface investigation of TPEs electrochemical activity,  $100 \times 100 \mu\text{m}^2$  SECM images were taken using three different redox probes with fast electron transfer kinetics, which is required in unbiased feedback mode imaging: ferrocene (Fc), ferrocyanide ( $\text{Fe}(\text{CN})_6^{3-/4-}$ ), and dopamine.<sup>32</sup> The graphical summary for PMMA and COC SECM images is shown in Figure 5.3. The three different redox probes were chosen with the SECM experiments because each gives

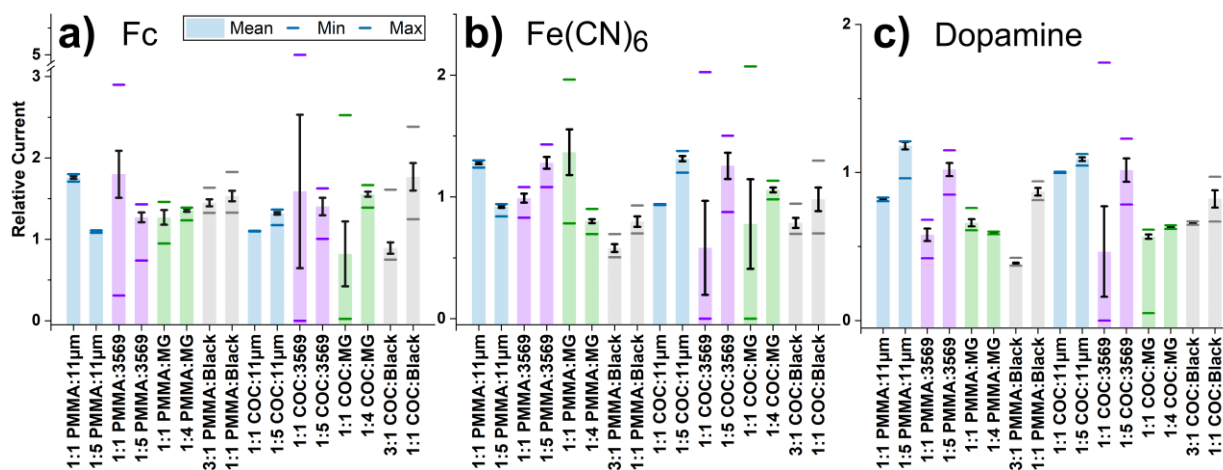


**Figure 5.3:** SECM image summary results of PMMA and COC TPEs using (a)  $\text{Fc}(\text{MeOH})_2$  in 100 mM  $\text{H}_2\text{SO}_4$ , (b)  $\text{Fe}(\text{CN})_6^{3-/4-}$  in 500 mM KCl, and (c) dopamine in 100 mM  $\text{H}_2\text{SO}_4$ . The column bars represent the mean value, black error bars represent mean  $\pm 1$  RMS (electrochemical), and the upper and lower bars represent the maximum and minimum current, respectively. Relative current values are the measured current normalized by the infinite current.

us different information. Ferrocene is not known to be surface sensitive due to its outer sphere character. On the contrary,  $\text{Fe}(\text{CN})_6^{3-/4-}$  and dopamine are surface sensitive (inner sphere character), and more specifically, dopamine is known to be surface sensitive to oxides with adsorption required.<sup>33,34</sup>

As expected, with increasing the relative amount of carbon, there is a trend that the mean normalized current is higher with all three redox probes. The few exceptions to this trend often have relatively high RMS values (variability in the image's current values, not physical surface roughness) with the lower thermoplastic to carbon ratio. The high RMS values leads to a less significant change between the two means. An example can be seen with the COC:3569 TPEs, where the 1:1 ratio (ferrocene redox probe) normalized current mean is 1.59 with an RMS of 0.944, and the 1:5 ratio normalized current mean is 1.40 with an RMS of 0.109. A decrease in normalized current mean is not seen with  $\text{Fe}(\text{CN})_6^{3-/4-}$  and dopamine as redox probes. The high RMS values seen with the 3569 graphite may be due to the larger and broader range of particle sizes relative to the others. The 3569 graphite is  $\leq 75 \mu\text{m}$  where the 11  $\mu\text{m}$  graphite is 7-11  $\mu\text{m}$ , the MG graphite is 15  $\mu\text{m}$ , and the carbon black is 50 nm.

Another observed trend that accompanies increasing carbon mass loading is a decrease in RMS values, which can be explained by the high concentrations of carbon (from 50% to 83% carbon for the 11  $\mu\text{m}$  and 3569 electrodes) leading to a more homogenous graphitic surface with smaller "islands" of polymer. It is important to note that the carbon black RMS values followed the opposite trend and had increased RMS values with increasing carbon mass loading. This change may be from the smaller particle sizes and/or the fabrication difficulties associated with the carbon black, leading to a maximum of 1:1 thermoplastic:carbon ratio. It is also interesting to note that the 11  $\mu\text{m}$  graphite consistently has the lowest RMS value relative to the other carbon

types for both thermoplastics. The lower RMS values might become significant when using TPEs for electroanalytical chemistry and should be considered when evaluating carbon type.

Another difference in carbon type can be seen with the mean normalized current values of dopamine. The 11  $\mu\text{m}$  and 3569 graphite have a higher electrochemical response from dopamine than the MG graphite and carbon black. Dopamine requires adsorption onto the surface that is strongly dependent on oxide functional groups or hydrogen bonding electrocatalytic sites, and has higher activity at edge plane graphite.<sup>35,36</sup> While the electrocatalytic sites for dopamine may result from the polishing,<sup>18,35</sup> all the electrodes were similarly polished. It is unclear why the 11  $\mu\text{m}$  and 3569 graphite have more dopamine electrocatalytic sites, and it may be a combination of increased edge plane sites and surface oxides. There is a similar trend observed with  $\text{Fe}(\text{CN})_6^{3-/4-}$  though, but  $\text{Fe}(\text{CN})_6^{3-/4-}$  can have a variable response with its surface interactions.<sup>36</sup> For future studies evaluating analytes with similar electrochemical behavior similar to dopamine, choice of carbon type is important to increase or decrease the electrode response.

There are not large differences observed in the image results between PMMA and COC TPEs, which suggests that the carbon type dominates the electrochemical behavior of TPEs. It is seen, however, that the higher carbon ratio TPEs have higher maximum normalized current values than the equivalent PMMA surfaces, but COC surfaces often have lower minimum normalized current value relative to the comparable PMMA surface. This may be a result of how the polymer coats the carbon particles. The electrochemical activity differences seen here between COC and PMMA for a TPE are not large, and the use of either will likely depend on the analyte of interest and solution conditions (solvent, fabrication requirements, etc.). For example, COC was employed over PMMA when creating electrochemical biosensors because of COC's high purity, chemical resistance, and biocompatibility.<sup>19</sup>

## Electrochemical mapping of PCL TPEs Over Time

PCL electrodes provide an alternative, simpler fabrication process than the PMMA and COC TPEs and were recently used in microfluidic devices for droplet detection and organic synthesis.<sup>20</sup> In bulk electroanalytical experiments, however, the signals from PCL TPEs changed over time after fabrication, even when stored in air and polished before use. PCL is a well-known biodegradable polymer, but degradation time is not well controlled and takes up to two years in physiological conditions.<sup>37-39</sup> The PCL TPEs surfaces were investigated with ferrocene as a redox probe at three different times after fabrication (fresh, two days after, and two weeks after). Freshly fabricated PCL and graphite TPEs had higher electrochemical response to ferrocene than PMMA and COC graphite TPEs. Even though the electrodes were freshly polished before each measurement, changes in the surface electrochemical activity can be seen after fabrication (Figure 5.4). With the three different graphites (3569 graphite, MG graphite and 11  $\mu\text{m}$  graphite) at both

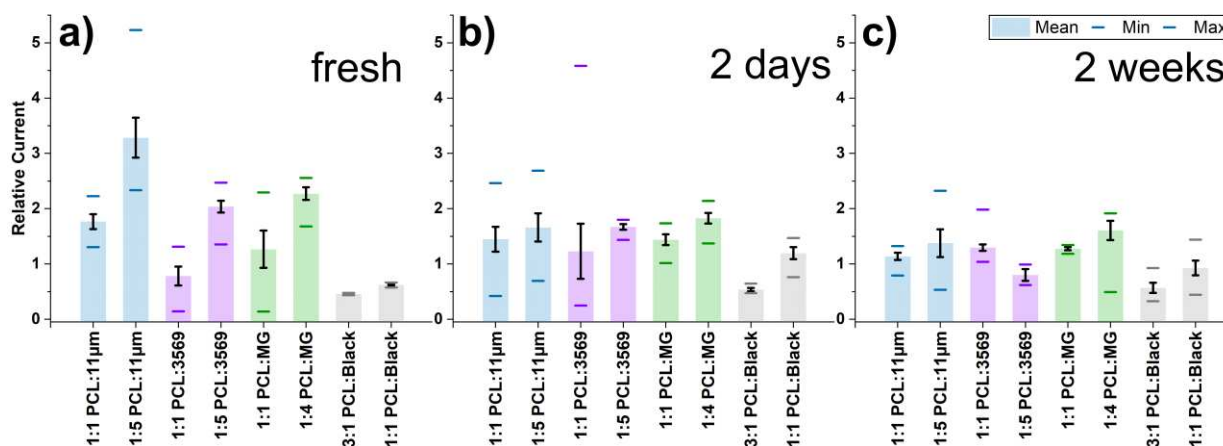


**Figure 5.4:** SECM image summary of PCL TPEs at three different times: freshly made (a, “fresh”), two days old (b, “2 days”), and 2 weeks old (c, “2 weeks”). The column bars represent the mean value, black error bars represent mean  $\pm$  1 RMS (electrochemical), and the upper and lower bars represent the maximum and minimum current, respectively. Relative current values are measured current normalized by the infinite current using 1 mM  $\text{Fc}(\text{MeOH})_2$  in 100 mM  $\text{H}_2\text{SO}_4$ . TPEs were freshly polished before obtaining images.

ratios, a decrease in activity over time was measured, and the higher carbon content TPEs have a greater change. The largest diminution over two weeks is seen with the 11  $\mu\text{m}$  graphite, with a

36% decrease with the 1:1 PCL:11  $\mu\text{m}$  and a 59% decrease with the 1:5 PCL:11  $\mu\text{m}$ . The 1:5 PCL:3569 and 1:4 PCL:MG have similar changes of 61% and 29%, respectively. The 1:1 PCL:3569 and PCL:MG normalized current values do not decrease over time, but both electrodes have large RMS values ( $\geq 0.1$ ), leading to less significant observed changes at the low carbon ratios. When using carbon black, however, PCL TPEs did not decrease over time. The lower carbon ratio TPE (3:1 PCL:Black) stayed about the same throughout the three times measured. The higher carbon ratio TPE (1:1 PCL:Black) normalized current values approximately doubled (0.62 to 1.20) from the freshly fabricated electrode to the two day old electrode and then decreased to 0.93 when measured two weeks after fabrication. Overall, if PCL TPEs are used for electroanalytical purposes, a more thorough electrode characterization to test their long-term stability and reproducibility is needed.

## **Conclusion**

A thorough local electrochemical characterization was successfully performed of carbon composite TPEs that have high electrochemical activity while being easy to fabricate and pattern. The TPE electrodes behave as a network of interactive diffusion microelectrode with high active islands isolated by less active areas. Thus, increasing carbon in the TPEs yields a more electroactive surface with lower surface current variation. Two graphite types, 11  $\mu\text{m}$  and 3569, have higher responses to dopamine, which impacts future decisions on what carbon type is best suited for the analyte of interest. There were not significant differences between PMMA and COC thermoplastic TPEs, suggesting that either thermoplastic is a viable option and the choice between either should depend on a different factor, e.g. fabrication ease or application. There were, however, significant changes observed over time with TPEs made with PCL, suggesting that future studies need to investigate and address the stability concern before usage.

## REFERENCES

1. W. Zhang, S. Zhu, R. Luque, S. Han, L. Hu and G. Xu, *Chem. Soc. Rev.*, 2016, **45**, 715-752.
2. K. Gong, Y. Yan, M. Zhang, L. SU, S. XIONG and L. MAO, *Anal. Sci.*, 2005, **21**, 1383-1393.
3. M. Yoshio, R. J. Brodd and A. Kozawa, *Lithium-ion batteries*, Springer, 2009.
4. N. Oliver, C. Toumazou, A. Cass and D. Johnston, *Diabetic Medicine*, 2009, **26**, 197-210.
5. I. Švancara, K. Vytřas, K. Kalcher, A. Walcarius and J. Wang, *Electroanalysis*, 2009, **21**, 7-28.
6. I. Švancara, A. Walcarius, K. Kalcher and K. Vytřas, *Open Chemistry*, 2009, **7**, 598-656.
7. S. H. Ng, J. Wang, K. Konstantinov, D. Wexler, S. Y. Chew, Z. Guo and H.-K. Liu, *J. Power Sources*, 2007, **174**, 823-827.
8. S. Sharma and M. Madou, *Bioinspired Biomim. Nanobiomater*, 2012, **1**, 252-265.
9. M. Vomero, P. van Niekerk, V. Nguyen, N. Gong, M. Hirabayashi, A. Cinopri, K. Logan, A. Moghadasi, P. Varma and S. Kassegne, *Journal of Micromechanics and Microengineering*, 2016, **26**, 025018.
10. S. Ranganathan, R. McCreery, S. M. Majji and M. Madou, *J. Electrochem. Soc.*, 2000, **147**, 277-282.
11. L. Falat and H. Cheng, *Anal. Chem.*, 1982, **54**, 2108-2111.
12. H. P. Henriques and A. G. Fogg, *Analyst*, 1984, **109**, 1195-1199.
13. M. Perween, D. B. Parmar, G. R. Bhadu and D. N. Srivastava, *Analyst*, 2014, **139**, 5919-5926.
14. S. Zhong, M. Kazacos, R. Burford and M. Skyllas-Kazacos, *J. Power Sources*, 1991, **36**, 29-43.
15. K. McLaren and G. Batley, *Journal of Electroanalytical Chemistry and Interfacial Electrochemistry*, 1977, **79**, 169-178.
16. D. E. Tallman and S. L. Petersen, *Electroanalysis*, 1990, **2**, 499-510.
17. X. Yao, H. Wu, J. Wang, S. Qu and G. Chen, *Chemistry—A European Journal*, 2007, **13**, 846-853.
18. K. J. Klunder, Z. Nilsson, J. B. Sambur and C. S. Henry, *J. Am. Chem. Soc.*, 2017, **139**, 12623-12631.
19. E. Noviana, K. J. Klunder, R. B. Channon and C. S. Henry, *Anal. Chem.*, 2019, **91**, 2431-2438.
20. K. J. Klunder, K. M. Clark, C. McCord, K. E. Berg, S. D. Minter and C. S. Henry, *Lab Chip*, 2019, **Submitted**.
21. D. O'Hare, J. V. Macpherson and A. Willows, *Electrochem. Commun.*, 2002, **4**, 245-250.
22. S. Ramírez-García, S. Alegret, F. Céspedes and R. J. Forster, *Analyst*, 2002, **127**, 1512-1519.
23. D. E. Weisshaar and D. E. Tallman, *Anal. Chem.*, 1983, **55**, 1146-1151.
24. D. Polcari, P. Dauphin-Ducharme and J. Mauzeroll, *Chem. Rev.*, 2016, **116**, 13234-13278.
25. A. J. Bard and M. V. Mirkin, *Scanning electrochemical microscopy*, CRC Press, 2012.
26. S. Amemiya, A. J. Bard, F.-R. F. Fan, M. V. Mirkin and P. R. Unwin, *Annu. Rev. Anal. Chem.*, 2008, **1**, 95-131.

27. G. Wittstock, M. Burchardt, S. E. Pust, Y. Shen and C. Zhao, *Angew. Chem. Int. Ed.*, 2007, **46**, 1584-1617.
28. C. Lagrost, Y. Leroux and P. Hapiot, *Electroanalysis*, 2016, **28**, 2680-2687.
29. D. Nečas and P. Klapetek, *Open Physics*, 2012, **10**, 181-188.
30. S. Lhenry, Y. R. Leroux and P. Hapiot, *Anal. Chem.*, 2013, **85**, 1840-1845.
31. O. Sklyan, G. Wittstock, C. Nunes Kirchner and A. Leash, *Journal*.
32. A. J. Bard, F.-R. F. Fan, D. T. Pierce, P. R. Unwin, D. O. Wipf and F. Zhou, *Science*, 1991, **254**, 68-74.
33. S. H. DuVall and R. L. McCreery, *J. Am. Chem. Soc.*, 2000, **122**, 6759-6764.
34. S. Lhenry, Y. R. Leroux and P. Hapiot, *Anal. Chem.*, 2012, **84**, 7518-7524.
35. R. L. McCreery, *Chem. Rev.*, 2008, **108**, 2646-2687.
36. R. L. McCreery and M. T. McDermott, *Anal. Chem.*, 2012, **84**, 2602-2605.
37. B. Saad and U. Suter, 2001.
38. R. L. Prabhakar, S. Brocchini and J. C. Knowles, *Biomaterials*, 2005, **26**, 2209-2218.
39. R. Perveen and A. Nasar, in *Applications of Nanocomposite Materials in Orthopedics*, Elsevier, 2019, pp. 111-126.

## CHAPTER 6. INCREASING APPLICATIONS OF GRAPHITE THERMOPLASTIC ELECTRODES WITH ARYL DIAZONIUM GRAFTING

### Chapter Overview

Carbon composite thermoplastic electrodes (TPEs) consist of graphite and thermoplastic from an easy, solvent-assisted fabrication. TPEs have the advantages of high conductivity, good electron transfer kinetics, low cost, reusability, and easy patterning, but have only been used with aqueous solvents thus far due to solvent compatibility with the poly(methyl methacrylate) (PMMA) template. The limited solvent compatibility hinders the range of applications. Here, cyclic olefin copolymer (COC) TPEs in a glass template are presented that are compatible with more solvents. The TPEs are grafted with various aryl diazonium salts through electroreduction in acetonitrile, showing covalent surface TPE modification for the first time. Further investigation of the surface modification is carried out with scanning electrochemical microscopy (SECM). The TPEs are then successfully post-functionalized with a ferrocene moiety via click chemistry. The diazonium grafting and click chemistry modifications opens up future studies and broader applications of TPEs. This work has been submitted to *Electrochimica Acta*.

### Introduction

Carbon electrodes have advantageous features, such as low cost, chemical inertness, biocompatibility, and wide potential windows but can suffer from low conductivity and are challenging to pattern.<sup>1-3</sup> Carbon composite electrodes (carbon mixed with a binder material) are the easiest to pattern but typically have low electrochemical performance.<sup>3,4</sup> The binder material affects the physical and electrochemical properties of the electrode; binders that have been used in carbon composite electrodes include pasting liquids for screen printed electrodes,<sup>5,6</sup> paraffin wax,<sup>7,8</sup> epoxy,<sup>9,10</sup> and various plastics.<sup>11-13</sup> Recently, a new form of carbon composite electrodes

called thermoplastic electrodes (TPEs) were reported that use a simple fabrication method to generate complex electrode geometries while maintaining high conductivity, good electron transfer kinetics, reusability, and low cost.<sup>14</sup> The first report used poly(methyl methacrylate) (PMMA) as the binder, but cyclic olefin copolymer (COC)<sup>15</sup> and polycaprolactone (PCL) (submitted manuscript to *Lab on A Chip*) have also been used as binders. While TPEs exhibit promising results, they have not yet been used in sensing applications nor have they been used in non-aqueous solutions, limiting the available surface modification possibilities.

Electrode modification is of great interest to many applications and is often required to achieve the desired sensitivity and/or selectivity.<sup>16-19</sup> Electrode modification with aryl diazonium salts has been studied since the seminal reports from 1992<sup>20</sup> because of the easy preparation, fast electroreduction, and strong covalent bond formed with carbon surfaces.<sup>21-28</sup> Although the initial report was the electroreduction grafting onto glassy carbon (GC) in acetonitrile,<sup>20</sup> variations to achieve grafted aryl layers on plate electrodes include using ionic liquids,<sup>29,30</sup> spontaneous reduction,<sup>21,31</sup> UV-assisted,<sup>32</sup> grinding a paste,<sup>33</sup> scratching,<sup>34</sup> and *in situ* generation of diazonium cations<sup>35,36</sup> have been reported. Because most screen printed carbon electrodes have limited solvent compatibility, they have primarily been modified via an *in situ* diazonium generation,<sup>37-39</sup> although there is one report of a screen printed electrode being modified in acetonitrile.<sup>40</sup> Once modified, post-functionalization and/or activation can be used to detect the target analytes.

A fast, easy, and selective post-functionalization method of a diazonium-modified surface is with click chemistry.<sup>19,41-45</sup> Click chemistry is a Cu(I)-catalyzed, 1,2,3-triazole forming reaction between terminal alkynes and azides using a variation of the Huisgen 1,3-dipolar cycloaddition. Li *et al.* used click chemistry with an alkyne-terminated diazonium surface and an azide-terminated polystyrene to tether the polymers.<sup>46</sup> Click chemistry has become commonly used

across many fields of chemistry, including reproducible functionalization of electrodes for sensing applications.<sup>47</sup> The covalent bond enables fast electron transfer kinetics, relative to adsorption, of bio-compounds (enzymes, antibodies, etc.) and is especially useful for fabricating biosensors due to the reaction's selectivity in mild conditions.<sup>47,48</sup>

Here, TPEs was fabricated in a glass template to achieve a wider range of solvent compatibility, including non-aqueous solvents. The TPEs were successfully modified with the aryl diazonium salt electroreduction in acetonitrile, showing covalent TPE surface modification for the first time. The surface modification was further investigated with scanning electrochemical microscopy (SECM).<sup>49</sup> Finally, the aryl diazonium modified TPEs were functionalized with a ferrocene moiety via click chemistry. The present study greatly expands upon the possible future use of TPEs by the ability to use non-aqueous solvents and to perform surface modifications and post functionalization.

## **Experimental**

All solutions were prepared with 18.2 M $\Omega$ ·cm water (Milli-Q system, Billerica, MA, USA), and the chemicals were reagent grade from Sigma-Aldrich (MO, USA). Two graphite types were used: 3569 graphite ("3569", 99.9% purity carbon, 96.9% is  $\leq 75$   $\mu\text{m}$  diameter, Asbury Graphite Mills Inc, NJ, USA) and MG-1599 ("MG", 99.5-99.9% purity carbon, 16  $\mu\text{m}$  diameter, Great Lakes Graphite Inc., MA, USA). TPEs were fabricated as previously described.<sup>14,15</sup> Briefly, COC (8007, TOPAS, MI, USA) was dissolved in toluene. Graphite was added in 1:3 plastic:carbon by mass (25% carbon by mass) and thoroughly mixed. The solvent was evaporated, and the carbon composite material was heat pressed into 2.5 mm diameter Pyrex glass electrode templates. The excess material was sanded off. TPEs were freshly polished with P4000 (5  $\mu\text{m}$  grit) sand paper before testing.

Bulk electrochemical experiments were performed with an Autolab PGSTAT 12 (Metrohm, Utrecht, Netherlands) using a saturated calomel electrode (SCE) reference and Pt wire counter electrode. SECM measurements were performed using a homemade setup to that described by Lhenry *et al.*,<sup>50</sup> with an Autolab PGSTAT 12 (Metrohm, Utrecht, Netherlands) potentiostat. The SECM setup is equipped with an adjustable stage for the tilt angle correction and controlled by the SECMx software written by Wittstock, G., *et al.*<sup>51</sup> SECM measurements were performed using a typical 3-electrode configuration in feedback mode, with a 10  $\mu\text{m}$  diameter Pt electrode (CH Instruments Inc, TX, USA) as the tip working electrode, Ag/AgCl (saturated KCl) reference electrode, and a Pt wire as a counter electrode. The applied potential at the tip electrode was at the diffusion plateau of the mediator to allow for fast electron transfer at the tip electrode. TPEs were not electrically connected (unbiased conditions). Tilt angle was manually corrected before imaging following a classical three points procedure.  $100 \times 100 \mu\text{m}^2$  images were taken at L (d/a) of 1, and values are reported as current relative to the infinite current with the following solutions: 1 mM Fc(MeOH)<sub>2</sub> in 100 mM KCl, 1 mM K<sub>4</sub>Fe(CN)<sub>6</sub> in 100 mM KCl (neutral), and 1 mM K<sub>4</sub>Fe(CN)<sub>6</sub> in 100 mM H<sub>2</sub>SO<sub>4</sub> (acidic). SECM image data analysis was performed with Gwyddion software.<sup>52</sup>

For aqueous derivatization of PMMA TPEs, the procedure described by Baranton and Bélanger was followed with 4-aminobenzoic acid.<sup>35</sup> CVs of 1 mM K<sub>4</sub>Fe(CN)<sub>6</sub> in 100 mM KCl were run before and after modification. For reductive aryl diazonium grafting in acetonitrile, TPEs (and a 2.5 mm diameter GC electrode) were modified in a 10 mM diazonium salt and 100 mM tetrabutylammonium hexafluorophosphate (TBA PF<sub>6</sub>) solution in an ice bath. CV modification parameters were as follows: +0.6 V to -0.5 V at 100 mV/s scan rate for four cycles. CVs of 1-5 mM aqueous solutions of Fc(MeOH)<sub>2</sub> and K<sub>4</sub>Fe(CN)<sub>6</sub> in 100 mM KCl were run before and after modification (same solution for each before and after modification CV). Post p-nitro aryl

diazonium modification CVs were run in 100 mM H<sub>2</sub>SO<sub>4</sub> with the following electrochemical parameters: +0.8 V to -0.8 V and back with 100 mV/s scan rate, twice. For the azidomethylferrocene click chemistry coupling, 1:1 water:ethanol solution of 100 mM CuSO<sub>4</sub> and 200 mM L(+)-ascorbic acid were stirred in the presence of 10 μM azidomethylferrocene and the modified TPE.<sup>53</sup>

## Results and Discussion

TPEs have been fabricated from PMMA, COC, and PCL thermoplastics, but they have always been used in a PMMA template<sup>14,15</sup> (submitted manuscript to *Lab On A Chip*). Because the PMMA template restricts solvent compatibility to aqueous solutions, *in situ* diazonium generation and modification was first attempted in aqueous solution using the method introduced by Baranton and Bélanger for GC surfaces.<sup>35</sup> However, Fe(CN)<sub>6</sub><sup>3-/4-</sup> detection after modification indicated the modification was unsuccessful (Figure 6.1). To circumvent the PMMA template solvent

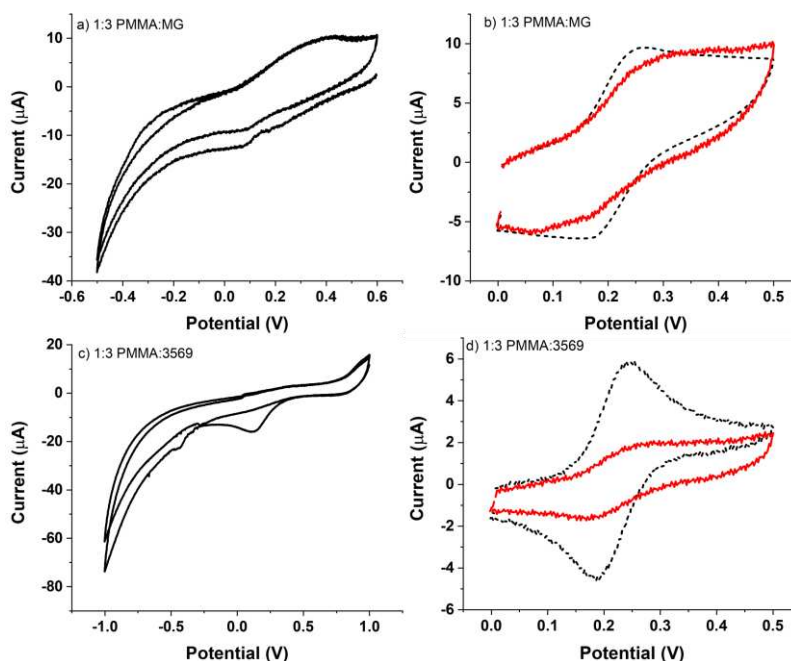


**Figure 6.1:** Aqueous 4-aminobenzoic acid derivatization of PMMA TPEs, (a) and (c) are modification CVs of 1:3 PMMA:MG and 1:3 PMMA:3569, respectively. (b) and (d) are before and after modification CVs of Fe(CN)<sub>6</sub><sup>3-/4-</sup> in 100 mM KCl. Potentials are vs SCE at 50 mV/s scan rate.

compatibility issues, a COC TPE in a glass template was fabricated. The combination of COC and glass enables a wider range of solvents to be used with TPEs because COC is compatible with polar solvents due to its hydrocarbon structure and glass is relatively inert in organic solvents.<sup>54</sup> The TPE surfaces were then able to be modified with aryl diazonium reduction via electrochemistry.<sup>20</sup> The TPEs were made from two carbon types, MG and 3569, using nitro-, carboxylic acid-, methyl-, and ethynyl-para substituted aryl diazonium compounds to show the general nature of the approach.

As expected, for the p-nitro aryl diazonium grafting CV (Figure 6.2) , there is a reduction

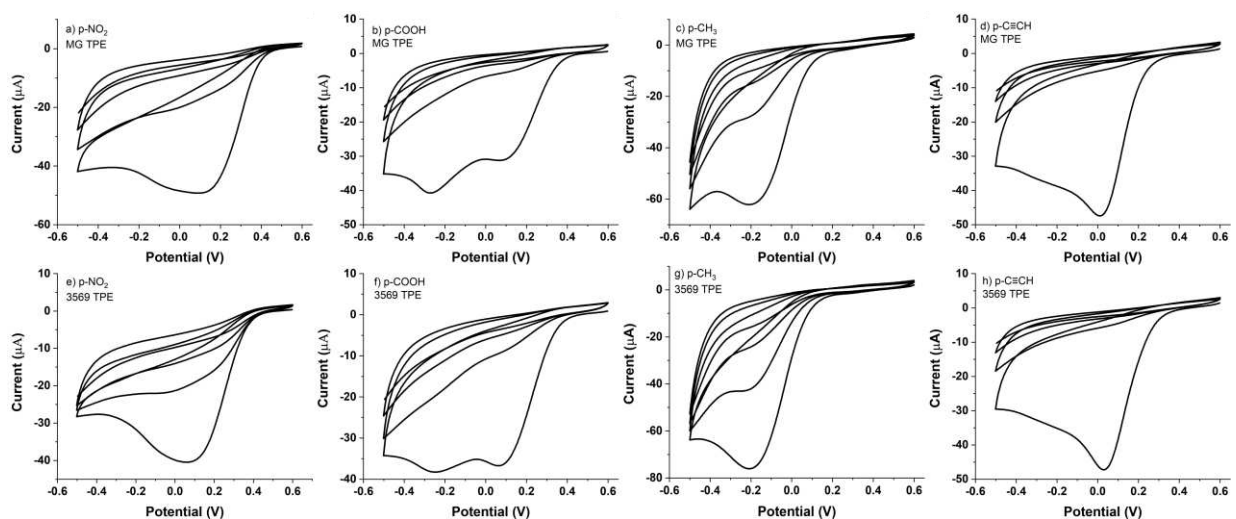


**Figure 6.2:** Grafting CVs of TPE modification in acetonitrile via aryl diazonium salt reduction with nitro- (a and e), carboxylic acid- (b and f), methyl- (c and g), and ethynyl (d and h) para substituents with two different carbon types, MG (a, b, c, and d) and 3569 (e, f, g, and h). 100 mV/s scan rate in 100 mM TBA PF<sub>6</sub> with SCE reference electrode.

peak at 0.1 V that disappears simultaneously with the lowering of the background current with subsequent cycles during CV, suggesting successful modification of the TPE electrodes. For both carbon types, there is not a significant Fe(CN)<sub>6</sub><sup>3-/4-</sup> redox peak after modification (Figure 6.3) . However, the before and after modification ferrocene CVs have the same peak height with a 10 mV increase in peak potential difference for both carbon types (Figure 6.4). The lack of Fe(CN)<sub>6</sub><sup>3-/4-</sup> detection with the ferrocene detection still intact suggests that the modification layer is thin (≤5

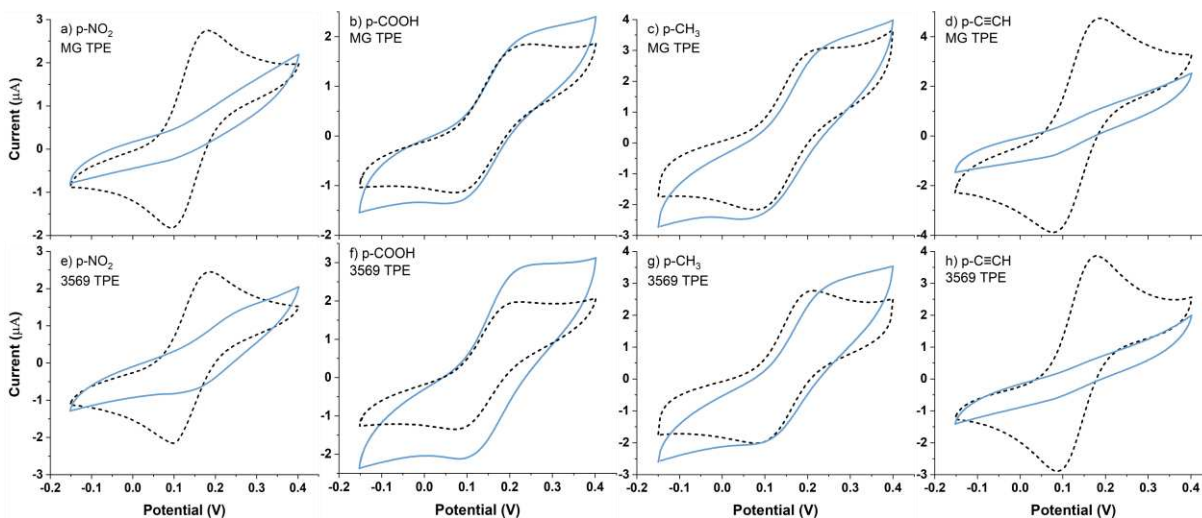


**Figure 6.3:** Grafting CVs of TPE modification in acetonitrile via aryl diazonium salt reduction with nitro- (a and e), carboxylic acid- (b and f), methyl- (c and g), and ethynyl (d and h) para substituents with two different carbon types, MG (a, b, c, and d) and 3569 (e, f, g, and h). 100 mV/s scan rate in 100 mM TBA PF<sub>6</sub> with SCE reference electrode.

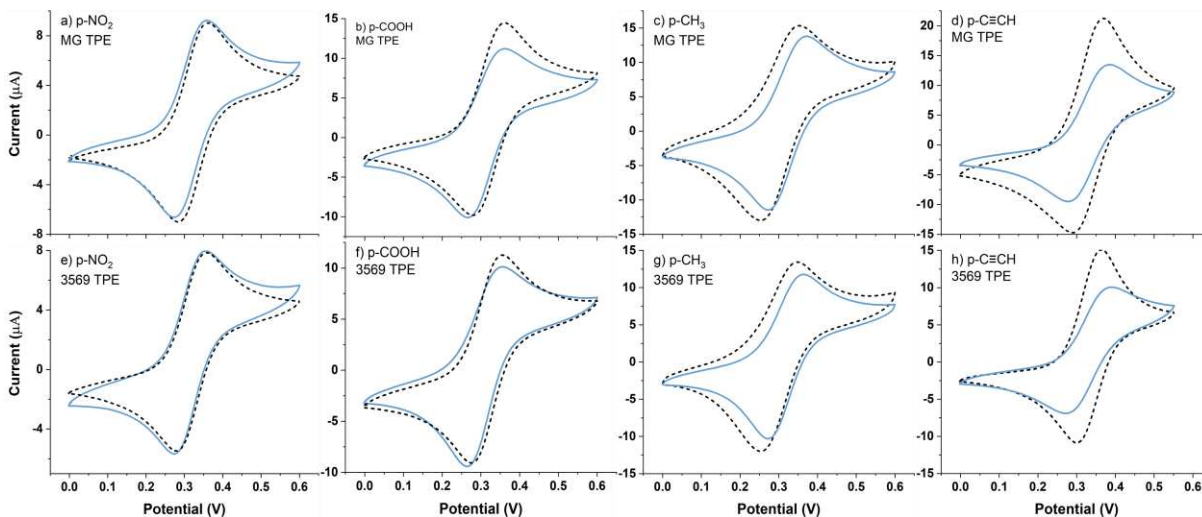


**Figure 6.4:** Ferrocene before and after TPE modification in acetonitrile via aryl diazonium salt reduction with nitro- (a and e), carboxylic acid- (b and f), methyl- (c and g), and ethynyl (d and h) para substituents with two different carbon types, MG (a, b, c, and d) and 3569 (e, f, g, and h). 100 mV/s scan rate in 100 mM KCl with SCE reference.

nm) because ferrocene is an outer sphere compound while  $\text{Fe}(\text{CN})_6^{3-/4-}$  exhibits inner sphere properties.<sup>55</sup> The GC electrode modified with the same method is unable to detect ferrocene or  $\text{Fe}(\text{CN})_6^{3-/4-}$  after modification indicating a thicker layer (Figure 6.5). The grafting difference between the GC and TPE is likely a result of the difference in surfaces, where the TPEs are

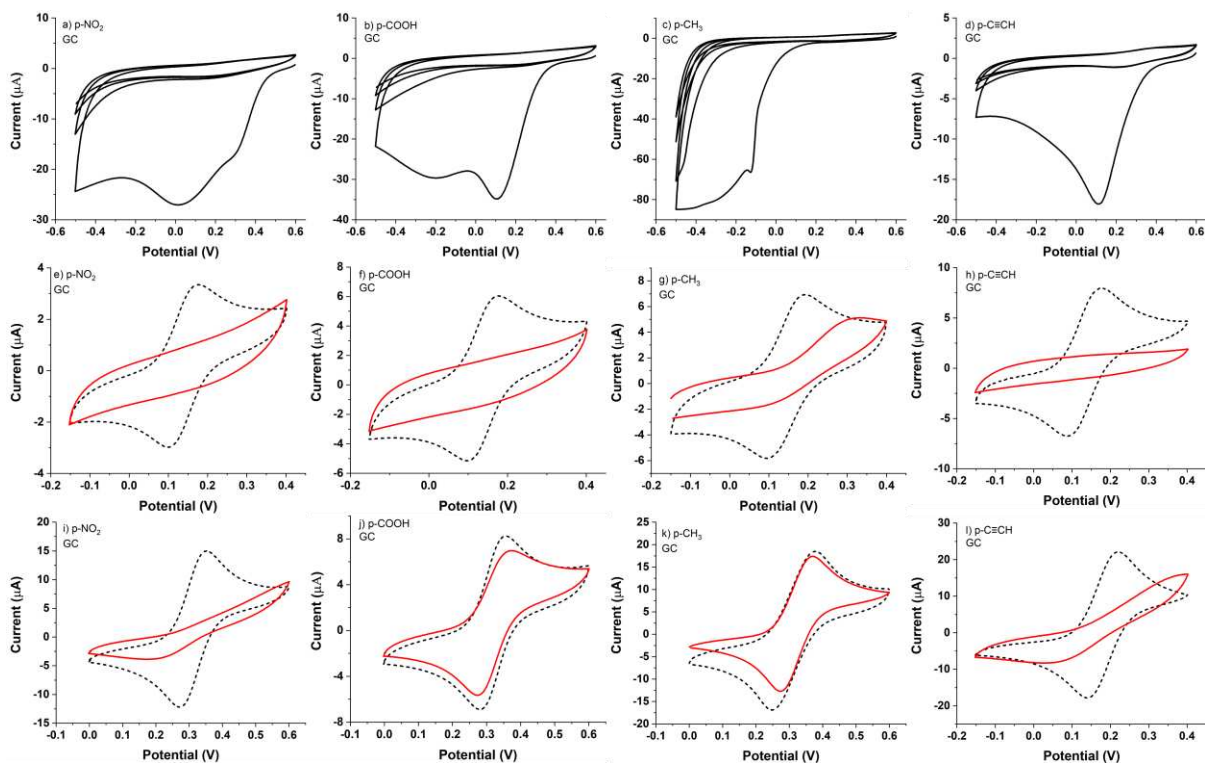


**Figure 6.5:** Grafting CVs (a, b, c, and d) of GC modification in acetonitrile via aryl diazonium salt reduction with nitro- (a, e, and i), carboxylic acid- (b, f, and j), methyl- (c, g, and k), and ethynyl (d, h, and l) para substituents. Modification with 100 mV/s scan rate in 100 mM TBA PF<sub>6</sub> with SCE reference electrode. Before and after modification CVs of Fe(CN)<sub>6</sub><sup>3-/4-</sup> (e, f, g, and h) and ferrocene (i, j, k, and l) in 100 mM KCl with 100 mV/s scan rate with SCE reference.

heterogeneous mixtures of plastic and carbon while the GC is uniform carbon. Post-modification CVs were also run to reduce the nitro group to an amino group (Figure 6.6) . The nitro group

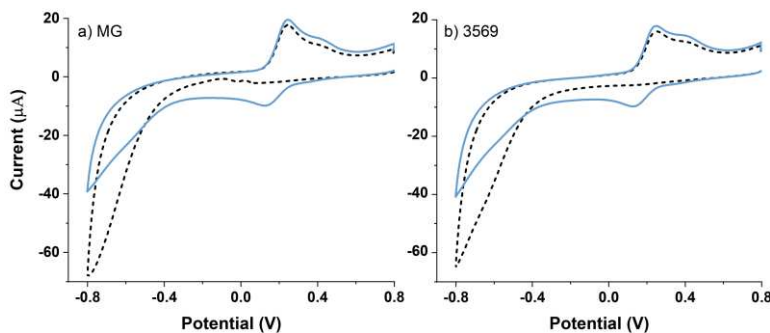


**Figure 6.6:** CVs (first cycle is dashed black, second cycle is blue) of p-nitro(benzene) modified electrodes with two carbon types: MG (a) and 3569 (b). 100 mV/s scan rate in 100 mM H<sub>2</sub>SO<sub>4</sub> with SCE reference.

reduction peak at 130 mV is not present during the first CV but is present in the second CV. The

oxidation peak at 250 mV with the introduction of the reduction peak at 130 mV matches with successful reduction of the nitro substituent to the amino substituent, further supporting successful nitro-aryl grafting.

Different modification results are seen with the p-carboxylic acid aryl diazonium salt. The diazonium electroreduction CVs for both carbon types show two peaks at 70 and -250 mV in the first cycle, and then on subsequent cycles, the peaks disappear and the background current is lower (Figure 6.2). For both TPEs, the  $\text{Fe}(\text{CN})_6^{3-/4-}$  redox peaks lose definition and the background appears to become more resistive (Figure 6.3), which may be a result of the  $\text{Fe}(\text{CN})_6^{3-/4-}$  interaction with the carboxylic acid groups, which are deprotonated at the neutral pH. Unlike with the nitro-aryl modification, the ferrocene peak currents were reduced by about two-thirds for the MG (or one-third for the 3569 carbon) for both oxidation and reduction accompanied by a 20 mV peak potential increase (Figure 6.4). The ferrocene signal persists but not the  $\text{Fe}(\text{CN})_6^{3-/4-}$ , which likely means that the modification layer is also thin ( $\leq 5$  nm) in areas and thicker in other areas because ferrocene, unlike  $\text{Fe}(\text{CN})_6^{3-/4-}$ , is not surface sensitive. The peak shape does not become sigmoidal, as seen with microelectrodes, which suggests that the areas with thin coverage are larger (tens of  $\mu\text{m}$ -scale).

Modification results similar to the p-carboxylic acid aryl diazonium are seen with the p-methyl- and p-ethynyl aryl diazonium. The p-carboxylic acid aryl electroreduction CV shows a peak at -200 mV that is still present during the subsequent reduction cycle (Figure 6.2). The peak and background current are both lower with each CV cycle. The effects of reducing the diazonium salt can be seen in the ferrocene and  $\text{Fe}(\text{CN})_6^{3-/4-}$  CVs. For both MG and 3569 carbon types, a clear  $\text{Fe}(\text{CN})_6^{3-/4-}$  peak is not present after TPE modification (Figure 6.3), but the ferrocene peak is still present with a one-fourth lower reduction peak current (Figure 6.4). The ferrocene peak potential

difference is the same before and after modification with each carbon type. For the p-ethynyl aryl modification,  $\text{Fe}(\text{CN})_6^{3-/4-}$  detection for both carbon types is non-existent after modification (Figure 6.3). Ferrocene peak height is also mitigated by about one-third for both carbon types (Figure 6.4), accompanied by a 30 mV peak potential difference increase for the MG TPE and a 50 mV increase for the 3569 TPE. Based on the similar  $\text{Fe}(\text{CN})_6^{3-/4-}$  and ferrocene data, it is likely that the p-methyl and p-ethynyl aryl modification layer is similar in structure to the p-carboxylic acid aryl layer, where the resulting grafted layer has varying thicknesses. The surface coverage variation is not surprising given TPEs heterogeneous surface of plastic and carbon. The layer thicknesses and variation within the layer is consistent with literature values using similar electroreduction conditions.<sup>27,56</sup>

To better understand the grafted layer,<sup>57-59</sup> before and after SECM images of the p-carboxylic acid aryl modified TPEs were taken with ferrocene,  $\text{Fe}(\text{CN})_6^{3-/4-}$  in a pH neutral solution, and  $\text{Fe}(\text{CN})_6^{3-/4-}$  in an acidic solution. The SECM images are shown in Figure 6.7. The  $\text{Fe}(\text{CN})_6^{3-/4-}$  redox couple is sensitive to surface oxides and has slower electron transfer kinetics with increasing pH attributed to the electrostatic repulsion between the surface bound carboxylate and the negatively charged redox couple.<sup>55,60,61</sup> Ferrocene is not sensitive to surface oxides and is good for comparison with the bulk solution measurements. For both MG and 3569 carbon types, ferrocene normalized current from the image decreased after modification (Figure 6.8), 1.21 to 0.87 for MG carbon and 1.47 to 1.07 for 3569 carbon, which is comparable to the bulk solution CVs. The 3569 carbon was more variable electroactive surface than MG before modification, as seen by the 0.146 and 0.002 RMS values, respectively. Both carbon types have similar RMS values (0.001 for MG and 0.003 for 3569) after modification though.  $\text{Fe}(\text{CN})_6^{3-/4-}$  normalized current in the neutral solution also decreased after modification for both carbon types, 0.88 to 0.63 for MG

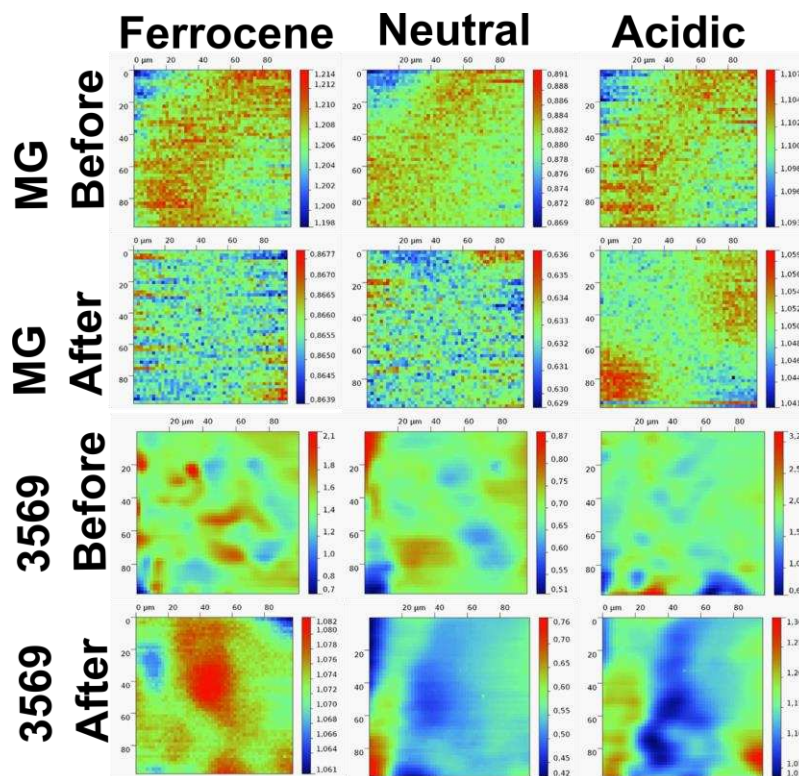


**Figure 6.7:** SECM images from before and after p-carboxylic acid aryl modification using ferrocene in 100 mM KCl,  $\text{Fe}(\text{CN})_6^{3-/4-}$  in 100 mM KCl (neutral),  $\text{Fe}(\text{CN})_6^{3-/4-}$  in 100 mM  $\text{H}_2\text{SO}_4$  (acidic). Values are current normalized by the limiting current.

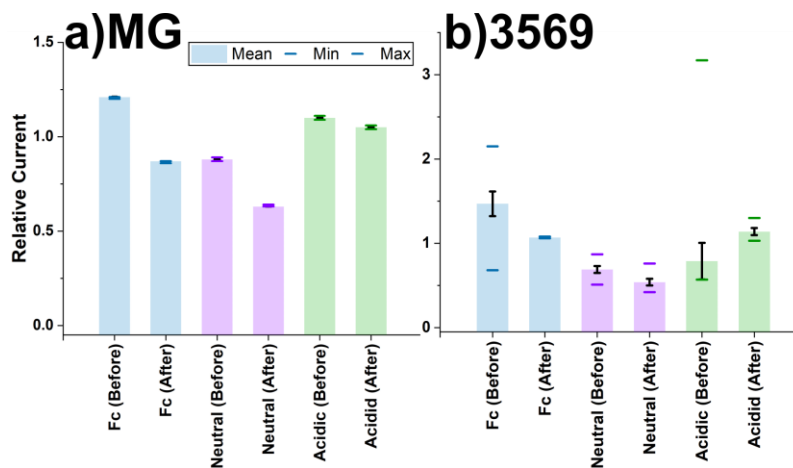


**Figure 6.8:** SECM image results from before and after p-carboxylic acid aryl modification using ferrocene in 100 mM KCl (Fc),  $\text{Fe}(\text{CN})_6^{3-/4-}$  in 100 mM KCl (neutral), and  $\text{Fe}(\text{CN})_6^{3-/4-}$  in 100 mM  $\text{H}_2\text{SO}_4$  (acidic). Relative current is the current normalized by the infinite current ( $i/i_{\text{inf}}$ ).

and 0.69 to 0.54 for 3569. In the acidic solution,  $\text{Fe}(\text{CN})_6^{3-/4-}$  normalized current values remained about the same or increased after modification with the p-carboxylic acid aryl layer. The MG TPE

was 1.10 (0.002 RMS) before modification and 1.05 (0.002 RMS) after modification. The 3569 TPE was 0.79 (0.217 RMS) before and 1.14 (0.042 RMS) after modification. The decrease in RMS values, along with the images, support the hypothesis that the grafted areas of a thin layer are larger ( $\mu\text{m}$  scale).

Finally, as a proof of concept, click chemistry was used to couple azidomethylferrocene with the p-ethynylphenyl modified TPE.<sup>53</sup> The post-functionalization CVs of each carbon TPE type are shown in Figure 6.9. By integrating the electrochemical current, the surface concentration

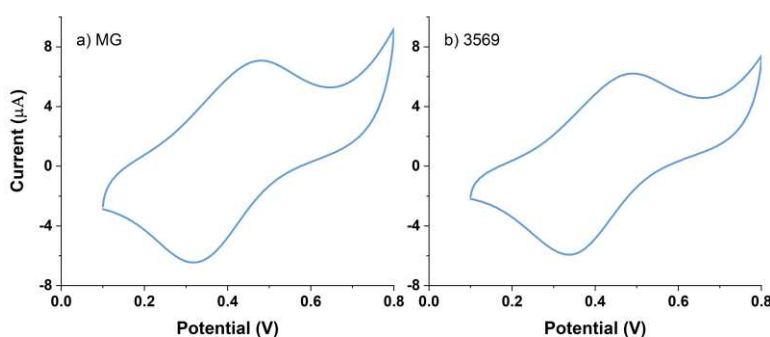


**Figure 6.9:** CVs of Fc-modified TPEs via click chemistry of two carbon types: (a) MG and (b) 3569. 100 mV/s scan rate in 50 mM KCl with SCE reference.

value of ferrocene moieties,  $\Gamma_{\text{Fc}}$ , was calculated to be  $4.3 \cdot 10^{-10} \text{ mol} \cdot \text{cm}^{-2}$  for the MG carbon and  $3.8 \cdot 10^{-10} \text{ mol} \cdot \text{cm}^{-2}$  for the 3569 carbon. The peak potential differences were 140 mV and 130 mV for MG and 3569 carbons, respectively. The different surface concentrations cause is unclear because the p-ethynyl aryl diazonium salt grafting results, as seen with  $\text{Fe}(\text{CN})_6^{3-/4-}$  and ferrocene redox couples, were similar with both carbon types. The two surface concentration values are close to the maximum possible surface concentration ( $4.5 \cdot 10^{-10} \text{ mol} \cdot \text{cm}^{-2}$ ).<sup>62</sup> Both surface concentrations are larger than those achieved with a GC electrode ( $2.2 \cdot 10^{-10} \text{ mol} \cdot \text{cm}^{-2}$ ) via the same method.<sup>53</sup>

## Conclusion

The presented work fabricated a carbon composite TPEs that has a broader range of solvent compatibility than previous TPEs, thus combining TPEs high electrochemical performance, low

cost, and easy fabrication with a broader range of viable electrochemistry. The TPE surfaces were successfully modified for the first time with various aryl diazonium salts using electroreduction. Post-functionalization click chemistry of the TPEs was then successful using a ferrocene moiety, showing that other click chemistry is possible in future studies and applications.

## REFERENCES

1. G. Zhao, H. Wang and G. Liu, *Int. J. Electrochem. Sci*, 2017, **12**, 8622-8641.
2. A. Ambrosi, C. K. Chua, N. M. Latiff, A. H. Loo, C. H. A. Wong, A. Y. S. Eng, A. Bonanni and M. Pumera, *Chem. Soc. Rev.*, 2016, **45**, 2458-2493.
3. I. Švancara, K. Vytrás, K. Kalcher, A. Walcarius and J. Wang, *Electroanalysis*, 2009, **21**, 7-28.
4. R. N. Adams, *Anal. Chem.*, 1958, **30**, 1576-1576.
5. K. Kalcher, J. M. Kauffmann, J. Wang, I. Švancara, K. Vytrás, C. Neuhold and Z. Yang, *Electroanalysis*, 1995, **7**, 5-22.
6. I. Švancara, A. Walcarius, K. Kalcher and K. Vytrás, *Open Chemistry*, 2009, **7**, 598-656.
7. C. Petit, A. Gonzalez-Cortes and J.-M. Kauffmann, *Talanta*, 1995, **42**, 1783-1789.
8. J. Wang and N. Naser, *Anal. Chim. Acta*, 1995, **316**, 253-259.
9. P. H. M. Buzzetti, G. C. de Oliveira, A. L. M. Azevedo, R. C. Michel, E. A. Ponzio and F. S. Semaan, *Advances in materials science research*, 2015, **21**, 1-23.
10. H. P. Henriques and A. G. Fogg, *Analyst*, 1984, **109**, 1195-1199.
11. J. Wang and M. Musameh, *Anal. Chem.*, 2003, **75**, 2075-2079.
12. M. Perween, D. B. Parmar, G. R. Bhadu and D. N. Srivastava, *Analyst*, 2014, **139**, 5919-5926.
13. A. Regel and S. Lunte, *Electrophoresis*, 2013, **34**, 2101-2106.
14. K. J. Klunder, Z. Nilsson, J. B. Sambur and C. S. Henry, *J. Am. Chem. Soc.*, 2017, **139**, 12623-12631.
15. E. Noviana, K. J. Klunder, R. B. Channon and C. S. Henry, *Anal. Chem.*, 2019, **91**, 2431-2438.
16. A. J. Bard, *Journal*, 1983.
17. C. Cao, Y. Zhang, C. Jiang, M. Qi and G. Liu, *ACS Applied Materials & Interfaces*, 2017, **9**, 5031-5049.
18. J. J. Gooding, *Electroanalysis: An International Journal Devoted to Fundamental and Practical Aspects of Electroanalysis*, 2008, **20**, 573-582.
19. S. Mahouche-Chergui, S. Gam-Derouich, C. Mangeney and M. M. Chehimi, *Chem. Soc. Rev.*, 2011, **40**, 4143-4166.
20. M. Delamar, R. Hitmi, J. Pinson and J. M. Saveant, *J. Am. Chem. Soc.*, 1992, **114**, 5883-5884.
21. A. Adenier, N. Barré, E. Cabet-Deliry, A. Chaussé, S. Griveau, F. Mercier, J. Pinson and C. Vautrin-UI, *Surf. Sci.*, 2006, **600**, 4801-4812.
22. P. Allongue, M. Delamar, B. Desbat, O. Fagebaume, R. Hitmi, J. Pinson and J.-M. Savéant, *J. Am. Chem. Soc.*, 1997, **119**, 201-207.
23. K. Boukerma, M. M. Chehimi, J. Pinson and C. Blomfield, *Langmuir*, 2003, **19**, 6333-6335.
24. T. Breton and D. Bélanger, *Langmuir*, 2008, **24**, 8711-8718.
25. D.-e. Jiang, B. G. Sumpter and S. Dai, *The Journal of Physical Chemistry B*, 2006, **110**, 23628-23632.
26. D.-e. Jiang, B. G. Sumpter and S. Dai, *J. Am. Chem. Soc.*, 2006, **128**, 6030-6031.
27. J. K. Kariuki and M. T. McDermott, *Langmuir*, 2001, **17**, 5947-5951.

28. P. Hapiot, C. Lagrost and Y. R. Leroux, *Current Opinion in Electrochemistry*, 2017.
29. J. Ghilane, P. Martin, O. Fontaine, J.-C. Lacroix and H. Randriamahazaka, *Electrochem. Commun.*, 2008, **10**, 1060-1063.
30. O. Fontaine, J. Ghilane, P. Martin, J.-C. Lacroix and H. Randriamahazaka, *Langmuir*, 2010, **26**, 18542-18549.
31. A. Adenier, E. Cabet-Deliry, A. Chaussé, S. Griveau, F. Mercier, J. Pinson and C. Vautrin-UI, *Chem. Mater.*, 2005, **17**, 491-501.
32. Y. Pan, B. Tong, J. Shi, W. Zhao, J. Shen, J. Zhi and Y. Dong, *The Journal of Physical Chemistry C*, 2010, **114**, 8040-8047.
33. G. G. Via, C. L. Shugart, S. L. Melnyk, S. R. Hupman and K. K. Cline, *Electroanalysis*, 2018, **30**, 2421-2426.
34. F. Anariba, S. H. DuVall and R. L. McCreery, *Anal. Chem.*, 2003, **75**, 3837-3844.
35. S. Baranton and D. Bélanger, *The Journal of Physical Chemistry B*, 2005, **109**, 24401-24410.
36. C. Saby, B. Ortiz, G. Y. Champagne and D. Bélanger, *Langmuir*, 1997, **13**, 6805-6813.
37. L. Civit, H. M. Nassef, A. Fragozo and C. K. O'Sullivan, *J. Agric. Food. Chem.*, 2008, **56**, 10452-10455.
38. A. Hayat, L. Barthelmebs, A. Sassolas and J.-L. Marty, *Talanta*, 2011, **85**, 513-518.
39. J.-P. Jasmin, K. Ouhenia-Ouadahi, F. Miserque, E. Dumas, C. Cannizzo and A. Chaussé, *Electrochim. Acta*, 2016, **200**, 115-122.
40. M. Alonso-Lomillo, C. Yardimci, O. Domínguez-Renedo and M. Arcos-Martínez, *Anal. Chim. Acta*, 2009, **633**, 51-56.
41. W. H. Binder and R. Sachsenhofer, *Macromol. Rapid Commun.*, 2007, **28**, 15-54.
42. W. H. Binder and R. Sachsenhofer, *Macromol. Rapid Commun.*, 2008, **29**, 952-981.
43. J. E. Moses and A. D. Moorhouse, *Chem. Soc. Rev.*, 2007, **36**, 1249-1262.
44. H. Nandivada, X. Jiang and J. Lahann, *Adv. Mater.*, 2007, **19**, 2197-2208.
45. W. Xi, T. F. Scott, C. J. Kloxin and C. N. Bowman, *Adv. Funct. Mater.*, 2014, **24**, 2572-2590.
46. H. Li, F. Cheng, A. M. Duft and A. Adronov, *J. Am. Chem. Soc.*, 2005, **127**, 14518-14524.
47. A. Cernat, M. Tertis, C. Cristea and R. Sandulescu, *Int. J. Electrochem. Sci*, 2015, **10**, 6324-6337.
48. F. Kong and Y. F. Hu, *Anal. Bioanal. Chem.*, 2012, **403**, 7-13.
49. D. Polcari, P. Dauphin-Ducharme and J. Mauzeroll, *Chem. Rev.*, 2016, **116**, 13234-13278.
50. S. Lhenry, Y. R. Leroux and P. Hapiot, *Anal. Chem.*, 2013, **85**, 1840-1845.
51. O. Sklyan, G. Wittstock, C. Nunes Kirchner and A. Leash, *Journal*.
52. D. Nečas and P. Klapetek, *Open Physics*, 2012, **10**, 181-188.
53. Y. R. Leroux, H. Fei, J.-M. Noël, C. Roux and P. Hapiot, *J. Am. Chem. Soc.*, 2010, **132**, 14039-14041.
54. P. S. Nunes, P. D. Ohlsson, O. Ordeig and J. P. Kutter, *Microfluidics and nanofluidics*, 2010, **9**, 145-161.
55. P. Chen and R. L. McCreery, *Anal. Chem.*, 1996, **68**, 3958-3965.
56. M. M. Chehimi, *Aryl diazonium salts: new coupling agents in polymer and surface science*, John Wiley & Sons, 2012.
57. M. Pellissier, D. Zigah, F. Barrière and P. Hapiot, *Langmuir*, 2008, **24**, 9089-9095.
58. P.-Y. Blanchard, T. Sun, Y. Yu, Z. Wei, H. Matsui and M. V. Mirkin, *Langmuir*, 2016, **32**, 2500-2508.

59. C. Lagrost, Y. Leroux and P. Hapiot, *Electroanalysis*, 2016, **28**, 2680-2687.
60. P. Chen, M. A. Fryling and R. L. McCreery, *Anal. Chem.*, 1995, **67**, 3115-3122.
61. R. L. McCreery, *Chem. Rev.*, 2008, **108**, 2646-2687.
62. K. Seo, I. C. Jeon and D. J. Yoo, *Langmuir*, 2004, **20**, 4147-4154.

## CHAPTER 7. CONCLUSION

There is a need to improve detection of environmental risk factors that affect human health. With improved detection of the risk factors, the millions of deaths and illnesses each year could be prevented. Large-scale pollution studies are needed for prevention but are often inhibited by the expense and slow turnaround time for data acquisition. Cheaper, faster, and easier assays were developed here that will help enable larger scale pollution studies to improve unsafe water and air pollution measurements. Electroanalytical chemistry with carbon electrodes was chosen for these measurements because of the reliability as an analytical method and carbon's low cost. Before the work here, carbon electrodes had significant limitations, which decrease the amount of possible applications that would benefit from the low cost and ease of use. The amount of potential applications was increased here for high performing carbon electrodes through fundamental characterization and subsequent modification.

Stencil printed carbon electrodes, made from commercially available carbon ink/graphite stenciled onto transparency film, were fabricated to determine Mn(II) content with an electrochemical technique, cathodic stripping voltammetry (CSV).<sup>1</sup> It has the advantages of being simple, economical, and suitable for field measurements with a detection limit as low as 500 nM (30 ppb) Mn. Measured manganese concentrations using this technique agreed with a traditional atomic absorbance spectroscopy method for two tea and yerba mate samples. The method is, however, susceptible to interferences from Al(III), Cu(II), Fe(II), and Pb(II), which are other common heavy metals found in water supplies. Before the Mn(II) assay developed here, Mn(II) assays had limited usage as they were expensive, not suitable for the field, and/or not sensitive enough. The developed Mn(II) assay here is inexpensive, disposable, portable, and sensitive with

low detection limits, which will increase the number of Mn(II) measurements and thus prevention of Mn(II) toxicity.

While homemade stencil printed electrodes are easy to fabricate for a laboratory with electrochemical equipment, it is not as straightforward for laboratories without that equipment. Commercially available stencil printed carbon electrodes were used with the dithiothreitol (DTT) assay for PM<sub>2.5</sub> oxidative potential analysis.<sup>2</sup> The system was validated through comparison to the UV/vis assay, and this work is the first time, to our knowledge, that the electrochemical DTT assay has been applied to a large sample size (211 samples). The time and labor was reduced by using an end-point assay instead of the kinetic assay. The end-point electrochemical assay presented here increases the sample throughput to five samples per hour. The electrochemical DTT assay with commercially available equipment will encourage more laboratories to use this higher throughput assay that requires less materials, enabling more PM<sub>2.5</sub> measurements to be performed, which will inform researchers on PM<sub>2.5</sub> human health effects.

The sample throughput of the DTT assay was further increased to six samples per hour while reducing reagent costs and manual labor with a custom carbon composite thermoplastic electrode (TPE) and HPLC autosampler. A TPE (a high performing and inexpensive carbon electrode) was used instead of the commercially available stencil printed carbon electrode because it enabled twice the sample throughput rate, also while allowing a 40% cost reduction of consumable products, which helps enable large-scale air pollution studies to be performed. During the assay development, it was discovered that the TPE's response changed over time, so further investigation was warranted. The semi-automated DTT assay will have a significant impact on the field because it will help enable large-scale PM<sub>2.5</sub> air pollution studies to directly research how PM<sub>2.5</sub> affects human health.

A thorough local electrochemical characterization using scanning electrochemical microscopy (SECM) was then successfully performed of carbon composite TPEs that have high electrochemical activity while being easy to fabricate and pattern. The TPE electrodes behave as a network of interactive diffusion microelectrode with high active islands isolated by less active areas. There were not significant differences between PMMA and COC thermoplastic TPEs, suggesting that either thermoplastic is a viable option and the choice between either should depend on a different factor, e.g. fabrication ease or application. There were, however, significant changes observed over time with TPEs made with PCL. Knowing the mechanism of how TPEs behave will enable future work to easily optimize their performance, making them more accessible for many different electroanalytical techniques.

Since surface modification is often required for desired sensitivity and/or selectivity for an analyte of interest, the high performing and low cost TPEs were then modified to have a broader range of viable applications. In order to be modified, however, the TPEs must be non-aqueous solvent compatible, and the TPE template was changed to glass. The TPE surfaces were successfully modified for the first time with various aryl diazonium salts using electroreduction. Post-functionalization click chemistry of the TPEs was then successful using a ferrocene moiety, showing that other click chemistry is possible in future studies and applications. TPEs have the potential of becoming widely used for many applications. TPEs becoming widely used in electroanalytical techniques would enable more measurements, including large scale pollution measurements, to be done because they are cheap, simple, and sensitive electrodes.

### **Future Directions**

Even though the research here made progress towards environmental health risk detection, improvements are still needed. Increased spatiotemporal resolution would increase knowledge to

prevent personal exposure. Great strides have been made to fabricate personal exposure air quality monitors with increased spatiotemporal resolution<sup>3-6</sup> and development towards small and portable analytical devices for heavy metal personal exposure monitoring.<sup>7,8</sup> Research and development of these products still needs to continue to create an inexpensive, user-friendly commercial product.

As PM oxidative potential assays are a relatively new concept (about 20 years old), there are several improvements to be made as well. There are many procedural inconsistencies between laboratories that prevent a uniform assay from being used. This is partially due to the constant ongoing research that is being done to discover the best oxidative potential assay. Another possible improved oxidative potential assay is proposed in Appendix 2. The assay would more directly measure hydroxyl radical formation. Once the PM oxidative potential assay is streamlined, air quality regulations can evaluate oxidative potential as well for a more accurate health prediction.

Even though carbon electrodes have been long established for electrochemistry, new variations of carbon composites, including carbon paste, electrodes are constantly being developed. TPEs are a very promising carbon composite electrode, but they are also in the infancy of development. More research needs to be performed to make consistent electrodes between users, as well as exploring different plastic types and applications.

## REFERENCES

1. K. E. Berg, J. A. Adkins, S. E. Boyle and C. S. Henry, *Electroanalysis*, 2016, **28**, 679-684.
2. K. E. Berg, L. R. Turner, M. L. Benka-Coker, S. Rajkumar, B. N. Young, J. L. Peel, M. L. Clark, J. Volckens and C. S. Henry, *Aerosol Sci. Technol.*, 2019, 1-8.
3. C. Quinn, D. D. Miller-Lionberg, K. J. Klunder, J. Kwon, E. M. Noth, J. Mehaffy, D. Leith, S. Magzamen, S. K. Hammond and C. S. Henry, *Environmental science & technology*, 2018, **52**, 11267-11275.
4. J. Volckens, C. Quinn, D. Leith, J. Mehaffy, C. S. Henry and D. Miller - Lionberg, *Indoor air*, 2017, **27**, 409-416.
5. J. Gulliver and D. Briggs, *Atmos. Environ.*, 2004, **38**, 1-8.
6. S. Steinle, S. Reis and C. E. Sabel, *Sci. Total Environ.*, 2013, **443**, 184-193.
7. W. Yantasee, Y. Lin, K. Hongsirikarn, G. E. Fryxell, R. Addleman and C. Timchalk, *Environ. Health Perspect.*, 2007, **115**, 1683-1690.
8. Y. Yang, E. Noviana, M. P. Nguyen, B. J. Geiss, D. S. Dandy and C. S. Henry, *Anal. Chem.*, 2016, **89**, 71-91.

## APPENDIX 1. MONITORING REACTION KINETICS WITH INFRARED SPECTROSCOPY IN MICROFLUIDIC DEVICES

### Appendix Overview

Microfluidics can bring low material consumption and automation advantages to traditionally laborious and expensive kinetic studies of organic reactions. Infrared (IR) spectroscopy can be used as a qualitative and quantitative detection motif; however, IR spectroscopy is not integrated with traditional microfluidic devices due to strong IR absorption of the materials. The devices also have limited organic-solvent compatibility. This work reports the efforts towards fabricating microfluidic devices with IR-transparent calcium fluoride and various optically thin polymers to enable better tracking of organic reaction kinetics. Due to difficulty in organic solvent-compatible device fabrication, kinetics of various aqueous reactions were monitored as model systems. Dr. Scott Noblitt collaborated on this project.

### Introduction

Chemical kinetic studies are significant because they yield valuable reaction information. Understanding reaction kinetics can provide optimized reaction conditions to improve future experimental setups. The studies also offer mechanistic insight, which helps further the understanding of the fundamental reaction chemistry, aiding in future research endeavors.<sup>1-7</sup> While kinetic studies have great value, there is also a large time, labor, and material investment necessary to carry out these experiments. For example, a traditional optimization study of a small-molecule organic synthesis can use grams of starting materials, a liter or more of solvent, and over a month of investigation. However, reducing the amount of materials consumed and labor required of these studies can be achieved through the use of microfluidic devices.

Microfluidics can lower the cost of kinetic studies by reducing the quantity of material required and hazardous waste generated, while achieving analogous results.<sup>1,8,9</sup> For example, one report showed a 52-fold improvement in both substrate and enzyme consumption when downscaling from traditional laboratory methods to a microfluidic approach using ultra-violet (UV) detection.<sup>9</sup> The reactor volumes decreased by a factor of 261 when utilizing a microfluidic device as compared to the similar batch process in a 30-mL flask. In conclusion, comparable results between the flask and microfluidic setup were achieved showing accuracy can be retained during the scale-down of a system. Unfortunately, UV detection, along with visible light and fluorescence, has limited utility with respect to monitoring reaction kinetics because electronic transitions are analyzed. As a result, only molecules with substantial changes (often only model systems) can be tracked using these optical methods.

One detection method that can provide more explicit chemical information and can be utilized with microfluidics is infrared (IR) spectroscopy, which probes bond vibrations. IR spectroscopy has the inherent advantages of being both qualitative and quantitative. It aids in chemical identification through the correspondence of particular functional groups to given light frequencies. Concentrations of chemicals can be ascertained through the Beer-Lambert law:

$$A = -\log\left(\frac{T}{T_o}\right) = \epsilon bc$$

where  $A$  is absorbance at a given wavelength measured by relative transmittance,  $T/T_o$ , which is related to concentration,  $c$  (mol/L), at a given pathlength,  $b$  (cm, typically defined by the channel height in transmission IR microfluidic applications), and molar absorptivity,  $\epsilon$  (L/mol·cm, intrinsic molecular property). Combining IR microscopy with microfluidics can yield simultaneous spatial and temporal resolution. Spatial resolution can be achieved within the microfluidic channel by employing a focal plane array (FPA) detector, a two-dimensional image sensor containing

detection elements sensitive to IR radiation. Temporal resolution within the microfluidic device can be achieved by scanning distinct positions along the channel. These positions correspond to various residence times ( $\tau$ ), calculated from the channel volume ( $V$ ) divided by the flow rate ( $Q$ ). The goal of the research project is to use microfluidic devices to monitor the kinetics of organic reactions *in situ* using IR absorbance spectroscopy. The principal challenge is that most traditional microfluidic device substrates (e.g. glass and plastics) used to fabricate devices are not IR transparent. One solution to this problem is to fabricate devices with substrates that are inherently IR transparent, such as calcium fluoride.<sup>10</sup>  $\text{CaF}_2$  also has the advantage of being inert towards a wide range of chemicals, with the exception of strong acids.<sup>11</sup> However, device fabrication methods using solely  $\text{CaF}_2$  are uncommon. Previously fabricated microfluidic devices contain another material combined with the  $\text{CaF}_2$ , such as waxes and photoresists, to define the channel pattern.<sup>12-14</sup> Although these additional materials facilitate the fabrication of a  $\text{CaF}_2$  device, the chemical compatibility is more limited, and in some cases, the temperature compatibility is problematic.

Another solution for constructing IR-transparent devices is to use optically thin (typically <100  $\mu\text{m}$ ) layers of traditionally IR-incompatible materials (Figure A1.1).<sup>15,16</sup> This approach is

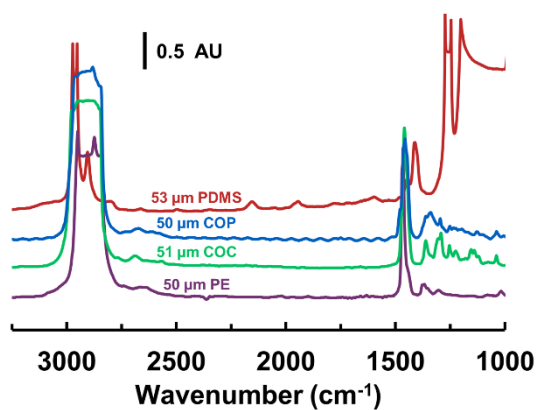


**Figure A1.1:** IR spectra of various polymers: poly(dimethylsiloxane) (PDMS), cyclic olefin polymer (COP), cyclic olefin copolymer (COC), and polyethylene (PE).

appealing because it can be achieved using common fabrication methods such as soft lithography. IR spectra of some materials: poly(dimethylsiloxane) (PDMS), cyclic olefin copolymer (COC), cyclic olefin polymer (COP), and polyethylene (PE), are shown here. PDMS is attractive due to low cost and facile fabrication but can be swollen by organic solvents,<sup>17</sup> and COC and COP are soluble in many common nonpolar solvents.

The initial goal was to develop methods for generating several types of IR-transparent devices. Using one of these systems (thin PDMS), kinetics of aqueous reactions were monitored. The long-term goal was to perform chemical kinetic studies of a broad range of organic reactions using IR microscopy.

## **Experimental**

All IR measurements were taken with a Bruker Hyperion 3000 IR microscope, equipped with two detectors: a single-element mercury cadmium telluride (MCT) and an FPA. The FPA consists of a  $64 \times 64$  pixel array over a  $170 \mu\text{m} \times 170 \mu\text{m}$  area.

### *This PDMS Devices*

The molds were made by standard lithography techniques,<sup>18</sup> which include developing a negative photoresist, SU-8, onto a silicon wafer with UV light through a patterned mask. PDMS (10:1 oligomer: curing agent) was spin coated onto the patterned mold to be less than  $50 \mu\text{m}$  thick. A thicker (few millimeters) piece of PDMS with a window cut out of it was plasma bonded to the thin PDMS for structural support before removing the PDMS from the silicon wafer. The same was done with PDMS onto a blank silicon wafer. Once inlet and outlet tubing holes were punched through the patterned PDMS, channels were sealed by plasma bonding both thin PDMS sides together.<sup>19</sup> This yields a device with IR transparency through the thin PDMS window (Figure A1.2).

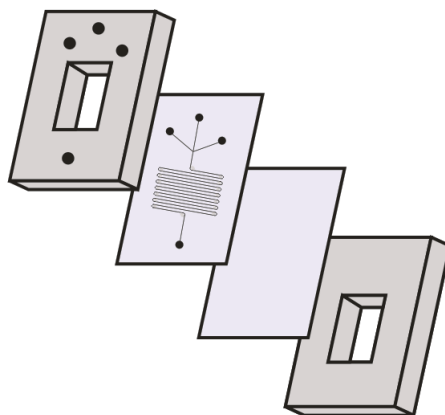


**Figure A1.2:** Fabrication scheme of thin PDMS device. Shown is 500 mm long serpentine channel design.

### *Thin Thermoplastic Devices*

The SU-8 molds on silicon wafers were fabricated as described previously. COC or COP were hot embossed with the mold pattern by heating to 105 °C or 165 °C, respectively, at 500 psi for 30 minutes using a heated press. Inlet and outlet holes were then punched through the patterned COC or COP. For devices with straight, short channels (less than 60 mm), the channels could be sealed to a “blank” (unmolded) piece of COC by putting the two pieces together through a laminator with a temperature of at least 170 °C. This procedure resulted in improper sealing in devices that had longer channels than about 60 mm. To address the improper sealing, attempts were made to thermally bond the device by varying the heat source, pressure, and time. Molds with outgassing channels were also attempted (thick, straight lines surrounding the microfluidic channels). Attempts to chemically bond COC were attempted with various combinations of hexane, toluene, and their vapors. These attempts did not result in a properly sealed device, and therefore, no reactions were run in these devices. It was also attempted to thermally bond PP membranes (51  $\mu\text{m}$  thick) and PE (14-100  $\mu\text{m}$  thick) in a manner similar to above, but these efforts also did not yield a properly sealed device. Further investigation into thin thermoplastic devices was discontinued.

## CaF<sub>2</sub> Devices

CaF<sub>2</sub> devices were fabricated by melting a polymer with a channel design cut out between two CaF<sub>2</sub> wafers, one of which contained drilled inlet and outlet holes (Figure A1.3). The polymer

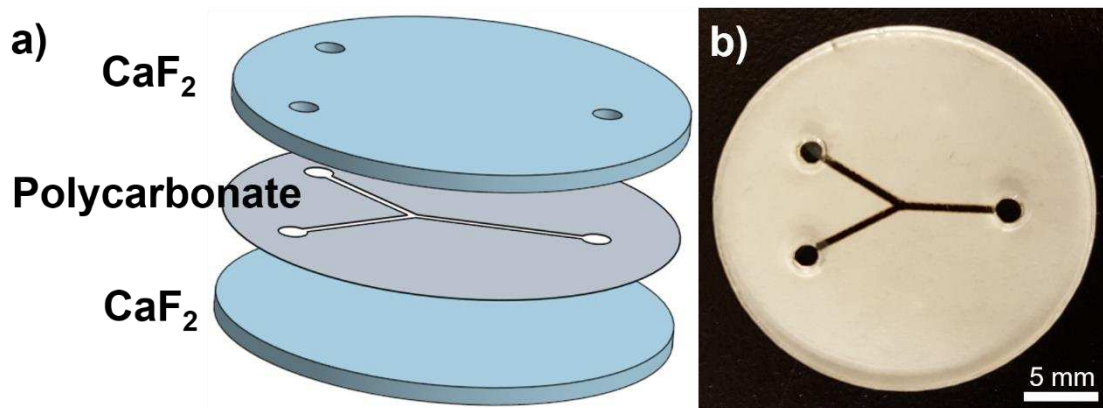


**Figure A1.3:** Device fabrication of polycarbonate membrane sandwiched between two CaF<sub>2</sub> windows. a) Schematic and b) completed device picture with a Y-channel.

used successfully was COC. COC, 50.8 to 140  $\mu\text{m}$ , was cut using a commercial craft cutter. Only straight and Y-shaped channels were successful due to the craft cutter's precision. Shorter channel lengths are also limited by the fragility of the thin polymer. Brief attempts using polycarbonate (PC) membranes, PP, and PE, separately, were also done, but they did not form a seal while simultaneously maintaining channel integrity between the CaF<sub>2</sub> wafers.

## Results and Discussion

### *PDMS Device Characterization*

Preliminary work began with PDMS devices because of their well-known, simple fabrication. A thin PDMS device with channel dimensions of 500 mm long x 200  $\mu\text{m}$  wide x 35  $\mu\text{m}$  tall was fabricated. When fluid was flowed through the channel, the channels became distorted, increasing in height from increasing back pressure. Specifically, a 60% increase in average height was observed from a less than 5-psi difference. Intensity maps from the integration of the water peak (1930-2470  $\text{cm}^{-1}$ ) at various distances along the channel are shown with a total flow rate of

3  $\mu\text{L}/\text{min}$  (Figure A1.4). Another perspective of this distortion can be seen in Figure A1.5, in which

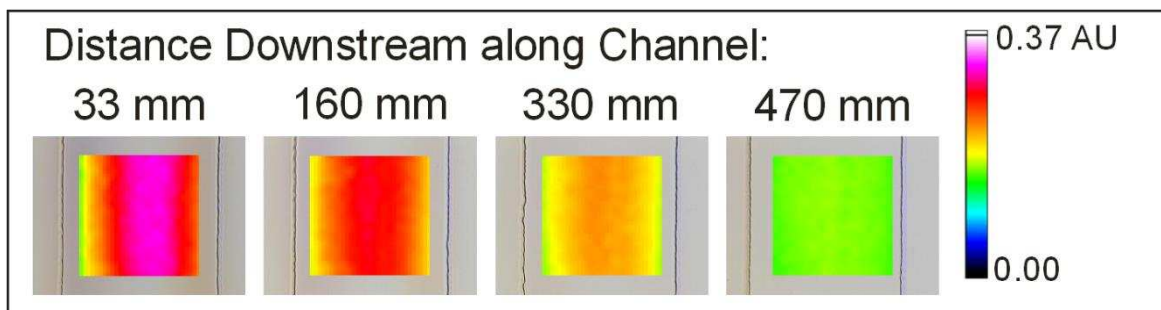


**Figure A1.4:** Intensity maps from the integration of the water peak ( $1930\text{-}2470\text{ cm}^{-1}$ ) at various distances along the channel from the inlet with a total flow rate of  $3\text{ }\mu\text{L}/\text{min}$

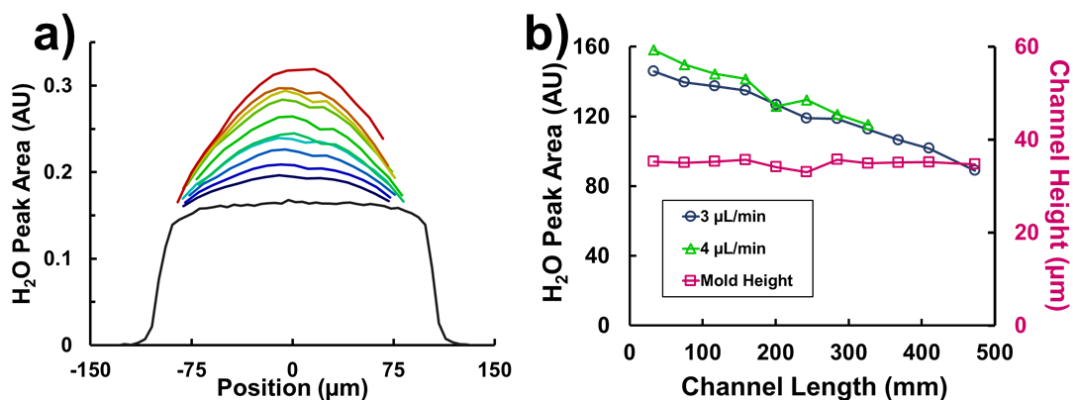


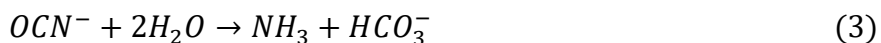
**Figure A1.5:** a) the “cross-sectional view” of the channel distortion as determined by the integration of the water peak ( $1930\text{-}2470\text{ cm}^{-1}$ ), where red corresponds to 33 mm after the intersection and black is 470 mm. b) the channel heights with and without fluid in the device.

the cross-sectional area of the channel, measured by the integrated water peak, is plotted at different distances downstream. Increased bowing is seen at the channels with higher back pressure (further upstream). The maximum height change within a channel observed was a 100% increase with less than a 5-psi difference. Figure A1.5 compares the channel heights with fluid flow relative to without fluid flow along the length of the channel. This also shows the difference of channel height with changing the flow rates within the device, further supporting the hypothesis that the PDMS is bowing due to increasing back pressure as higher flow rates result in higher back pressure. Various distortions in thin ( $\leq 100\text{ }\mu\text{m}$ ) PDMS have been observed previously.<sup>20,21</sup> This

bowing property of thin PDMS devices causes the spectral analysis to be more complex due to the changing PDMS background absorbance, refraction effects, and variable pathlength. The changing PDMS thickness and refraction effects are not solved in the following experiments. Correcting for the changing pathlength is approached by analyzing the relative intensity integration ratios of the peaks of interest to the water peak.

#### *Acidic Decomposition of Cyanate*

The decomposition of cyanate in acidic solutions has been well studied<sup>22</sup> and was chosen as an example reaction to test the system, partially due to the easily traceable IR peaks in aqueous systems. Cyanate reacts with acid to yield isocyanic acid, which then predominantly reacts with a hydronium ion and decomposes into ammonium and carbon dioxide (reaction 1 below). In this system at low pH, there are two side reactions that also occur (reactions 2 and 3 below). The isocyanic acid can react with water to form ammonia and carbon dioxide, and the cyanate ion can react with two water molecules to form ammonia and bicarbonate, as shown below.



The rate of isocyanic acid decomposition is pH dependent; thus, many different reaction rates can easily be studied in microfluidic devices by simply changing incoming flow rates of solutions. In the thin PDMS microfluidic device described above, the kinetics of isocyanic acid's decomposition in sulfamic acid were calculated. The intensity maps of the isocyanic peak (2210-2190  $\text{cm}^{-1}$ ) for 3 and 4  $\mu\text{L}/\text{min}$  total flow rates from three inlet channels each are shown in Figure

A1.6. Artifacts most likely resulting from refractive distortion of the PDMS can be seen. The

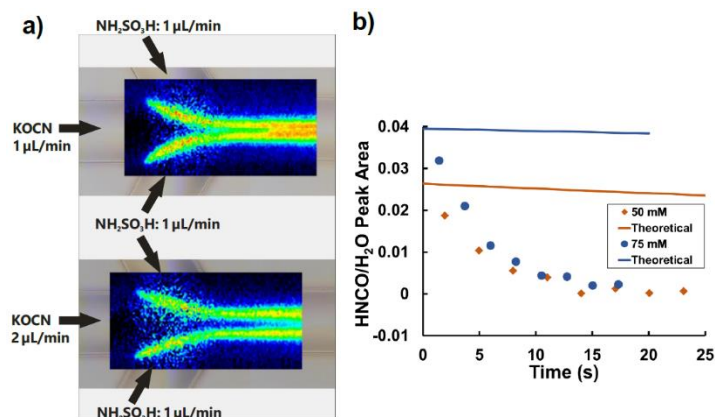


**Figure A1.6:** a) intensity maps of 150 mM potassium cyanate and 150 mM sulfamic acid mixing at 3 (top) and 4 (bottom)  $\mu\text{L}/\text{min}$  total flow rates b) kinetic curves of measured and theoretical isocyanic acid decomposition in thin PDMS, concentrations are initial potassium cyanate concentrations.

isocyanic acid's absorbance, which is proportional to concentration, was monitored at various distances down the channel in the IR viewing window. Figure A1.6 shows the concentration of isocyanic acid versus reaction time found in the microfluidic device compared to the predicted expectations calculated from the following integrated rate law:

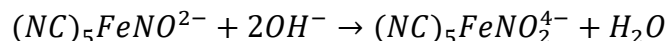
$$[HNC(O)] = [HNC(O)]_o e^{-t(k_1[H_3O^+] + k_2 + k_3[OCN^-]_o)}$$

where the  $k$  values corresponding to the reactions above. Two different reaction conditions are shown. The first reaction condition is 50 mM potassium cyanate with a calculated pH of 1.57. The second reaction condition is 75 mM potassium cyanate with a calculated pH of 2.41. These reaction conditions were chosen to give predicted half-lives of 206 and 496 s, respectively,<sup>22</sup> which can be monitored in the device. Unfortunately, the experimental and theoretical reaction conditions do not match with half-lives of 3.9 and 3.1 s, respectively. This disagreement is most likely from the volatilization of isocyanic acid through the PDMS. Isocyanic acid's Henry's law constant has been reported as 21 M/atm at a pH of 3.<sup>23</sup> This corresponds to a vapor pressure of  $2.4 \times 10^{-3}$  and  $3.6 \times 10^{-3}$  atm, respectively, for the reactions run. PDMS is well known as a porous,

gas-permeable material for small molecules,<sup>24,25</sup> so it is reasonable that the isocyanic acid would volatilize through the PDMS. The inherent flaw of the isocyanic evaporation resulted in improper kinetic comparison to bulk solution; therefore, this reaction has not been studied further. Future plans involve studying the kinetics of this reaction in a microfluidic device that is less gas permeable than PDMS, such as CaF<sub>2</sub>, so as to prevent significant volatilization of isocyanic acid.

### *Nitroprusside Ion*

Pentacyanonitrosylferrate(III), nitroprusside, similar to cyanate in that it is easily traceable with IR spectroscopy in aqueous systems, can yield a range of kinetic rates to probe that have previously been characterized.<sup>26-32</sup> The nitroprusside reaction monitored was the degradation in basic solution:



which has the following second-order reaction rate:

$$\frac{d[NP]}{dt} = -k[NP][OH^-]$$

where [NP] is the concentration of nitroprusside, [OH<sup>-</sup>] is the concentration of hydroxide, and k has been previously measured to equal 0.55 ± 0.01 M<sup>-1</sup>s<sup>-1</sup>.<sup>30</sup> This rate law was integrated to account for the 1: 2 stoichiometric ratio of nitroprusside to hydroxide in the reaction:

$$\frac{1}{([OH^-]_o - 2[NP]_o)} \ln\left(\frac{[NP]_o}{[NP]}\right) + \frac{1}{([NP]_o - [OH^-]_o)} \ln\left(\frac{[OH^-]_o}{[OH^-]^2}\right) = kt$$

where [NP]<sub>o</sub> and [OH]<sub>o</sub> are the initial concentrations of nitroprusside and hydroxide, respectively. Within the thin PDMS device described above, total concentrations of 70 mM nitroprusside and 170 mM sodium hydroxide were reacted to yield the product. The NO peak area absorbance (1908-1964 cm<sup>-1</sup>), relative to concentration, degrades over time. The solid line plotted is the theoretical concentration over time, adjusted to the same initial absorbance value for direct comparison

(Figure A1.7). The coefficient of determination,  $R^2$ , between the measured values and theoretical

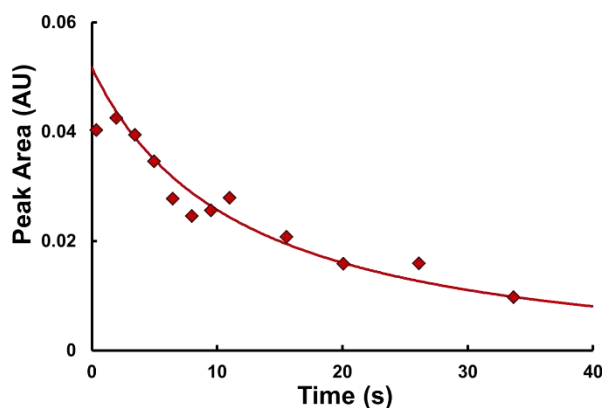
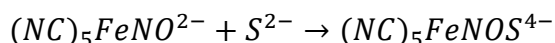


**Figure A1.7:** Decomposition of nitroprusside in aqueous hydroxide solution by monitoring the NO peak ( $1908\text{-}1964\text{ cm}^{-1}$ ) compared to the theoretical concentration (solid line).

concentration is 0.9341. The next reaction that can be studied is that between nitroprusside and hydrogen sulfide:



which has been reported to have changing IR spectra over time<sup>27,28</sup> that can be monitored in a thin PDMS device. Other nitroprusside reactions that can be monitored include thiol-containing organic compounds, e.g. cysteine, that are mostly diffusion-limited reactions.<sup>33</sup> This diffusion-limited reaction could be monitored in Y-channel devices, such as the polymer–CaF<sub>2</sub> devices.

## Conclusion

For microfluidic devices to be applicable to kinetic studies of organic syntheses with IR absorbance spectroscopy, the devices need to be IR and organic-solvent compatible. While attempts were being made to develop organic reaction-compatible devices, preliminary studies were done to characterize and monitor aqueous reaction kinetics in microfluidic devices with previously known fabrication methods. A limitation of thin-PDMS devices was observed in that the channels bowed with increased back pressure, making analysis more difficult due to a variable pathlength, changing substrate background, and refraction effects. The pathlength differences

were corrected for by comparing the peak of interest to a reference peak, e.g. solvent or other internal standard. Another limitation of PDMS was discovered while trying to monitor the decomposition of isocyanic acid due to its volatilization through the PDMS, yielding a falsely low half-life. This will need to be monitored in future conditions but can be minimized by utilizing a less gas-permeable material. The decomposition kinetics of an easily traceable IR compound, nitroprusside, in aqueous hydroxide were monitored in a thin PDMS device and found to correspond to previously reported results. A thermoplastic, organic-compatible, IR-transparent device has yet to be manufactured, despite efforts with COC, COP, PP, and PE. However, a COC-CaF<sub>2</sub> device, which is functional with polar organic solvents, has been fabricated but is limited in channel length, and therefore is not applicable to many organic reactions.

In order for applicability to chemical kinetic studies of a broader range of reactions, i.e. organic reactions, devices need to be manufactured that have a broader range of solvent compatibility while maintaining relevant resident times. Future plans involve fabricating devices from SU-8 epoxy-based photoresist and CaF<sub>2</sub> wafers, where the entire channel wall is composed of SU-8, which has the desired advantage of broad solvent compatibility.<sup>18</sup> A thin layer (< 1  $\mu\text{m}$ ) will be cured onto a CaF<sub>2</sub> wafer. A thicker, channel height defining, layer of SU-8 will then be cured on top of that, and tubing holes will be drilled into the CaF<sub>2</sub>. The CaF<sub>2</sub> will be drilled after the application of SU-8 in order to prevent the risk of SU-8 obstructing the holes before curing. On another CaF<sub>2</sub> wafer, an adhesive layer of SU-8 will be spin coated then bonded to the channel-defining SU-8 layer. The adhesive layer would be ideally as thin as possible while still maintaining bonding integrity. Similar devices with this SU-8 technique have previously been fabricated<sup>34,35</sup> with the adhesive layer of SU-8 reported as low as 10  $\mu\text{m}$ , which is suitable for transmission IR spectroscopy. With the shorter adhesive-layer heights, there was a higher percentage of non-

bonded area, so the fabrication parameters would require optimization. These optimization parameters include but are not limited to: bonding temperature, bonding pressure, outgassing channel incorporation, and adhesive-layer thickness. Once organic solvent and IR-compatible devices have been fabricated, the limitations, e.g. dimensions and solvent compatibility, of the devices will be explored. After these limitations are taken into account, reactions will be investigated and analyzed within the device.

## REFERENCES

1. K. S. Elvira, X. C. i Solvas and R. C. Wootton, *Nature chemistry*, 2013, **5**, 905-915.
2. D. M. Ratner, E. R. Murphy, M. Jhunjhunwala, D. A. Snyder, K. F. Jensen and P. H. Seeberger, *Chem. Commun.*, 2005, 578-580.
3. K. Geyer, T. Gustafsson and P. H. Seeberger, *Synlett*, 2009, 2382-2391.
4. K. F. Jensen, *MRS Bull.*, 2006, **31**, 101-107.
5. J. S. Moore and K. F. Jensen, *Organic Process Research & Development*, 2012, **16**, 1409-1415.
6. J. P. McMullen and K. F. Jensen, *Organic Process Research & Development*, 2010, **14**, 1169-1176.
7. R. L. Hartman, J. P. McMullen and K. F. Jensen, *Angew. Chem. Int. Ed.*, 2011, **50**, 7502-7519.
8. H. Song and R. F. Ismagilov, *J. Am. Chem. Soc.*, 2003, **125**, 14613-14619.
9. J. Fagaschewski, S. Bohne, D. Kaufhold, J. Müller and L. Hilterhaus, *Green Processing and Synthesis*, 2012, **1**, 337-344.
10. I. Silverwood, N. Al-Rifai, E. Cao, D. Nelson, A. Chutia, P. Wells, S. Nolan, M. Frogley, G. Cinque and A. Gavriilidis, *Rev. Sci. Instrum.*, 2016, **87**, 024101.
11. B. Lehmkuhl, S. D. Noblitt, A. T. Krummel and C. S. Henry, *Lab Chip*, 2015, **15**, 4364-4368.
12. W. Buchegger, C. Wagner, B. Lendl, M. Kraft and M. J. Vellekoop, *Microfluidics and Nanofluidics*, 2011, **10**, 889-897.
13. K. L. A. Chan, X. Z. Niu, A. J. de Mello and S. G. Kazarian, *Lab Chip*, 2010, **10**, 2170-2174.
14. T. Pan, R. T. Kelly, M. C. Asplund and A. T. Woolley, *J. Chromatogr. A*, 2004, **1027**, 231-235.
15. M. V. Barich and A. T. Krummel, *Anal. Chem.*, 2013, **85**, 10000-10003.
16. M. Srisa-Art and Y. Furutani, *Bull. Chem. Soc. Jpn.*, 2016.
17. J. N. Lee, C. Park and G. M. Whitesides, *Anal. Chem.*, 2003, **75**, 6544-6554.
18. H. Lorenz, M. Despont, N. Fahrni, N. LaBianca, P. Renaud and P. Vettiger, *Journal of Micromechanics and Microengineering*, 1997, **7**, 121.
19. S. Bhattacharya, A. Datta, J. M. Berg and S. Gangopadhyay, *Microelectromechanical Systems, Journal of*, 2005, **14**, 590-597.
20. J. R. Anderson, D. T. Chiu, R. J. Jackman, O. Cherniavskaya, J. C. McDonald, H. Wu, S. H. Whitesides and G. M. Whitesides, *Anal. Chem.*, 2000, **72**, 3158-3164.
21. C. Liu, D. Cui, H. Cai, X. Chen and Z. Geng, *Electrophoresis*, 2006, **27**, 2917-2923.
22. M. B. Jensen, *Acta Chem. Scand*, 1958, **12**, 1657-1670.
23. J. M. Roberts, P. R. Veres, A. K. Cochran, C. Warneke, I. R. Burling, R. J. Yokelson, B. Lerner, J. B. Gilman, W. C. Kuster, R. Fall and J. de Gouw, *Proceedings of the National Academy of Sciences*, 2011, **108**, 8966-8971.
24. A. Singh, B. Freeman and I. Pinnau, *J. Polym. Sci., Part B: Polym. Phys.*, 1998, **36**, 289-301.
25. M. W. Toepke and D. J. Beebe, *Lab Chip*, 2006, **6**, 1484-1486.
26. C. Andrade and J. H. Swinehart, *Inorg. Chem.*, 1972, **11**, 648-650.

27. M. R. Filipovic, M. Eberhardt, V. Prokopovic, A. Mijuskovic, Z. Orescanin-Dusic, P. Reeh and I. Ivanovic-Burmazovic, *J. Med. Chem.*, 2013, **56**, 1499-1508.
28. P. A. Rock and J. H. Swinehart, *Inorg. Chem.*, 1966, **5**, 1078-1079.
29. J. Swinehart, *Coord. Chem. Rev.*, 1967, **2**, 385-402.
30. J. H. Swinehart and P. A. Rock, *Inorg. Chem.*, 1966, **5**, 573-576.
31. J. H. Swinehart and W. G. Schmidt, *Inorg. Chem.*, 1967, **6**, 232-237.
32. S. K. Wolfe, C. Andrade and J. Swinehart, *Inorg. Chem.*, 1974, **13**, 2567-2572.
33. M. D. Johnson and R. G. Wilkins, *Inorg. Chem.*, 1984, **23**, 231-235.
34. S. Li, C. B. Freidhoff, R. M. Young and R. Ghodssi, *Journal of Micromechanics and Microengineering*, 2003, **13**, 732.
35. S. Tuomikoski and S. Franssila, *Sensors and Actuators A: Physical*, 2005, **120**, 408-415.

## APPENDIX 2. ELECTROCHEMICAL DETECTION OF 2-HYDROXYTEREPHTHALATE FOR IMPROVED PARTICULATE MATTER TOXICITY: A PROPOSAL

### Appendix Overview

Particulate matter (PM<sub>2.5</sub>) air pollution is linked to millions of human deaths and diseases worldwide each year. The toxicity mechanism is unknown, but the current hypothesis is that the PM generates reactive oxygen species (ROS), which creates oxidative stress and inflammation. PM's oxidative potential (OP), the ability to oxidize target molecules, is used for PM toxicity analysis. Initial OP assays monitored the depletion of antioxidants, ascorbic acid (AA) and glutathione (GSH), but a more common OP assay is to monitor PM-catalyzed dithiothreitol (DTT) oxidation. While both assays are simple to perform, there is some debate about the correlation of these assays with relevant biomarkers and health outcomes. 2-hydroxyterephthalate (2-OHTA), product of terephthalate and a hydroxyl radical, was recently shown to have better correlation with PM<sub>2.5</sub> toxicity when measured concurrently with the DTT or antioxidant assays than the other assays alone. 2-OHTA was measured via fluorescence but could be measured electrochemically, which enables simultaneous detection without a separation step; however, there is still value in measuring antioxidants and DTT (PM OP), as they have been more thoroughly characterized. I hypothesize that electrochemical detection of 2-OHTA, DTT, AA, and GSH will enable simultaneous detection that will lead to a more accurate toxicity assay and an increased understanding of PM<sub>2.5</sub> health effects without significantly more time, labor, and cost. While 2-OHTA has been previously used in fluorescent assays, little is known about its electrochemistry. As a result, the first step is to detect 2-OHTA and optimize the electrochemical parameters for quantification. Figures of merit, such as sensitivity, limit of detection, and interferences from other antioxidants, will be established. The second aim is to design a microfluidic device to

simultaneously detect 2-OHTA, DTT, AA, and GSH with a flow injection analysis system. The third step is to compare the relative reactivities of the compounds to show the applicability of this method for more accurately measuring PM<sub>2.5</sub> effects on human health relative to the antioxidant assays alone. Comparing reactivities will also determine if this assay's results can be directly compared to previous assay results. The compounds' reactivities will be measured when reacting alone with the PM sample and compared to the reactivity when multiple compounds are present in solution. The data collected will inform epidemiologists, as there is great interest in the specific health effects of PM<sub>2.5</sub> pollution. It will also provide information about the accuracy of the assays when compared to epidemiological data. If this method is proven viable, large-scale PM<sub>2.5</sub> health studies will be more accurate without significantly more time, labor, and cost of other chemical assays.

*Aim 1: Determine electrochemical parameters for 2-OHTA detection and test for interferences*

The first hypothesis is that if 2-OHTA electrochemical detection is performed with a high-performing, carbon-based thermoplastic electrode (TPE) in the presence of the assay's other compounds, there will not be interferences due to differences in oxidation potentials. This hypothesis will be tested by comparing limit of detection, sensitivity, and linear range of 2-OHTA detection with and without the other assay compounds present.

*Aim 2: Detect 2-OHTA, DTT, GSH, and AA compounds simultaneously*

My second hypothesis is that if a wall-jet, multiple ring-disc electrode configuration in a microfluidic device is incorporated into a semi-automated injection system, then 2-OHTA, DTT, GSH, and AA can be simultaneously detected. Simultaneous detection will be tested using TPEs because they are easily integrated into microfluidic devices. The device design and electrochemical parameters will be chosen based on literature and the first hypothesis' testing results.

*Aim 3: Verify 2-OHTA, DTT, GSH, and AA have equivalent reactivity rates with PM<sub>2.5</sub> samples*

The final hypothesis is that if PM OP are measured for each compound individually, the reactivity rates of the compounds will not be significantly different when the compounds are simultaneously detected. This is important to test if: 1) there are interferences between the compounds and 2) the OP values can be directly compared to existing literature values.

## **Introduction**

Human exposure to particulate matter (PM) air pollution has been linked to millions of deaths globally, as well as many cardiovascular and respiratory diseases.<sup>1,2</sup> PM is from natural and anthropogenic sources, is composed of liquid droplets and particles suspended in that air, and can include acids, organic compounds, metals, and dust.<sup>3</sup> PM is typically classified by the aerodynamic diameter, with PM<sub>2.5</sub> (<2.5 μm, or fine PM) having the most significant long-term impact on human health.<sup>4</sup> The mechanism of PM's toxicity is unknown, but the current hypothesis is that PM generates reactive oxygen species (ROS, i.e. hydrogen peroxide, hydroxyl radicals) that leads to a state of oxidative stress, which leads to inflammation and various diseases in the body.<sup>3,5,6</sup> PM toxicity is dependent on several factors, including size, concentration, and chemical composition.<sup>7</sup> The oxidative potential (OP) of PM is the measurement of PM's ability to oxidize target molecules and is theoretically a more biologically relevant measurement of PM toxicity than PM mass alone (only PM mass is currently regulated).<sup>8-10</sup> The different OP of various PM samples results from the differences in chemical composition and the corresponding chemical reactivities to form oxidative reactions.<sup>11</sup> For example, an area with high PM amounts, with PM that is less reactive with the human body, can be less toxic than an area with a lower amount of highly reactive PM.

PM OP has been measured several different ways: direct ROS detection<sup>12,13</sup> and indirect detection through antioxidant monitoring.<sup>14,15</sup> Direct ROS detection, while promising, often

requires expensive equipment, a lot of labor, and gives inconsistent OP assay responses with different PM chemical composition.<sup>11,15</sup> PM OP through indirect ROS measurements are usually performed by monitoring the loss of an antioxidant and/or the formation of the oxidized product. Ascorbic acid (AA) and glutathione (GSH) are common antioxidants and are attractive due to their natural occurrence in the human body. There is debate in the literature about the accuracy of the AA and GSH assays as some literature argues that AA and GSH are not always accurate due to their sensitivity to the PM chemical composition.<sup>15</sup> Both AA and GSH have high reactivity to Cu and GSH is also sensitive to Fe, which causes an OP measurement that does not correlate well with relevant biomarkers in PM samples high in Cu and Fe.<sup>14,16</sup>

Dithiothreitol (DTT) is a commonly used reducing agent for PM OP measurements since its introduction in 2005.<sup>8</sup> Of the developed assays thus far, DTT reacts with the widest range of compounds found in PM<sub>2.5</sub> and correlates with oxidative stress and inflammation biomarkers.<sup>9,15,17</sup> In the DTT assay, PM catalyzes DTT oxidation to the disulfide, and the remaining DTT is quantified over time with the degradation rate equivalent to the PM OP.<sup>8</sup> Recently, it was proposed to add disodium terephthalate, a hydroxyl radical scavenger, to the DTT assay to obtain an ROS estimation of PM samples because DTT is well correlated with hydrogen peroxide, but not hydroxyl radical, formation.<sup>15</sup> A follow-up study found that measuring ROS via 2-hydroxyterephthalate (2-OHTA, product of terephthalate and a hydroxyl radical) quantification in the presence of either DTT or an antioxidant mixture was the highest correlation to PM<sub>2.5</sub> cytotoxicity in Chinese hamster ovarian cells.<sup>18</sup> This new finding makes 2-OHTA promising for PM<sub>2.5</sub> toxicity studies in further detail.

The reported DTT and 2-OHTA assays were measured with UV-vis and fluorescence, respectively.<sup>18</sup> DTT can also be quantified in PM OP studies with electrochemistry using carbon-

based electrodes modified with cobalt(II) phthalocyanine (CoPC).<sup>19</sup> The electrochemical DTT assay gives comparable precision and accuracy as the UV-vis assay but is simpler to perform.<sup>20</sup> Our lab recently developed a semi-automated electrochemical DTT assay that improved the sampling throughput from one to six samples per hour with reduced labor.<sup>21</sup> The time and labor required for the DTT assay is a major hurdle in the field for large-scale (>100 samples) health studies, and there has only been one report of a semi-automated system, but it only reduced the labor required without increasing the sampling throughput.<sup>22</sup>

Here, simultaneous electrochemical detection of 2-OHTA, DTT, AA, and GSH in the semi-automated sampling system is proposed for an improved PM<sub>2.5</sub> toxicity assay that can provide more information to epidemiologists without significantly more sample processing time, labor, and cost. The first step is to electrochemically detect 2-OHTA in the presence of the other compounds in the PM<sub>2.5</sub> toxicity assay. The detection will be performed on homemade, carbon-based, high-performing thermoplastic electrodes (TPEs). Carbon electrodes are often used to detect AA (no modification),<sup>23</sup> GSH and DTT (with CoPC modification).<sup>19</sup> The next step is to create an application-specific microfluidic device for simultaneous detection with multiple TPE rings. TPEs have been shown to be easily fabricated and integrated into microfluidic devices.<sup>24</sup> The microfluidic device will then be combined with the semi-automated flow injection analysis system developed by our lab.<sup>21</sup> After testing and optimizing the simultaneous detection, OP and ROS measurements on real, collected PM<sub>2.5</sub> aerosol filter samples to provide more information related to human health. Being able to analyze a large sample number with an assay that yields more data without considerably more time or labor will show the feasibility of this method for future large-scale health studies and thus improving pertinent health information from PM<sub>2.5</sub> air pollution.

## Research Design and Methods

The aims here are towards the simultaneous, electrochemical detection of 2-OHTA, DTT, AA, and GSH within a microfluidic device that will be integrated with a semi-automated flow injection analysis system for a more accurate PM<sub>2.5</sub> toxicity assay without significantly more time, labor, and cost. Once the simultaneous detection in a microfluidic device (Aims 1 and 2) is developed, the accuracy will be assessed by comparing the relative PM<sub>2.5</sub> reactivities of the compounds alone and together in solution (Aim 3).

*Aim 1: Determine electrochemical parameters for 2-OHTA detection and test for interferences*

Recently, using terephthalate as a hydroxyl radical scavenger, which produces 2-OHTA (Figure A2.1),<sup>25</sup> was shown to be more accurate for PM<sub>2.5</sub> toxicity assays when measured in the presence of DTT or antioxidants GSH and AA, than DTT alone.<sup>18</sup> 2-OHTA has higher solubility,

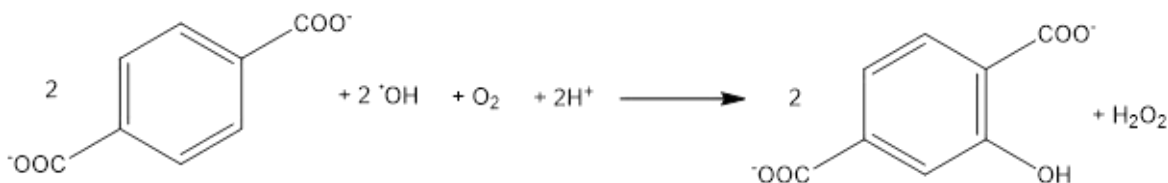


**Figure A2.1:** Hydroxylation of terephthalate in aerobic conditions. It is hypothesized to undergo a perhydroxyl radical intermediate that dissociates into hydrogen peroxide and molecular oxygen.

stability, and yield (partly due to terephthalate's symmetry leading to the same hydroxylated product) than other hydroxyl radical chemical probe products for fluorescence detection.<sup>25,26</sup> 2-OHTA is measured with fluorescence detection and little is known about its electrochemistry. However, more is known about the electrochemical properties of similar structured compounds, such as salicylic acid.<sup>27,28</sup> Salicylic acid hydroxylation has been electrochemically detected, but the hydroxylation of benzoic acid to produce salicylic acid suffers from lower yields.<sup>25</sup>

This work first proposes to investigate electrochemical quantification of 2-OHTA. The quantification will be completed on high-performing, carbon-based TPEs.<sup>23</sup> Preliminary work

has been done to investigate the electrochemical activity of 2-OHTA. A cyclic voltammogram (CV) of 2-OHTA (Figure A2.2) with a TPE was performed in phosphate buffer, pH 7.4, as the

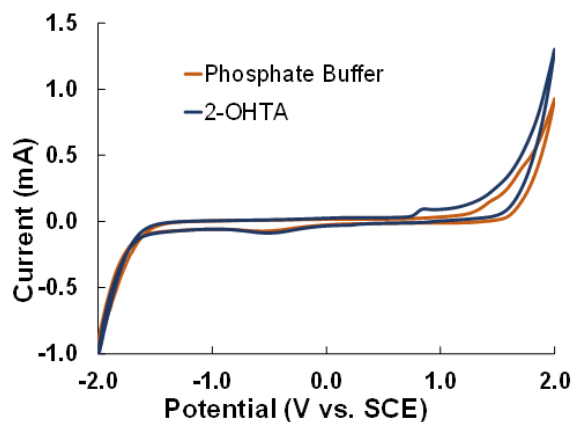


**Figure A2.2:** CV of 500  $\mu\text{M}$  2-OHTA in phosphate buffer (blue) and phosphate buffer, pH 7.4, background (orange) with a TPE.

same background electrolyte used in  $\text{PM}_{2.5}$  assays. The CV shows promise for 2-OHTA electrochemical detection with TPEs because there is a 45  $\mu\text{A}$  oxidation peak at 0.85 V vs. SCE. Analytical figures of merit (limit of detection, sensitivity, linear range) will be determined in a microfluidic device with flow injection analysis. The figures of merit need to be in the nM range based on previous assays.<sup>15,18</sup> Variables that can be altered to optimize the figures of merit include flow rate, injection volume, electrode size, and channel dimensions.<sup>29</sup> The TPE size is easily defined and prototyped with a  $\text{CO}_2$  laser cutter in a poly(methyl methacrylate) (PMMA) template down to 150  $\mu\text{m}$  resolution.<sup>23</sup> The PMMA pieces are easily tapped (for microfluidic connections), stacked, and bolted together. The bolts facilitate reusable PMMA and electrode pieces, as well as rapid prototyping of designs. The channel height is defined by the spacer used, which can also be easily changed as needed.

The individual electrochemical behavior of DTT, GSH, and AA also needs testing on TPEs before simultaneous detection. AA and DTT have already been detected with TPEs.<sup>21,23</sup> AA requires no electrode modification and has an oxidation peak at  $\sim 0.0\text{V}$  vs. SCE. DTT detection

( $\sim 0.3$  V vs. SCE) gives poor limits of detection and sensitivity using unmodified carbon-composite electrodes and requires CoPC catalyst electrode modification. TPEs are easily modified with CoPC, with the CoPC addition in the same step as the carbon, and this also leads to reusable modification. GSH has not yet been detected on TPEs, but it is known in the literature to also have slow kinetics on unmodified carbon electrodes,<sup>30,31</sup> and as such, will likely also require a CoPC-modified TPE. Based on similar CoPC-modified, carbon composite electrodes, GSH will likely be detected with an oxidation potential at  $\sim 0.8$  V vs. SCE.<sup>19</sup>

The first problem that may be encountered is that 2-OHTA detection is not sensitive enough with TPEs. If this problem occurs, a catalyst addition to the TPEs will be tested, such as Pt nanoparticles or PbO<sub>2</sub> that have been previously used to detect other alcohol-substituted benzoic acids.<sup>32,33</sup> The fabrication would not be significantly more difficult with a catalyst addition in the same step as the carbon addition. A commercial electrode will be considered if needed. If the 2-OHTA detection is still not sensitive enough, detection at metal (e.g. Au or Pt) electrodes will be tested. If 2-OHTA detection is not sensitive enough using electrode materials suitable for integration in microfluidic devices, then benzoic acid will be explored as a hydroxyl radical scavenger. 2-hydroxybenzoic acid's (or salicylic acid) electrochemistry is better known and has been integrated with high performance liquid chromatography (HPLC) for hydroxyl radical detection and has an oxidation potential at  $\sim 0.8$  V vs SCE.<sup>34-36</sup> The second possible problem, as with many simultaneous detection techniques, is interferences between the compounds being detected. Due to both being thiols that require CoPC modification, the most likely interference would be between DTT and GSH. If there is an interference between GSH and DTT, measuring 2-OHTA and DTT or 2-OHTA, GSH, and AA would still result in the goal of obtaining concurrent ROS and OP PM measurements.

*Aim 2: Detect 2-OHTA, DTT, GSH, and AA compounds simultaneously*

After analyzing individual electrochemical behavior of the compounds, the microfluidic device for simultaneous detection will be planned and fabricated. A wall-jet (perpendicular fluid flow to the electrode surface), with multiple subsequent rings will be used to increase electrode area relative to a flow-over electrode. Historically, wall-jet devices are more difficult to fabricate and model than a flow over electrode device; however, TPEs are easily integrated into either device design. The device will be similar to a previously fabricated TPE wall-jet device.<sup>21</sup> (Figure A2.3)

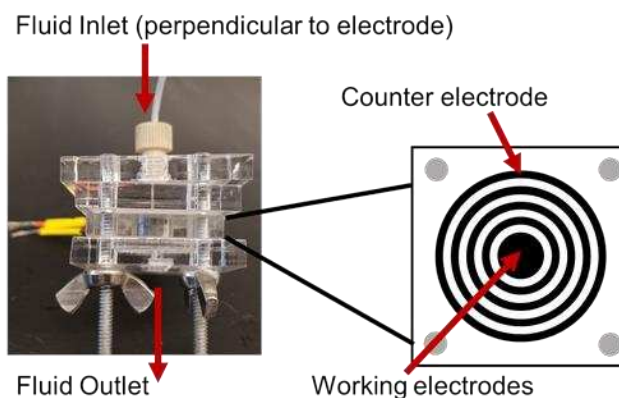


**Figure A2.3:** Side view of wall jet TPE device and electrode design with outer counter electrode and multiple electrode rings for simultaneous detection

and will contain 4 PMMA layers consisting of the following (in direction of fluid flow): 1) tapped piece for inlet tubing connection from fluid pump, 2) a defined inlet hole, 3) TPEs and 4) controlled outlet fluid flow. The device design will be cut with a CO<sub>2</sub> laser cutter and bolted together to hand tightness with o-rings to prevent leaking. A spacer will be used to define the channel height between the fluid inlet and the electrodes. The TPEs will be connected to a potentiostat that can measure 4 working electrodes with a common counter and reference electrode.

Following the direction of the fluid flow within the device (perpendicular flow to the center of the electrodes and then spreads outward across the rings in Figure A2.3), the compounds will be detected with increasing oxidation potentials. For quantitative analysis, current subtraction of

former electrodes from later electrodes will be used.<sup>37</sup> With the known and predicted oxidation potentials (Aim 1), the order the compounds will likely be detected is: 1) AA, 2) DTT, 3) GSH, and 4) 2-OHTA. Due to the slow kinetics, GSH should not be detected on the 4<sup>th</sup> electrode, intended for 2-OHTA detection, if the electrode is unmodified, even though the detection potentials will likely be similar. There will be an outer-ring that will act as the counter electrode. The reference electrode will be externally placed in the fluid outlet, similar to previously work.<sup>21</sup>

Once the device is fabricated, calibration curves of each compound can be made. Calibration curves also need to be validated of each compound with varying levels of the other compounds present in the solution. For example, a DTT calibration curve will be made while changing the amounts of GSH, AA, and 2-OHTA. Traditionally, DTT, GSH, and AA have starting concentrations of 100, 100 and 200  $\mu\text{M}$ , respectively, and the rate is followed to about 75% of the initial concentration.<sup>18</sup> Terephthalate is initially present at 60  $\mu\text{M}$ , and less than 1  $\mu\text{M}$  will be lost during the PM OP assay,<sup>18</sup> so calibration curves with 60  $\mu\text{M}$  terephthalate should be performed. After calibration curves and lack of interferences from compounds are established, molecules with known reactivities, e.g. Cu(II), should be tested to verify the accuracy of the system. Cu(II) reactivity with DTT is well known and often used as a positive control in DTT assays.<sup>38-40</sup>

If a metal electrode was required for sensitive 2-OHTA detection, a poly(dimethylsiloxane) (PDMS) device will be used as microwire are easily incorporated into the devices.<sup>41</sup> PDMS devices are still easy to fabricate with photolithography.<sup>42,43</sup> However, the device design would be a flow-over electrode, which changes the analytical figures of merit. Because thiol detection (DTT and GSH) on metals requires large overpotentials and fouls easily,<sup>19</sup> an alternative device design would also be needed. The options would be to incorporate TPEs into the PDMS device similar to carbon paste electrodes,<sup>19</sup> to split the flow between PDMS and TPE detection devices, or to have both.

*Aim 3: Verify 2-OHTA, DTT, GSH, and AA have equivalent reactivity rates with PM<sub>2.5</sub> samples*

DTT, AA, and GSH degradation are not monitored until completion in the respective assays to maintain linearity with the pseudo first order reaction rate; typically, the rates are monitored until ~ 25% degradation.<sup>8,44,45</sup> While AA and GSH are often run simultaneously,<sup>11,45,46</sup> DTT has not been run with antioxidants present to my knowledge. 2-OHTA formation relates to the hydroxyl radicals produced during the DTT or antioxidant assays,<sup>18</sup> so the correlation of 2-OHTA and cytotoxicity is likely dependent on the presence of the other compounds. However, having both DTT and the antioxidants present may change the 2-OHTA production such that it is no longer correlated with cytotoxicity. 2-OHTA generation rate was higher with the antioxidant assay (0.3-1.5 pmol/min/m<sup>3</sup>) than the DTT assay (0.01-0.25 pmol/min/m<sup>3</sup>),<sup>18</sup> so the 2-OHTA generation rate will likely change but not double. There is also the possibility that the antioxidant assay produced the maximum amount of hydroxyl radicals from the PM samples, which would render no 2-OHTA change from the addition of DTT. Therefore, the plan is to run pieces of the same PM<sub>2.5</sub> filter (repeated for 20+ filters) with the following compounds present: 1) Terephthalate, DTT, GSH, and AA; 2) Terephthalate, GSH, and AA; 3) Terephthalate and DTT; 4) DTT; 5) GSH and AA; 6) Terephthalate. I hypothesize that the DTT, AA, and GSH reactivity rates with each PM<sub>2.5</sub> filter sample will not change in the presence of other compounds because the compounds are not known to react with each other in these conditions but do react with PM<sub>2.5</sub> acting as the degradation catalyst. The reactivity of only terephthalate and PM<sub>2.5</sub> has not been measured. I hypothesize that no significant 2-OHTA generation will occur with only terephthalate in the solution to react with PM<sub>2.5</sub> as the PM<sub>2.5</sub> likely does not inherently contain measurable hydroxyl radicals due to their high reactivity, but a background signal for 2-OHTA generation should still be obtained to confirm no other reactivity between the PM<sub>2.5</sub> and terephthalate. If all

of the compounds were not able to be simultaneously detected during Aim 2, the above list will be modified appropriately to account for such changes.

The work here proposes a more accurate toxicity assay for  $PM_{2.5}$  aerosol filters without significantly more time, labor, and cost. Simultaneous detection of 2-OHTA, DTT, GSH, and AA will allow for ROS and OP measurements of  $PM_{2.5}$  aerosol filter samples. Combining this detection with the semi-automated analysis system will allow for more data to be acquired and analyzed from large-scale aerosol filter studies, which will lead to an increased understanding of  $PM_{2.5}$  health effects.

## REFERENCES

1. A. J. Cohen, M. Brauer, R. Burnett, H. R. Anderson, J. Frostad, K. Estep, K. Balakrishnan, B. Brunekreef, L. Dandona, R. Dandona, V. Feigin, G. Freedman, B. Hubbell, A. Jobling, H. Kan, L. Knibbs, Y. Liu, R. Martin, L. Morawska, C. A. Pope, III, H. Shin, K. Straif, G. Shaddick, M. Thomas, R. van Dingenen, A. van Donkelaar, T. Vos, C. J. L. Murray and M. H. Forouzanfar, *The Lancet*, 2017, **389**, 1907-1918.
2. O. M. Morakinyo, M. I. Mokgobu, M. S. Mukhola and R. P. Hunter, *International journal of environmental research and public health*, 2016, **13**, 592.
3. J. O. Anderson, J. G. Thundiyil and A. Stolbach, *Journal of Medical Toxicology*, 2012, **8**, 166-175.
4. R. D. Brook, S. Rajagopalan, C. A. Pope, J. R. Brook, A. Bhatnagar, A. V. Diez-Roux, F. Holguin, Y. Hong, R. V. Luepker, M. A. Mittleman, A. Peters, D. Siscovick, S. C. Smith, L. Whitsel and J. D. Kaufman, *An Update to the Scientific Statement From the American Heart Association*, 2010, **121**, 2331-2378.
5. A. A. Alfadda and R. M. Sallam, *BioMed Research International*, 2012, **2012**.
6. J. T. Bates, R. J. Weber, J. Abrams, V. Verma, T. Fang, M. Klein, M. J. Strickland, S. E. Sarnat, H. H. Chang, J. A. Mulholland, P. E. Tolbert and A. G. Russell, *Environmental Science & Technology*, 2015, **49**, 13605-13612.
7. A. De Vizcaya-Ruiz, M. Gutiérrez-Castillo, M. Uribe-Ramirez, M. Cebrián, V. Mugica-Alvarez, J. Sepúlveda, I. Rosas, E. Salinas, C. Garcia-Cuéllar and F. Martínez, *Atmos. Environ.*, 2006, **40**, 583-592.
8. A. K. Cho, C. Sioutas, A. H. Miguel, Y. Kumagai, D. A. Schmitz, M. Singh, A. Eiguren-Fernandez and J. R. Froines, *Environ. Res.*, 2005, **99**, 40-47.
9. B. Crobeddu, L. Aragao-Santiago, L.-C. Bui, S. Boland and A. Baeza Squiban, *Environ. Pollut.*, 2017, **230**, 125-133.
10. P. J. A. Borm, F. Kelly, N. Künzli, R. P. F. Schins and K. Donaldson, *Occupational and Environmental Medicine*, 2007, **64**, 73-74.
11. N. A. H. Janssen, A. Yang, M. Strak, M. Steenhof, B. Hellack, M. E. Gerlofs-Nijland, T. Kuhlbusch, F. Kelly, R. Harrison, B. Brunekreef, G. Hoek and F. Cassee, *Sci. Total Environ.*, 2014, **472**, 572-581.
12. A. M. Arangio, H. Tong, J. Socorro, U. Pöschl and M. Shiraiwa, *Atmospheric Chemistry and Physics*, 2016, **16**, 13105-13119.
13. H. Shen and C. Anastasio, *Atmos. Environ.*, 2012, **46**, 665-668.
14. T. Fang, V. Verma, J. Bates, J. Abrams, M. Klein, M. Strickland, S. Sarnat, H. Chang, J. Mulholland and P. Tolbert, *Atmospheric Chemistry & Physics Discussions*, 2015, **15**.
15. Q. Xiong, H. Yu, R. Wang, J. Wei and V. Verma, *Environmental science & technology*, 2017, **51**, 6507-6514.
16. E. Vidrio, H. Jung and C. Anastasio, *Atmos. Environ.*, 2008, **42**, 4369-4379.
17. N. Li, C. Sioutas, A. Cho, D. Schmitz, C. Misra, J. Sempf, M. Wang, T. Oberley, J. Froines and A. Nel, *Environ. Health Perspect.*, 2003, **111**, 455.
18. Y. Wang, M. J. Plewa, U. K. Mukherjee and V. Verma, *Atmos. Environ.*, 2018, **179**, 132-141.

19. Y. Sameenoi, M. M. Mensack, K. Boonsong, R. Ewing, W. Dungchai, O. Chailapakul, D. M. Crokek and C. S. Henry, *Analyst*, 2011, **136**, 3177-3184.
20. Y. Sameenoi, K. Koehler, J. Shapiro, K. Boonsong, Y. Sun, J. Collett, J. Volckens and C. S. Henry, *J. Am. Chem. Soc.*, 2012, **134**, 10562-10568.
21. K. E. Berg, K. M. Clark, X. Li, E. Carter and C. S. Henry, *in preparation*, 2018.
22. T. Fang, V. Verma, H. Guo, L. King, E. Edgerton and R. Weber, *Atmospheric Measurement Techniques*, 2015, **8**, 471.
23. K. J. Klunder, Z. Nilsson, J. B. Sambur and C. S. Henry, *J. Am. Chem. Soc.*, 2017, **139**, 12623-12631.
24. K. J. Klunder, K. M. Clark, C. McCord, K. E. Berg and C. S. Henry, *Lab Chip*, 2018, **in preparation**.
25. M. Saran and K. H. Summer, *Free Radical Res.*, 1999, **31**, 429-436.
26. Y. Son, V. Mishin, W. Welsh, S.-E. Lu, J. Laskin, H. Kipen and Q. Meng, *International Journal of Environmental Research and Public Health*, 2015, **12**, 13678.
27. Y. Park, D. S. Shin, S. H. Woo, N. S. Choi, K. H. Shin, S. M. Oh, K. T. Lee and S. Y. Hong, *Adv. Mater.*, 2012, **24**, 3562-3567.
28. H. Urano, S. Sunohara, H. Ohtomo and N. Kobayashi, *J. Mater. Chem.*, 2004, **14**, 2366-2368.
29. J. A. Cooper and R. G. Compton, *Electroanalysis: An International Journal Devoted to Fundamental and Practical Aspects of Electroanalysis*, 1998, **10**, 141-155.
30. O. Oyesanya, 2008.
31. N. Pereira-Rodrigues, R. Cofré, J. H. Zagal and F. Bedioui, *Bioelectrochemistry*, 2007, **70**, 147-154.
32. S. Ai, Q. Wang, H. Li and L. Jin, *J. Electroanal. Chem.*, 2005, **578**, 223-229.
33. Z. Wang, F. Ai, Q. Xu, Q. Yang, J.-H. Yu, W.-H. Huang and Y.-D. Zhao, *Colloids and Surfaces B: Biointerfaces*, 2010, **76**, 370-374.
34. W. Freinbichler, L. Bianchi, M. A. Colivicchi, C. Ballini, K. F. Tipton, W. Linert and L. D. Corte, *J. Inorg. Biochem.*, 2008, **102**, 1329-1333.
35. Y.-S. Fung and S.-F. Luk, *Analyst*, 1989, **114**, 943-945.
36. A. A. J. Torriero, J. M. Luco, L. Sereno and J. Raba, *Talanta*, 2004, **62**, 247-254.
37. R. Thangaraj, S. Nellaiappan, R. Sudhakaran and A. S. Kumar, *Electrochim. Acta*, 2014, **123**, 485-493.
38. J. Charrier, N. Richards-Henderson, K. Bein, A. McFall, A. Wexler and C. Anastasio, *Atmospheric Chemistry and Physics*, 2015, **15**, 2327-2340.
39. J. G. Charrier and C. Anastasio, *Atmospheric chemistry and physics (Print)*, 2012, **12**, 11317-11350.
40. J. G. Charrier, A. S. McFall, K. K. T. Vu, J. Baroi, C. Olea, A. Hasson and C. Anastasio, *Atmos. Environ.*, 2016, **144**, 325-334.
41. S. D. Noblitt and C. S. Henry, *Anal. Chem.*, 2008, **80**, 7624-7630.
42. R. Martinez-Duarte and M. J. Madou, *Journal*, 2011, **2**, 231-268.
43. G. M. Whitesides, E. Ostuni, S. Takayama, X. Jiang and D. E. Ingber, *Annual review of biomedical engineering*, 2001, **3**, 335-373.
44. M. Y. Chung, R. A. Lazaro, D. Lim, J. Jackson, J. Lyon, D. Rendulic and A. S. Hasson, *Environmental Science & Technology*, 2006, **40**, 4880-4886.

45. I. S. Mudway, N. Stenfors, S. T. Duggan, H. Roxborough, H. Zielinski, S. L. Marklund, A. Blomberg, A. J. Frew, T. Sandström and F. J. Kelly, *Arch. Biochem. Biophys.*, 2004, **423**, 200-212.
46. J. G. Ayres, P. Borm, F. R. Cassee, V. Castranova, K. Donaldson, A. Ghio, R. M. Harrison, R. Hider, F. Kelly, I. M. Kooter, F. Marano, R. L. Maynard, I. Mudway, A. Nel, C. Sioutas, S. Smith, A. Baeza-Squiban, A. Cho, S. Duggan and J. Froines, *Inhalation Toxicology*, 2008, **20**, 75-99.